Absolute measurements of cross-sections of nuclear reactions induced by fast neutrons

Colin George Bruce Williams Williams

"Absolute measurements of cross-sections of nuclear reactions induced by fast neutrons"

THESIS

presented in candidature for the degree of

DOCTOR OF PHILOSOPHY

in the

UNIVERSITY OF DURHAM

by

COLIN GEORGE BRUCE WILLIAMS, M.Sc. (Birmingham).

Memorandum

The work described in this thesis was carried out at the Londonderry Laboratory for Radiochemistry, University of Durham, between January 1963 and September 1964, and at the University of Kent at Canterbury, between October 1964 and December 1965 under the supervision of Professor G.R. Martin, Professor of Chemistry, University of Kent at Canterbury.

This thesis contains the results of some original research by the author; no part of the material offered has previously been submitted by the candidate for a degree in this, or any other University. When use has been made of the results and conclusions of other authors in relevant investigations, care has always been taken to ensure that the source of information is clearly indicated, unless it is of such a general nature that indication is impracticable.

C.J. Williams.

ABSTRACT

Nuclear reactions induced by 2.3 MeV and 14.7 MeV neutrons in some light and medium weight elements (nitrogen, oxygen, fluorine, phosphorus, calcium, iron, copper and selenium) have been investigated by activation techniques. The cross-sections of (n,p), (n,t), (n,α) (n,2n), (n,n^1) and (n,γ) reactions have been measured, and are discussed with reference to the predictions of the nuclear models.

The 2.3 MeV neutrons were obtained from the $^2H(d,n)^3He$ reaction while those of 14 MeV were obtained from the $^3H(d,n)^4He$ reaction. The deuterons were accelerated on a 200 kV Cockcroft-Walton and a 400 kV S.A.M.E.S. accelerator. A method was developed to determine the absolute flux at both energies using the associated particle method. Recoil particles were counted on a silicon surface barrier detector mounted in the accelerator drift tubes.

Absolute disintegration rates were determined by end-window proportional counters, annular liquid sample Geiger-Müller counters and on various NaI(Tl) γ-ray scintillation spectrometers. These were calibrated using sources which were standardised using $4\pi\beta$ counting and

$4\pi\beta/\gamma$ or β/γ coincidence techniques. The active species resulting from irradiation were separated radiochemically before further identification and determination by counters.

CONTENTS

CHAPTER I

Introduction

Much of the information now available on the structure and characteristics of the atomic nucleus has been obtained by the study of the interaction of particles and photons with particular nuclides. A number of different models have been proposed to account for the observed data. These are the Bohr liquid drop model[1] and the nuclear shell model[2], with the many other variants which have been developed from these. As the amount of experimental data grows these models are suitably modified and become more sophisticated in order to explain the observations. Ideally the behaviour of the atomic nucleus should be calculated from first principles, but so little is known of the nuclear interaction forces and the many - body - problem calculations are so complicated that this is quite impossible at present.

Of the many probes available (neutrons, protons, α- particles and others) the neutron is one of the most useful since it has no nuclear charge, and therefore it does not experience a repulsive Coulomb barrier and can interact with nuclei over the entire range of the available energy (10^{-4} - 10^{10} eV).

In the energy region of interest here (the fast neutron region, which extends from about 1 to 50 MeV) elastic,

inelastic and capture reactions of the types (n,γ), (n,n), $(n,n'\gamma)$, (n,p), (n,α), (n,x), $(n,2n)$, (n,np), $(n,n\alpha)$ and (n,nx) are possible, (together with (n, fission) for heavy elements). A measure of the probability of such an event taking place is expressed as a cross-section for the reaction and is measured in units of 10^{-24} cm^2 which are called barns. The contribution of each process to the total cross-section depends on the neutron energy and the target nucleus. To obtain the complete data which might be useful for theoretical discussion a study should be made of each nuclide over the complete energy range with monoenergetic beams of neutrons.

In the past,large gaps were left in the energy range because of the limits of the available machines but now systematic excitation functions (curves of the variation of cross-section with energy) are being increasingly carried out.

Since 1947 when quantities of tritium produced from the $^{6}Li(n,t)^{4}He$ reaction in nuclear reactors became available, much work has been done at an energy of 14 MeV; neutrons of this energy may be produced using small accelerators (< 200 keV) by using the reaction ^{3}H (d,n) ^{4}He + 17.586 MeV. (DT reaction).

At this energy the three main inelastic processes are

(n,p), (n,α), and (n,2n). These have largely been investigated using the activation method, as in the present work. This involves the bombardment of a sample of some target material with a known flux of neutrons to produce residual nuclei which are radioactive. The activity of the sample is determined by suitable detectors to find the number of radioactive nuclei produced and hence the cross-section for the reaction.

Other methods have been developed in which the recoil particles are detected by using nuclear emulsions, or directly with scintillators, gas or solid state counters. These latter methods can yield more information on the actual reaction process than the activation method since the spatial and energetic distribution of the particles may be determined.

In the case of (n,2n) reactions various multiplication methods have also been used. Here the cross section is calculated from the increase in the number of neutrons counted by a suitable detector when the sample is placed between a neutron source and a detector. In 4π detector methods neutrons from a sample are detected by a suitably loaded bath of liquid. In the 'manganese bath' method[3] neutrons are moderated in a solution of potassium permanganate and react to give the active nuclide ^{56}Mn. The amount of

activity serves as a measure of the number of neutrons produced. In another method neutrons are detected in a large cadmium loaded liquid scintillation counter surrounding the sample.[4]

Two theories for reaction mechanisms have been developed from experimental data. The first, the compound nucleus theory, was developed by Bohr[5] from his liquid drop model of the nucleus. In this the interaction between neighbouring particles is regarded as being very strong and thus the mean free path of a nucleon is very short compared with nuclear dimensions. The incoming particle shares its energy with the entire nucleus so forming the compound nucleus. This may decay through one of a number of different channels, by photon , particle ,or photon and particle emission. Since the process is in two definite stages the compound nucleus is considered to have 'forgotten' its mode of formation and subsequent decay is thus independent of this. The angular distribution of particles emitted should be isotropic.

Weisskopf and Ewing[6] successfully developed this theory into the statistical theory which, to be strictly applicable, requires that the incident energy of the incoming particle should be sufficient to lift the excitation of the compound

nucleus into the energy level continuum which, having many possible states, allows a statistical treatment to be applied.

In the second approach, the direct interaction process, the individual nucleons are considered to interact only very weakly and the nucleon mean free path is of the order of nuclear dimensions (as in the shell model for nuclear structure). Hence the incoming particle reacts with only one or a few nucleons any of which may then be directly emitted. Most of the energy and angular momentum of the incident particle is transferred directly to the emitted particle and therefore an anisotropic distribution (strongly peaked in the forward direction) is obtained. This reaction is thought to take place near the surface of the nucleus since it is here that the chance of the particle escaping before undergoing a second collision is highest.

Together these very different mechanisms account for a wide range of reaction phenomena. In an attempt to reconcile these independent and collective approaches the optical model has been developed. This treats a nuclear reaction in analogy with the propagation of light through a partially absorbing medium. The model involves the interaction of the incoming particle wave with a complex potential. The real part of this gives elastic scattering which

describes a single particle behaviour, while the imaginary part attenuates the incident wave and is directly associated with the mean free path of the incident particle in the nucleus. From the latter, compound nucleus and direct interactions are derived.

The first large experimental survey made in this field using activation techniques was that of Paul and Clarke.[7] These workers measured (n,p), (n, α) and (n,2n) reactions for 57 elements using 14.5 MeV neutrons from the DT reaction. The resultant activities were determined by β -particle and γ-ray detection, reliance being placed on half life determinations to analyse decay curves.

Comparison was made with the statistical compound nucleus theory of Weisskopf and Ewing[6] which has been outlined above; their values below a mass of $A \simeq 70$ were found to be within a factor of 9 but above $A \simeq 70$ the discrepancy rose to up to a factor of 100 (1600 for ^{208}Pb). Paul and Clarke suggested a direct interaction mechanism to explain the disagreement between experimental and theoretical values.

Later, more accurate work than that of Paul and Clarke, such as that by Blosser et al.[8,9] and Levkovskii et al.[10] who used radiochemical techniques to isolate the isotope under investigation and more quantitative counting techniques,

revealed that the discrepancy between experiment and theory at the heavier masses was not as large as that found originally. However, from purely compound nucleus considerations, the difference was still significant. Brown and Muirhead[11] calculated contributions from the compound nucleus model and direct interaction model and showed that the sum of these for (n,p) reactions agreed within a factor of 3 with most of the later measurements.

Since 1960 a considerable amount of work has been carried out on fast neutron induced reactions. Compilations of data have been made by a number of workers including (at 14 MeV) Gardner[12] for (n,p) reactions, Chatterjee[13,14] for (n,p), (n,d), (n,t) and (n,α) reactions, Bormann[15] for (n,2n) reactions and Neuert and Pollehn.[16] Liskien and Paulsen[17] have collected and reviewed single points and excitation functions for (n,p), (n,α) and (n,2n) reactions in the energy range 1 to 20 MeV.

These lists show disparities in reported values much larger than the reported errors and also that many gaps exist in the data. Discrepancies may arise in neutron flux determinations and absolute counting of individual activities; also much of the work has been carried out without chemical isolation of reaction products. Generally the nuclides were distinguished by half life and β and γ-energy

determinations. Many measurements have been made relative to reference reactions which themselves may not have been accurately determined. Excitation functions may be in error if they have been normalised to a single point determined by some other worker.

Nevertheless, definite trends have been noticed in the value of cross-sections. Levkovskii[10], and later, Gardner[12], pointed out that for (n,p) and (n,α) cross-sections at 14 MeV the cross-section of each succeeding isotope of any element was about one half the value of the preceeding isotope (Levkovskii trend). Gardner also noticed that a semi-log plot of (n,p) cross-section values against mass number seemed to lie on parallel, equally spaced, straight lines, one for each element. He derived a semi-empirical equation to predict the (n,p) cross section for any isotope from the statistical model. The results agree with observation in a number of cases.

Chatterjee[18,19] plotted (n,p) and (n,α) cross-section values against proton and neutron number of the residual nuclei and showed the existence of minima in the cross-sections in all the major proton shell closure positions and subsidiary minima in proton subshell closure regions. The minima due to neutron shell closures were less obvious. The shell theory also suggests that the presence of unpaired nucleons might affect the values of the cross-sections; this

was noted by Gardner[20,21] and Chatterjee.[18] A similar analysis has been carried out by Bormann[15] for (n,2n) reaction cross-sections; the effects of closed neutron shells were observed.

More recently with the higher fluxes available from modern machines attempts have been made to detect, and estimate the cross-sections of the rarer reactions such as (n,t), (n,^{3}He) and (n, α n) which have cross-sections in general of a millibarn or less. Only a few cases of these can be measured by the activation method and then in most cases only upper limits have been quoted. Heinrich and Tanner[22] and Poularikos and Gardner[23] on the other hand have both measured (n,t) cross sections by counting the resulting tritium.

The purpose of this work, therefore, has been to improve on the accuracy of previous determinations by taking greater care with neutron flux determination and absolute counting techniques; chemical separations were carried out when necessary. Some cross-sections have also been measured which do not appear to have been previously reported.

The cross-sections for two widely used reference reactions have been determined by the associated particle method (this is described later). Measurements were also made on two (n,t) reactions for which only upper limits had been previously reported.

An attempt was made to investigate (n, particle) cross-sections at 2.5 MeV neutron energy using neutrons from the ^{2}H (d,n) ^{3}He reaction. Unfortunately the conditions necessary for good energy resolution result in a very low neutron flux and the small cross-sections generally found in this energy region made the induced activities too weak to measure with present equipment.

CHAPTER 2

Part 1. General methods of neutron production and flux measurement.

The value of a nuclear reaction cross-section varies, often very rapidly, with energy of the bombarding neutrons and therefore the study and measurement of nuclear reactions requires a source of neutrons as nearly monochromatic as possible.

The simplest neutron sources are the radioactive type in which neutrons are produced by (α, n) or (γ,n) processes. In the first an α-emitter such as ^{226}Ra or ^{210}Po is intimately mixed with light elements such as beryllium or boron. The neutron spectra from these sources are complex and neutrons with energy up to 12 MeV are present. The second type are monoenergetic having neutron energies up to about 1 MeV; they are usually formed by surrounding an intense γ-source by beryllium or deuterium. Both of these types have been displaced from use to some extent by other methods which give a higher neutron intensity; they are retained since they are excellent neutron flux standards, have a constant output, and are very compact.

Nuclear reactors supply very high fluxes of neutrons; up to 10^{14}n $cm^{-2}s^{-1}$ over the fission spectrum. These can be

thermalised in a thermal column or certain energy regions may be selected using crystal diffraction (0.01 - 10 eV) or slow (10^{-4} - 0.2 eV) and fast (1 eV - 10 keV) chopper techniques.

Intense, almost monoenergetic,beams of fast neutrons can be produced from accelerators using one of the following reactions:

^{3}H (p,n) ^{3}He	Q = - 0.764 MeV
^{7}Li (p,n) ^{7}Be	Q = - 1.645 MeV
^{2}H (d,n) ^{3}He	Q = + 3.266 MeV
^{3}H (d,n) ^{4}He	Q = +17.586 MeV

The energy resolution of the neutrons produced by this method is affected by the factors described below.

Any energy spread of the primary beam of the accelerator will cause a corresponding variation in the energy of the neutrons produced. Linear accelerators (Cockcroft-Walton and Van der Graaff types) give more nearly monochromatic beams than cyclotrons. The number of molecular ions (such as $^{2}H_{2}^{+}$) in the primary beam must be reduced as these will give neutrons of different energy to those produced by protons and deuterons. A similar, but larger, effect is the loss of energy of the primary beam in the target; neutrons can possibly be produced by particles from the maximum to

minimum energy. The relative effect of these is reduced the higher the Q value of the neutron producing reaction and the lower the energy of the primary beam.

Geometry factors are also usually far from ideal; the neutrons are produced from a non-point source, and the sample subtends a large angle at the source to take advantage of the neutron flux available. Samples and detectors are often placed at 90° to the incident beam where variation of energy with angle is greatest but where the actual energy spread is a minimum.

Neutrons are scattered and degraded in energy by surrounding supporting materials and therefore these should be kept to a minimum and the target placed as far from walls as possible. Secondary neutrons may be produced by the primary beam striking accelerator components and contaminants of the target. With low energy primary beams this is a small effect except in the cases of deuterium build up in a target bombarded by deuterons; this will give rise to 3 MeV neutrons.

The ^{3}H (p,n) ^{3}He reaction is used to produce neutrons up to an energy of 6 MeV and has largely displaced the ^{7}Li (p,n) ^{7}Be reaction for this energy range since the latter has two groups of neutrons; the second arises from an excited state of ^{7}Be. Just above its threshold (1.019 MeV)

the ^{3}H (p,n) ^{3}He reaction also has a second group of neutrons caused by centre of mass motion at the compound nucleus.

The ^{3}H (d,n)^{4}He and ^{2}H (d,n) ^{3}He reactions are those most widely used since they have large positive Q values and are thus available to low energy accelerators (150 kV). The first is used in the range 10 to 40 MeV and the second from 1 to 14 MeV.

Deuterium and tritium targets may be either gaseous or may be absorbed into a thin layer of titanium. Heavy ice, D_3PO_4 and NaOD have also been used for deuterium.

Above 50 MeV, neutrons may be produced by stripping high energy deuterons in light element targets such as beryllium.

Absolute determination of neutron flux

Since neutrons cannot be detected directly, fast neutron fluxes are usually determined by one of the following methods; the proton recoil method, the associated particle method, or by the use of relative or secondary methods.

In the proton recoil method a thin hydrogenous radiator is placed in the neutron beam and the recoiling protons counted by a variety of methods. These include proton recoil telescopes and plastic scintillators. At the energies of interest here collisions between neutrons and protons

are mainly elastic and therefore the scattering cross section can be determined by a transmission method.

By arranging the sample and monitor to subtend known solid angles at the source the neutron flux through the sample may be deduced from the proton count using known neutron angular distributions. The method assumes a fixed point source and also (since the solid angles must be accurately determined) a good geometrical arrangement with large sample - target and monitor - target distances. This also reduces the effect of a finite source size and finite sample thickness.

In the associated particle method the secondary recoil particle from the nuclear reaction producing the neutrons is counted within a known solid angle from which the number of neutrons passing through the sample, also subtending a known solid angle, may be calculated (since neutron and recoil particle distributions are known). Neutron fluxes at 14 MeV have been determined (by counting 3 MeV recoil α-particles from the ^{3}H (d,n) ^{4}He reaction) by Paul and Clarke[7] (using a proportional counter) and Cevolani and Petralia[24] (using a semi-conductor counter). A variation of this method has been developed in this laboratory by Hemingway et al[25] in which α-particles from the ^{3}H (d,n) ^{4}He reaction are trapped in aluminium foils which are then dissolved releasing

the helium, the volume of which is determined ($\sim 10^{-7}$ ml). As in the proton recoil method the sample must be irradiated in conditions of good geometry to minimise errors due to the finite size of the neutron source and the thickness of the sample.

The relative and secondary methods are most widely used in the determination of fluxes. The cross-section of almost any neutron induced reaction, once measured using one of the above methods, can provide a secondary means of measuring fluxes. Relative flux measurements can always be made using a neutron detector of which the efficiency is not known.

The cross-sections most widely used in the 14 MeV region as monitors are:

$^{56}Fe\ (n,p)\ ^{56}Mn$ $\quad (t_{\frac{1}{2}} = 155\ m)$

$^{63}Cu\ (n,2n)^{62}Cu$ $\quad (t_{\frac{1}{2}} = 10\ m)$

$^{27}Al\ (n,\alpha)^{24}Na$ $\quad (t_{\frac{1}{2}} = 14.85\ h)$

These materials may be irradiated with the sample as a sandwich with monitor foils on either side of a sample foil or as a homogeneous mixture when the monitor and sample are in powder or granular form. The iron monitor lends itself to the latter method since iron may be readily separated from a bulk sample by magnetic means. The homogeneous method

allows the sample to be irradiated close up to the neutron source thus making full use of the available flux which is essential in the determination of reaction cross-sections which are small or give rise to long lived products.

Relative counter methods are used most widely at the low energy end of the fast neutron range where neutron cross-sections are normally low. Of the wide variety of counters the fission counter and the Li^6I (Eu) scintillation crystal have been most frequently used.

In the first, the sample is irradiated in close proximity to a layer of ^{235}U on the inside surface of an ionisation chamber and the flux obtained from the number of fission fragments thus counted. This method has been used by Johnsrud et al.[26] up to an energy of 4 MeV; the counter used was calibrated using thermal neutrons. Barry[27] has also used this method from 1.6 to 14.7 MeV the calibration being made by the associated particle method at 14.1 MeV.

In the second, a thin crystal of ^6LiI(Eu) has been used to count α-scintillations from the ^6Li (n,t) ^4He reaction; the cross section was measured by the associated particle method. This method has been developed by Kern and Kreger[28] over the range of 2 to 20 MeV.

Part 2. Actual methods used for neutron production and flux measurement

The high fluxes of almost monoenergetic neutrons used in this work were produced using the reactions

$$^{3}H\ (d,n)\ ^{4}He \quad + \quad 17.586\ MeV \qquad 1$$

for neutrons of 14 MeV energy, and

$$^{2}H\ (d,n)\ ^{3}He \quad + \quad 3.266\ MeV \qquad 2$$

for 3 MeV energy. Deuterons of several hundred keV energy were incident on targets of titanium tritide or titanium deuteride respectively.

The excitation function of reaction (1) rises to a broad resonance of about 5 barns at 110 keV incident deuteron energy, and up to an energy of about 500 keV the reaction may be regarded as isotropic in the centre of mass co-ordinates.[29] Since neutrons are produced by deuterons of energy from zero to the maximum, the optimum bombarding energy is a little above 110 keV, because, although a greater neutron yield is obtained with an increase in deuteron energy, as more of the target becomes available the energy spread of the neutrons produced in the forward direction also increases.

For the second reaction the excitation function increases smoothly with energy but has a value of only 70 mb[30] at 400 keV and therefore to obtain a reasonable neutron yield

the maximum available bombarding energy must be used. The reaction is also anisotropic being peaked forward and back in the centre of mass system. Graphs of the variation of neutron energy with laboratory angle for various incident deuteron energies are shown in Fig. 1.

Suitable beams of deuterons were produced at Durham with a 200 kV Cockcroft-Walton accelerator built by Professor G.R. and Mrs. Martin,[31] and at Canterbury with a S.A.M.E.S. (Société Anonyme de Machines Électrostatiques) 400 kV 'T' type accelerator.

a) Durham Machine

A schematic arrangement of the Durham machine is shown in Fig. 2. Power from the mains supply (250 V, 50 c/s) is fed via a 100 kV peak transformer to the voltage quadrupling circuit and thence to the accelerating tube. Deuterons are extracted by a voltage of several kV from a radio-frequency ion source and then accelerated through 40 kV at the focusing gap. They are then further accelerated by two accelerating gaps and finally strike the target block at the end of the drift tube. This machine was used to produce 14 MeV neutrons the deuterons being accelerated to 160 keV; with a beam current of 200 μA yields of up to several times 10^9 neutrons per second were produced.

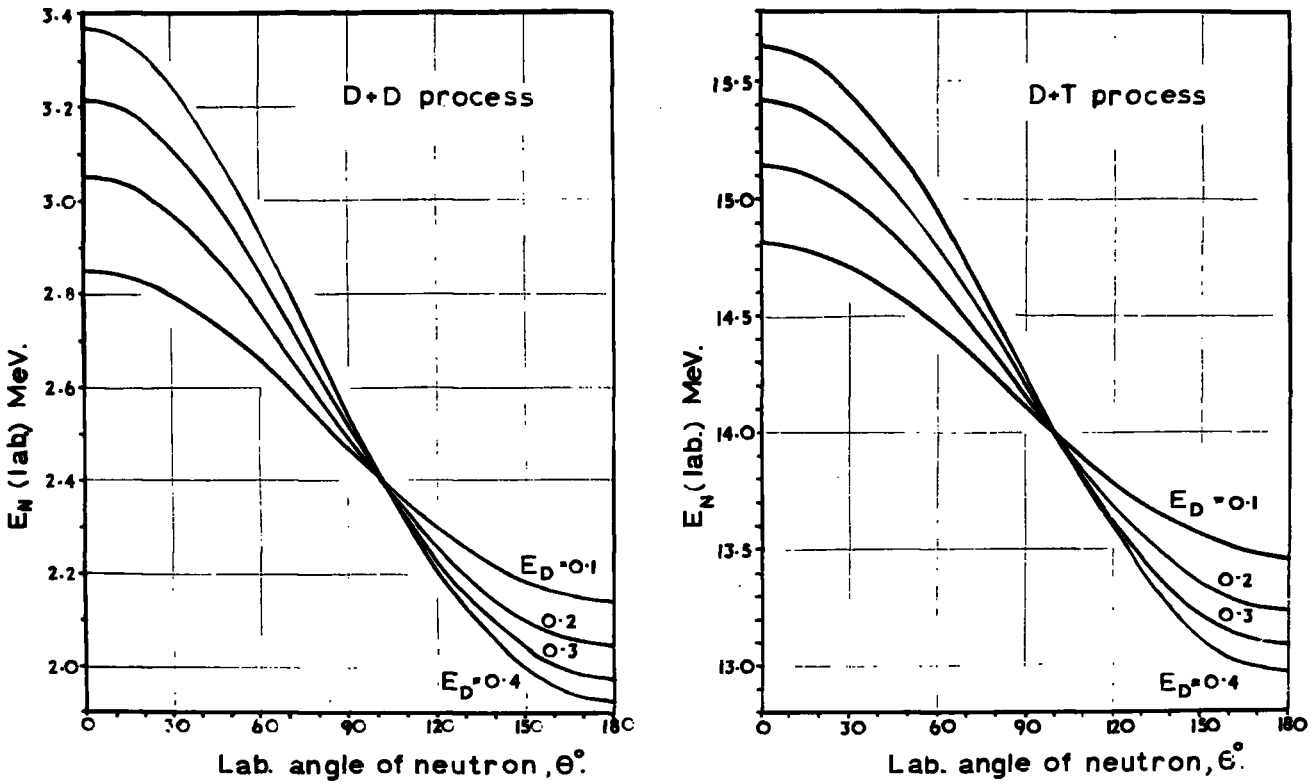

Fig.1. Neutron energy as a function of angle of emission and deuteron energy.

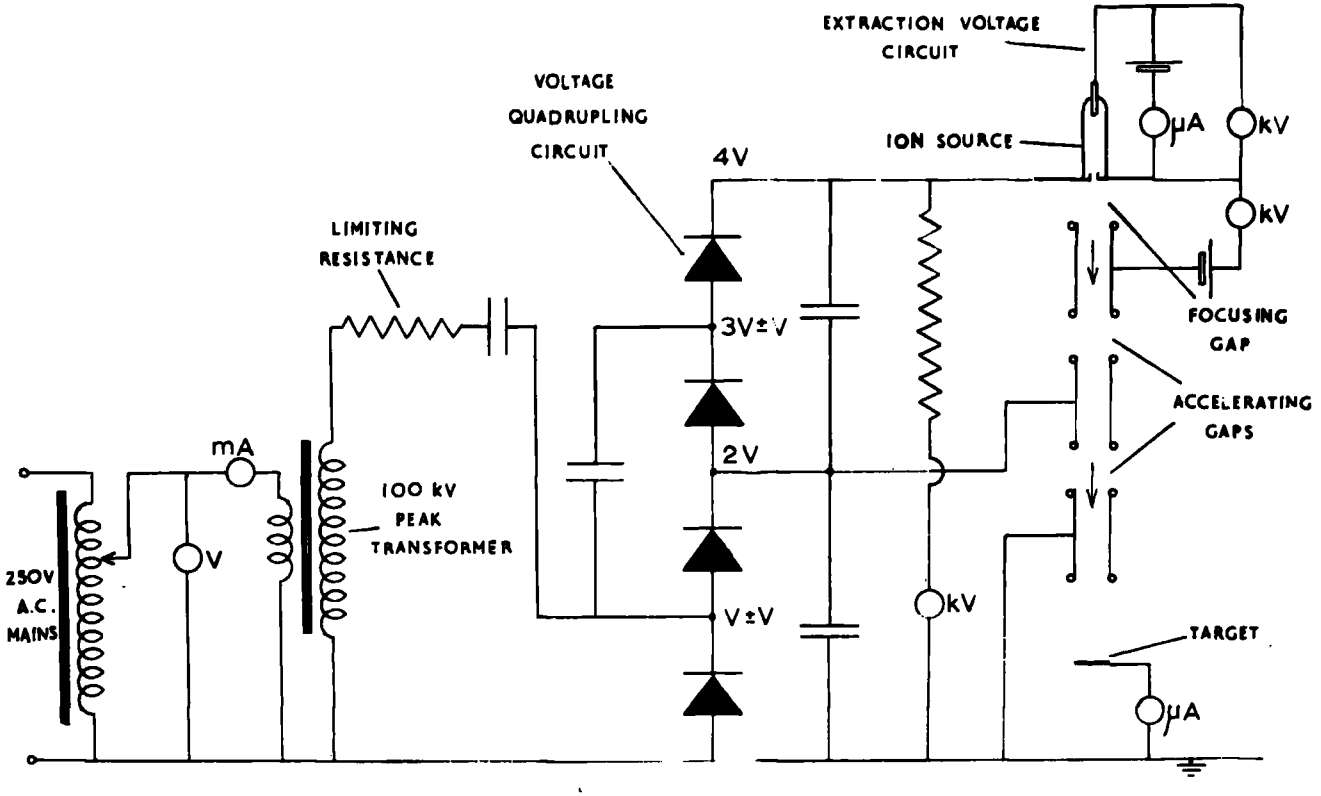

Fig.2.Schematic arrangement of the Durham Cockcroft-Walton accelerator.

b) S.A.M.E.S. Machine.

The S.A.M.E.S. machine is depicted in Figs. 3 and 4. Fig. 3 shows the principle of the electrostatic generator which is an 'insulating carrier' type, converting mechanical energy directly into d.c. high voltage electrical energy by the transfer of charge against the electric field.

A hollow cylinder made of insulating material, the rotor, is driven by an electric motor to effect the transfer of the charges. These are deposited or withdrawn from the rotor by thin metallic blades, ionisers, placed in close proximity to the outer surface of the rotor. Curved plates, inductors, are placed near the inner surface of the roter which induce a strong electric field in the sharp edge of the ioniser. To reduce any local concentrations of the electric field a glass (10^{12} ohm-cm) cylinder is placed between the inductors and the rotor. The complete sealed unit, generator and motor, is filled with hydrogen at 10 - 25 atmospheres which has excellent insulation properties combined with a high ion mobility.

The charging ioniser is set at a high negative voltage, up to -30kV, by the exciter unit which causes positively charged ions to flow from earth to be deposited on the rotor. These are then transferred against a tangential electric field to the discharging ioniser and thence to the high voltage

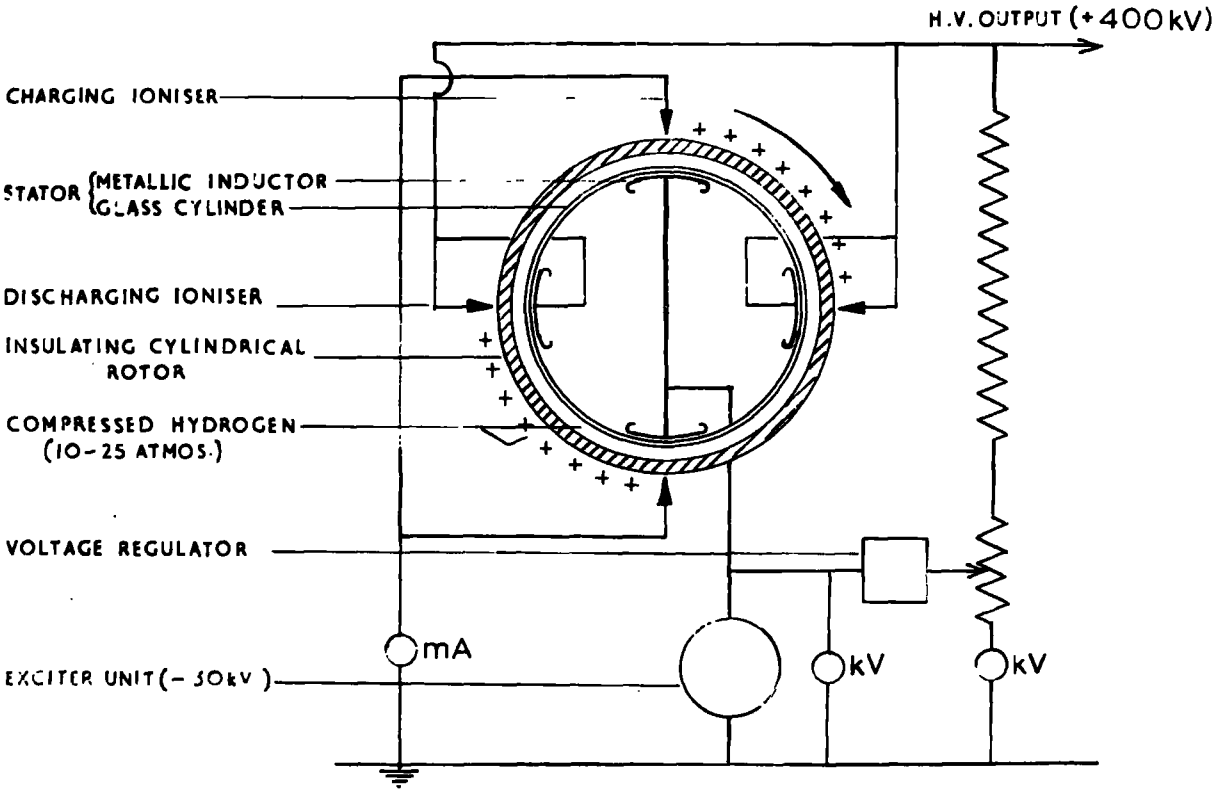

Fig.3. Circuit diagram of S.A.M.E.S. electrostatic generator.

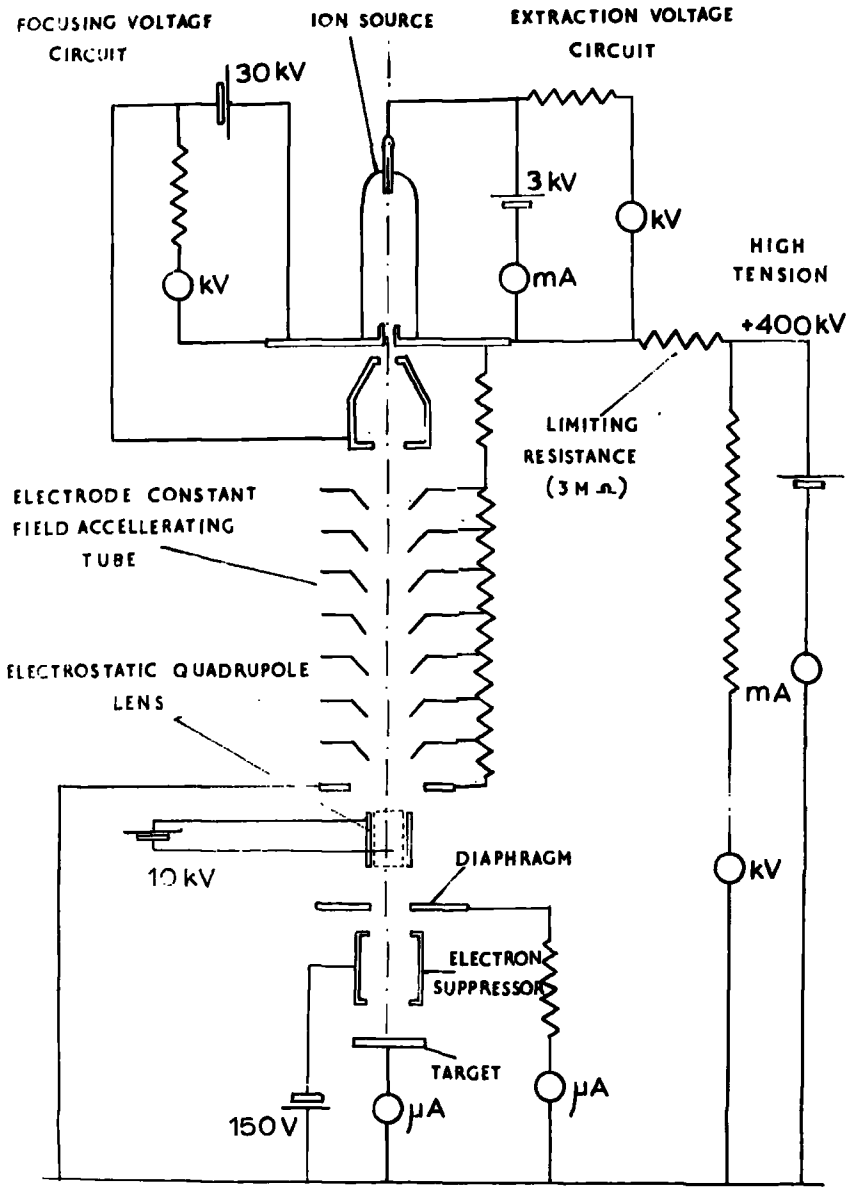

Fig.4.Schematic arrangement of the S.A.M.E.S.accelerator.

terminal of the accelerator.

The generator voltage is regulated by means of a feed-back loop by the output voltage of the excitation unit such that the generator current, which is proportional to the density of the ions deposited on the rotor, is equal to the current required by the accelerator thus maintaining a constant terminal voltage. A variation of output voltage of less than 1% is quoted by S.A.M.E.S. for our medium stability machine.

Deuterons from the R.F. ion source are again extracted through a narrow canal by a 3kV potential, focussed, and then accelerated down the eight gap constant field tube. They are further focussed by an electrostatic quadrupole lens before passing down the drift tube to the target block. At the centre of the drift tube is a diaphragm with a 2.5 cm diameter aperture. The ratio of the measured beam current striking this to that striking the target block serves as an indication of the focussing of the beam. A second diaphragm with a larger aperture placed immediately behind the first and set at -150v acts as a suppressor to the secondary electron current from the target.

The minimum accelerating voltage at which the machine has been found to run satisfactorarily is 220kV. With this setting and a beam current of 1mA a yield of up to

5×10^{10} 14 MeV neutrons per second has been achieved. A yield of 7×10^{8} neutrons per second has been obtained for 3 MeV neutrons using the full 400 kV acceleration and 1 mA beam current.

c) Targets.

The titanium tritide (TRT5) and deuteride (DBT6) target discs were obtained from the Radiochemical Centre, Amersham. The titanium layer of about 1mg cm^{-2} thickness is obtained on a thin copper backing disc of 2.5 cm diameter. When loaded with tritium or deuterium, an atomic ratio (H/Ti) equal to or greater than one is obtained; this corresponds to 0.23 ml cm^{-2} or 0.6 curies cm^{-2} for tritium. For convenience, each disc was divided into four segments which were bombarded separately. The segments were soldered on to water cooled metal blocks to keep the temperature below 240°C during an irradiation; above this temperature titanium hydride dissociates.[32]

The various types of target assembly used are illustrated in Figs. 5, 6, 7 and 8. The Durham target blocks were of brass and were fitted with a molybdenum shutter with which the deuteron beam could be stopped. For the S.A.M.E.S. machine a power dissipation of 200 - 400 watts was involved and therefore the target blocks were made from copper and the cooling water arranged to flow close to the segment. The separation between the segment and irradiated sample was kept

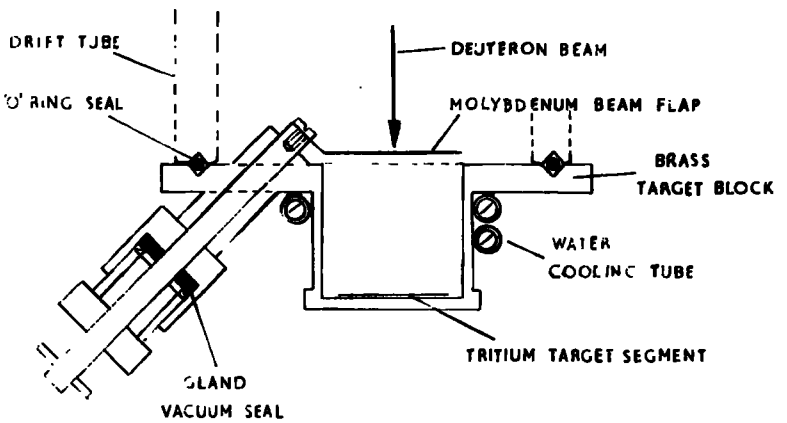

Fig.5.Durham target block.

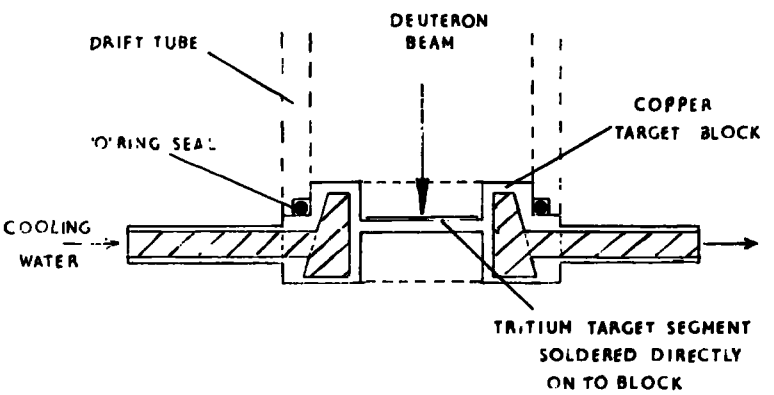

Fig.6.Canterbury D,T target block.

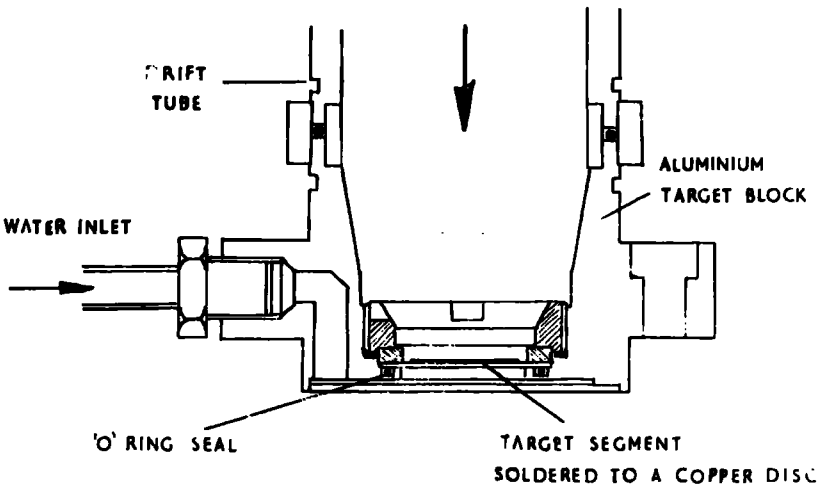

Fig.7. S.A.M.E.S. target block used for D,D irradiations.

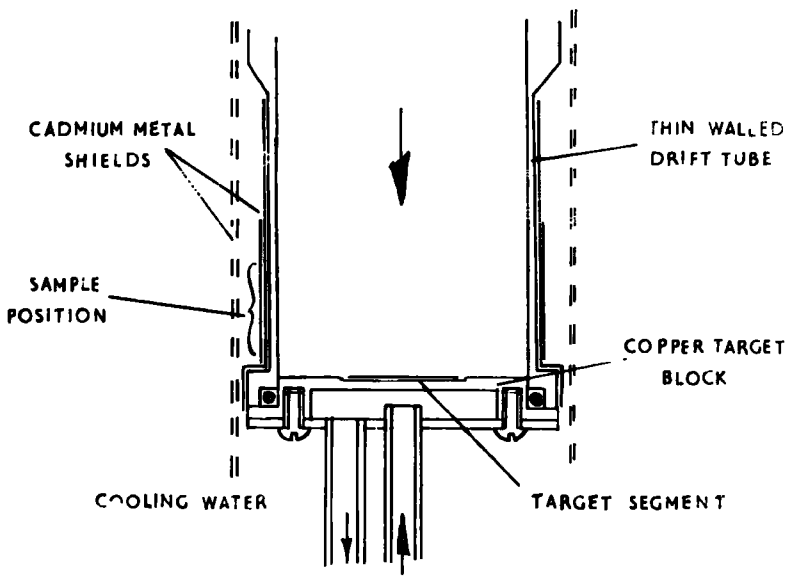

Fig.8. 90° target block.

down to 2 mm to enable full use to be made of the neutron flux available. In S.A.M.E.S. own target design cooling water is passed across the back of the target disc which increases the segment - sample separation to 5 mm; the amount of scattering material is also increased. The target shown in Fig. 8 was used to irradiate samples between 95° and 145° with 3 MeV neutrons. Here the drift tube wall was made thin to reduce the amount of scattering material near the samples.

The target blocks were all sited at the centre of the target chamber as far away from the concrete walls and other scattering materials as possible. Such materials increase the flux of scattered, degraded neutrons in the vicinity of the sample.

d) Neutron Flux Measurement.

The absolute neutron fluxes produced by both reactions have been measured using the associated particle technique. For the $T(d,n)^4He$ reaction α-particles were counted whilst for the $D(d,n)^3He$ reaction, protons from the other branch of the D + D process, the D(d,p) reaction, were counted. The branching ratio of this process has been measured by Preston et al.[30] and found to be approximately one at these energies.

A silicon semiconductor detector was mounted in the drift tube in such a way that the whole target area was 'seen' by the effective counting area of the silicon. Charged particles

from the target in an accurately measured solid angle at 175° to the incident deuteron beam were measured.

The counter used was an ORTEC Model No. SBDJ007 - 60 which is of the silicon surface barrier type described by Dernaley and Whitehead[33]. A cross sectional view of the device is shown in Fig. 11. The sensitive surface is coated with a thin layer of gold. The circular silicon wafer is mounted in a ceramic ring of which the back and front surfaces are metallised. The front surface of this insulator is grounded to the metal case whilst the rear surface is connected to the centre electrode of a standard Microdot minature connector which serves as the signal output and bias voltage connection.

The counter is made of n - type silicon having a resistivity of 900 ohm-cm and an active surface of 7 mm^2. At the maximum applied voltage of 50v the depletion depth is 110 microns which will totally absorb the energy of a 14.5 MeV α -particle, a 3.43 MeV proton or a 0.153 MeV β -particle. An energy resolution of 0.7% is claimed by the manufacturers for 5.5 MeV α-particles fromathin ^{241}Am source in vacuo.

The assembly used to mount the counter in the drift tube is shown in Fig. 10. After the rapid deterioration in performance experienced with unprotected solid state detectors made in the laboratory it was considered advisable

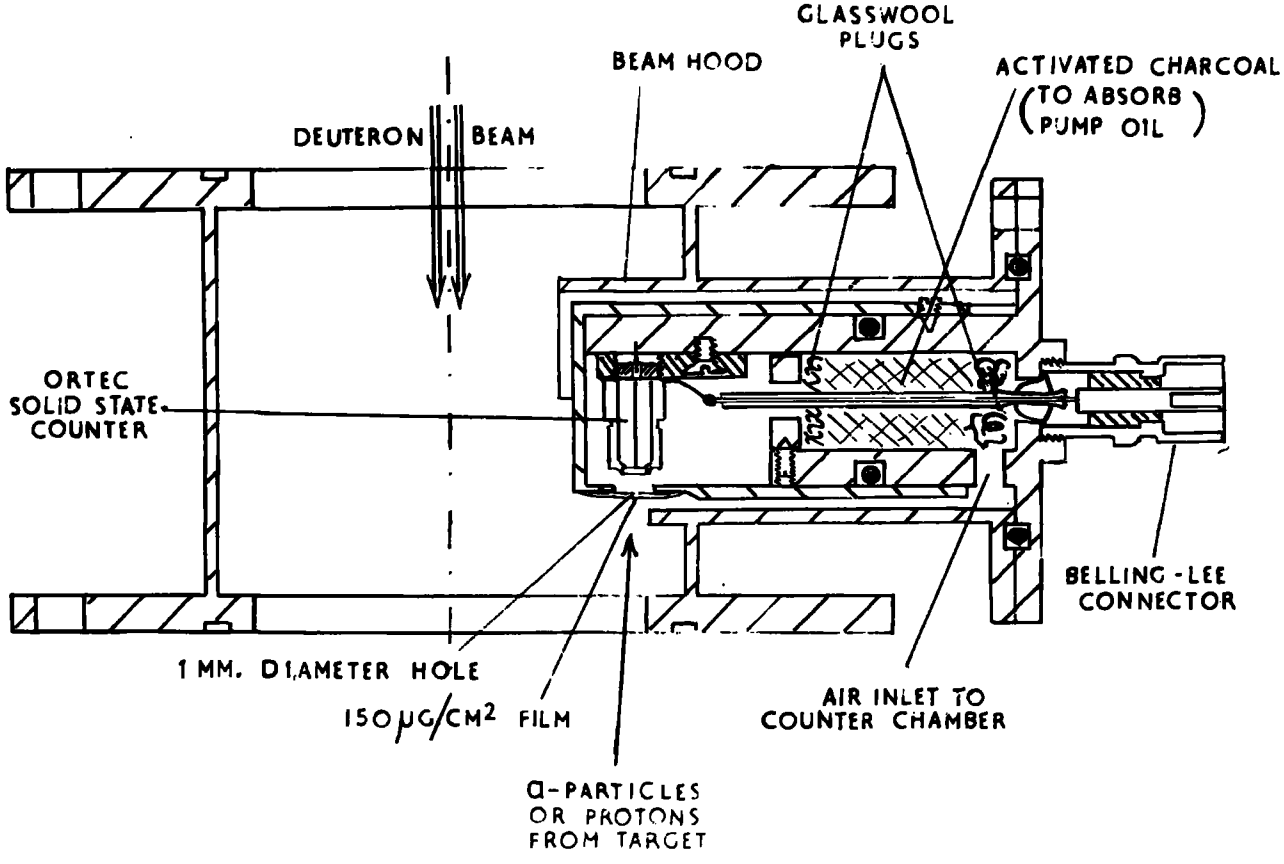

Fig.10. Ortec counter mount in accelerator drift tube.

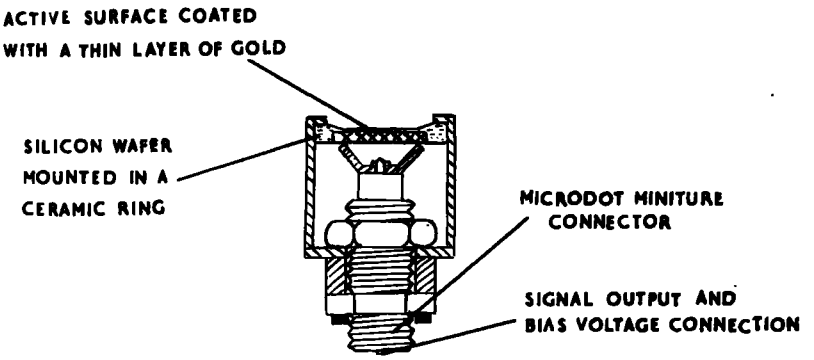

Fig.11. Cross section through ORTEC detector.

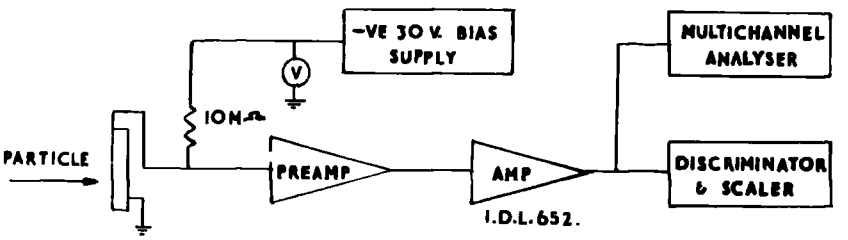

Fig.12. Block diagram of counting circuit.

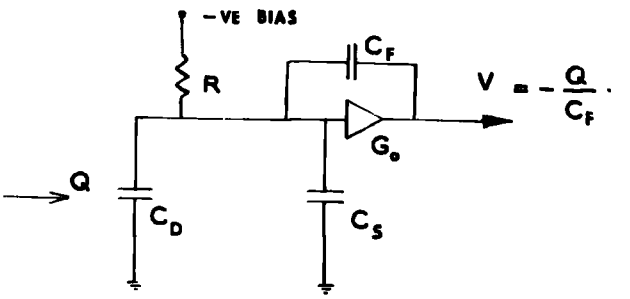

Fig.13. Capacitative feedback loop of the preamplifier.

to protect the ORTEC detector from vacuum pump oil in the accelerator. This was achieved by covering the defining aperture to the counter with either 1mg cm^{-2} Melinex or 0.15 mg cm^{-2} VYNS windows, and also by placing a few grams of activated charcoal at the entrance to the counter cell. The defining aperture was a 1 mm diameter hole drilled in 20 mg cm^{-2} polystyrene sheet; the diameter was accurately determined by comparison with a ruled graticule on a microscope. The window and aperture foil were glued to a flat area on the brass cover using 'Evostick' adhesive. The distance from the counter aperture to the target block was about 50 cm for the Durham machine and 70 cm for the S.A.M.E.S. machine; these distances gave solid angles subtended at the counter of 4×10^{-5} steradians and 2×10^{-5} steradians respectively.

The block diagram of the counter circuit is shown in Fig. 12. For solid state counters voltage amplification of the signal has the disadvantage that the dependence of the detector capacity, C_D, on the applied bias voltage leads to a corresponding bias dependence of the output signal voltage. If the charge collected is Q, and the total capacity, C_T, equal to the sum of C_D and C_S (the stray capacity) the voltage signal is Q/C_T. In the charge sensitive preamplifier with a capacitive feedback loop (see Fig. 13) the output pulse size

is independent of the bias. If G_O is the open loop amplifier voltage gain and C_F the feed back capacitance, the output voltage is now - Q/C_F which is independent of C_T provided $G_O C_F$ is much more than C_T. In general G_O is of the order of 1000 while C_S and C_D have a value of several pF. A low noise charge sensitive preamplifier was built to the design suggested by Chase et al.[34]. This circuit employs 5 R.C.A. type 7586 Nuvistor triodes which have a low tube capacity and good anti-microphonic qualities. A screened cascode first stage is followed by a long-tailed-pair whilst the output is driven by a cathode follower. The bias voltage was supplied by two 30v Everready B123 batteries connected in series through a potentiometer to the counter.

The counter has been operated at main amplifier settings of 0 - 4 dB with equal integration and differentiation time constants of 3 μs and scaler paralysis settings of 10 and 50 μ s; the output signal is then of the order of 20v in amplitude. The applied bias was adjusted between 0 and 30v depending on the particles being counted according to the particle range/bias relationships obtained from the nomogram of Blankenship[35]. Fig. 14 shows a graph of the variation of pulse height with bias for 0.8 MeV α-particles or 2.5 MeV protons obtained from the D,T and D,D reaction respectively after passing through the 1 mg cm^{-2} window. As can be seen the α-particle

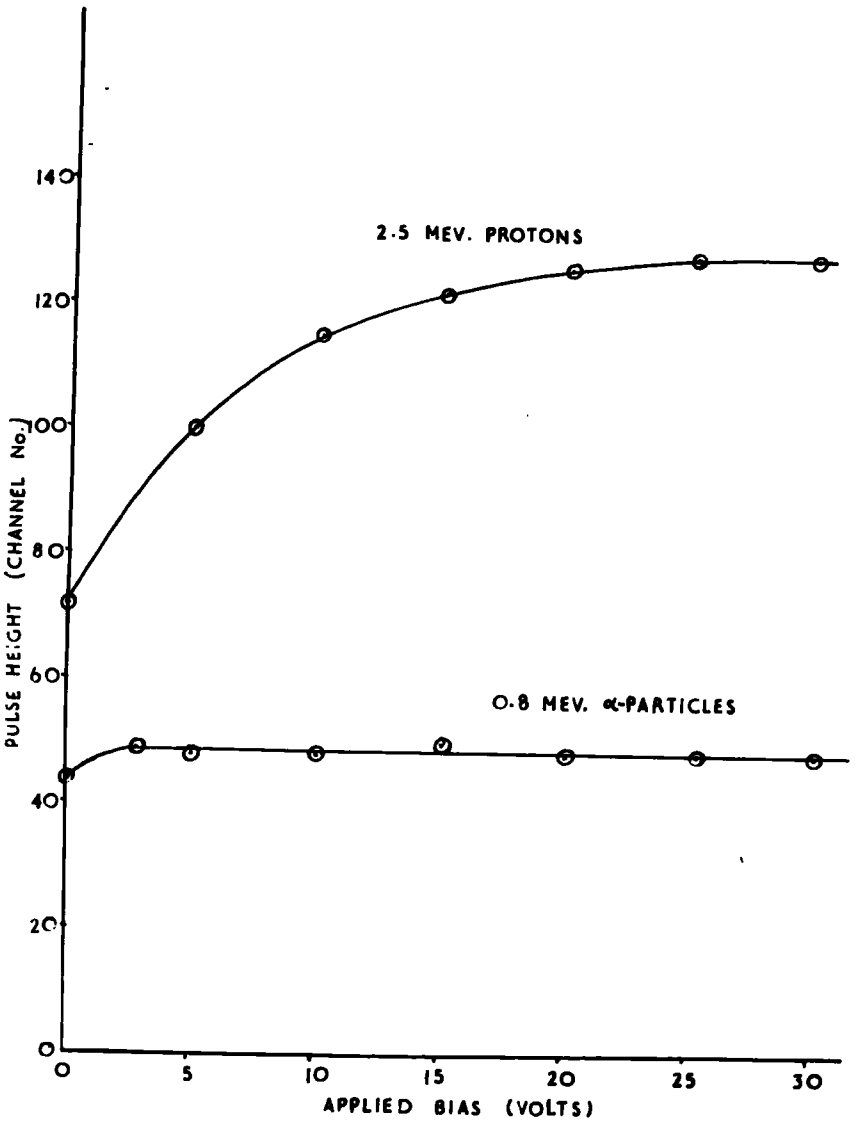

Fig.14.Ortec counter, variation of pulse height with applied bias.

pulse height rapidly saturates at 3v bias whilst the longer range of the proton requires a bias of 30v for saturation.

A resolution of 1.22% was obtained for 5.31 MeV α-particles from an uncollimated weightless source of $^{210}P_o$ counted in a vacuum through an 0.15 mg cm^{-2} VYNS window. Fig. 15 and 16 show typical spectra obtained with the counter on the accelerators. Fig. 15 shows the proton spectrum from the D,D reaction (bias 25v) the protons passing through a 1 mg cm^{-2} Melinex window. 0.6 MeV tritons from this reaction and 0.3 MeV ^3He particles from the accompanying $D(d,n)^3He$ reaction have insufficient energy to penetrate this window. The high energy tail of the proton peak is produced by protons from the reaction induced by deuterons of lower energy reacting deep in the target. Fig. 16 a and b show α-spectra from the D,T reaction. The first was taken with a bias of 25v and a 1 mg cm^{-2} window and the second with a bias of 2v and an 0.15 mg cm^{-2} window. In both cases the α-peak has a smaller peak on the high energy side caused by D_2^+ ions inducing the D,T reaction. These spectra also show the proton peak from the D,D reaction caused by the build up of deuterium in the target. With a 1 mg cm^{-2} window the proton peak is always above the α-peak even at zero applied bias while with the thinner window the pulse height of the protons only approaches that of the α-peak

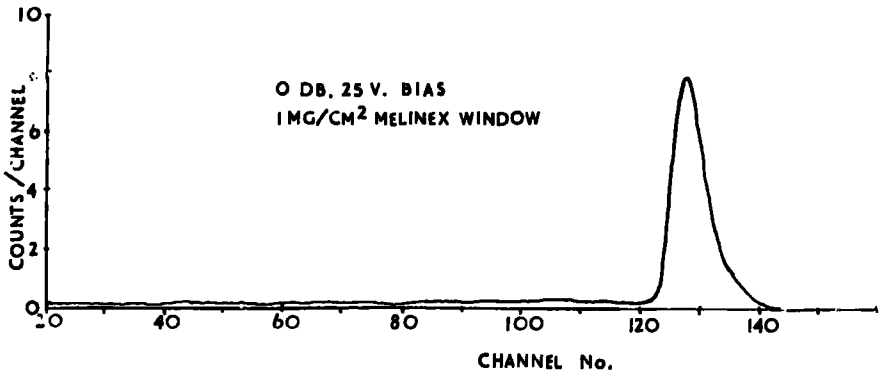

Fig.15. Proton spectrum , (D(d,p)T).

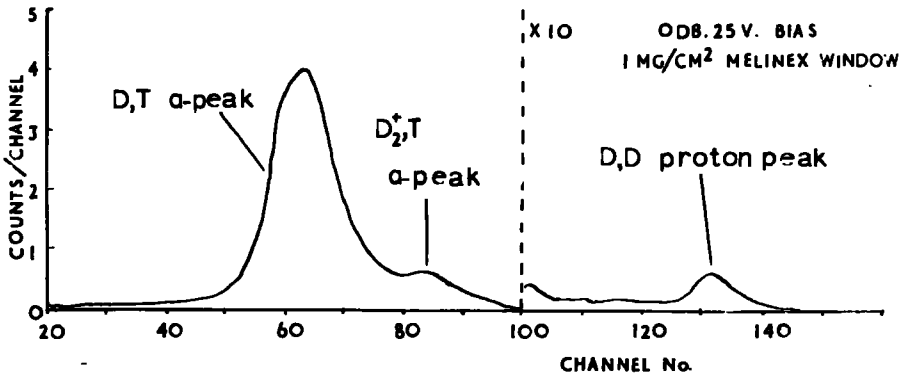

Fig.16a. α-particle spectrum, (T (d,n) α).

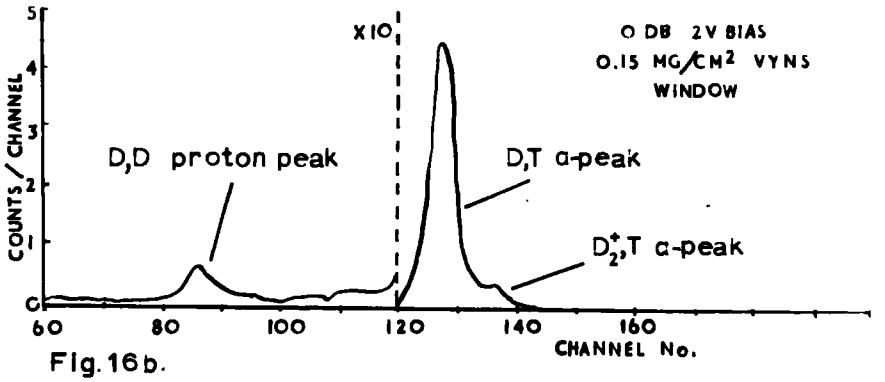

Fig. 16b.

at 30v bias. For measurements of neutrons from the D,T reaction a thin window and low bias setting were therefore used; the discriminator level could then be set above the proton peak.

When the solid state counter was not used the variation of neutron flux was monitored using a proton recoil scintillation counter placed in the target chamber. The variation of neutron flux during an irradiation must be known, for it is necessary to make corrections for the rate of formation and decay of the various activities induced during the irradiation. The ORTEC or scintillator monitor counts were recorded at time intervals short compared with the half-life of the shortest lived species under consideration.

c) Performance of targets

The yield of neutrons from tritium targets was found to fall with time as the tritium was lost from the heated surface or displaced by deuterium. It is hoped that this drop in yield may be reduced by the use of erbium tritide targets suggested by Redstone and Rowland[36] and Large and Hill[37] at S.E.R.L.. These have a higher maximum operating temperature (540°C) than that of the titanium tritide targets. As a target ages the accumulation of deuterium will cause the proportion of lower energy neutrons to the total number

of neutrons to increase. Many of the reactions studied at 14 MeV have thresholds above 3 MeV and therefore D,D neutrons did not often present a problem.

The neutron yield from a fresh TiD target was found to drop initially before levelling off at about half the initial value after two hours bombardment at 500 μA. It was found that an improvement in yield was obtained by rubbing the target surface gently with tissue; this suggested that the fall was caused to some extent by surface contamination.

Before leaving Durham the possibility of using self loading targets for D,D neutron production was investigated. Discs of copper, zinc, brass, gold plated copper and gold-palladium-gold plated copper were soldered in turn on to the accelerator target holder with Wood's metal. Each disc was bombarded at 165 keV with a beam current of 100 μA for about two hours. The production of 3 MeV neutrons was monitored by counting protons as already described. It was found that the yield at saturation and the time to reach saturation varied from material to material. The values obtained are shown in Table 1.

Table 1.

Target material	n/sec/ μA	Time to reach saturation (min)
Au	4.0×10^4	50
Au/Pd/Au	3.7	50
Cu	1.2	90
Zn	3.7	30
Brass	2.9	30
(DTi)	(2×10^5)	—

The value for deuterated titanium (DTi) is an estimate from work carried out at Canterbury. The results agree with those obtained by Fiebiger[38] which show that gold gives the highest yield for metals that have not been previously degassed but that this was only about 50% of that from a DTi target.

Part 3. Counting equipment used in the determination of activities.

The absolute disintegration rate of sources of radioactive nuclides are normally determined by $4\pi\beta$, $2\pi\beta$ or various coincidence counting methods. These techniques often require complex procedures which do not lend themselves to routine counting. It is usual therefore to use these primary methods to standardise a series of sources which can then be used to calibrate counters which are more convenient to use.

This method has been employed here; the counters used included end-window gas-flow proportional counters, a liquid sample Geiger Müller counter and various thallium activated sodium iodide (NaI(Tl)) crystal γ -ray scintillation detectors. Sources for the calibration were standardised using $4\pi\beta$ counting or $4\pi\beta/\gamma$ coincidence counting.

a) $4\pi\beta$-gas flow proportional counter

A cut-away view of the counter is shown in Fig. 17. The upper and lower halves of the polished aluminium body were hinged at one side to enable the source to be inserted into the equatorial plane of the counter. An 'O' ring clamped between the two halves acted as a gas seal. Two 0.001" tungsten wires each stretched across the diameter of one

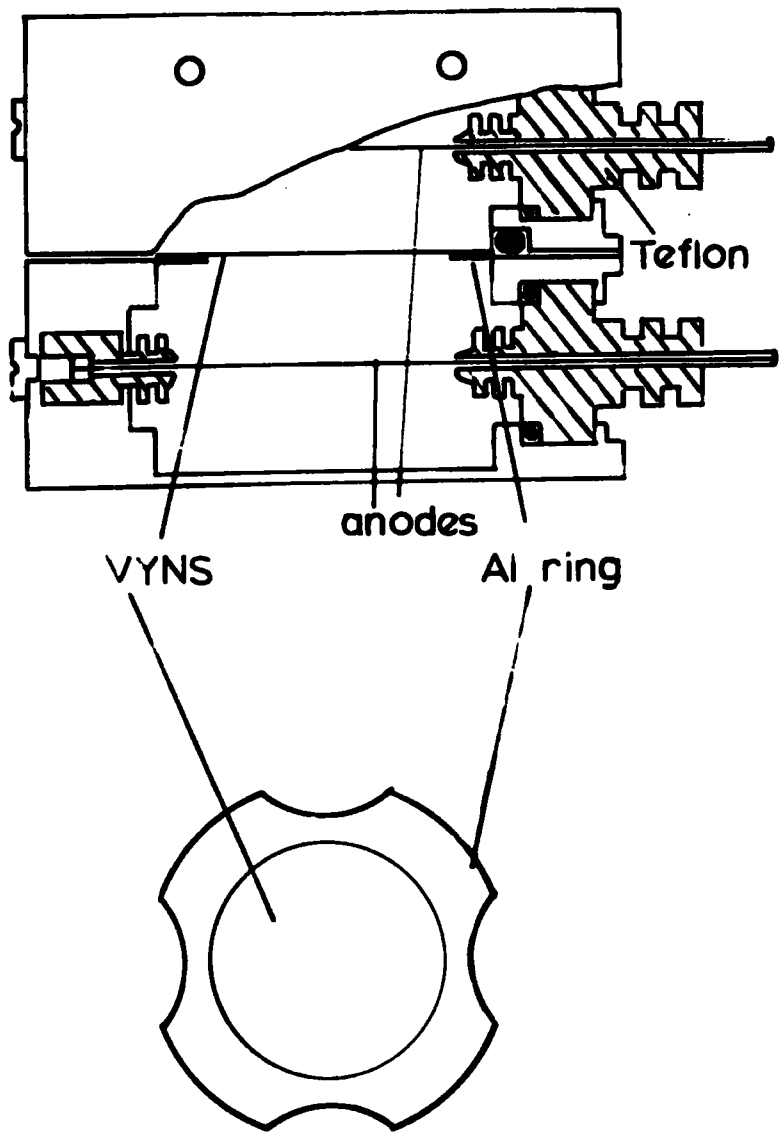

Fig.17. $4\pi\beta$ proportional counter.

counting volume between two Teflon insulators served as anodes. These were connected externally to the pre-amplifier.

The counter gas (a standard mixture of 90% argon and 10% methane obtained from the British Oxygen Co.) was dried by passing it through tubes containing silica gel and magnesium perchlorate then through a glass wool filter before allowing it to flow through the counter at atmospheric pressure. The flow rate was controlled by a needle valve and flow-meter and was usually about 0.7 ml sec^{-1}. A flow of less than 0.3 ml sec^{-1} could be shown to cause a drop in the count rate of a standard source. The electronic equipment and gas flow system were identical with that used for the end-window counter and are illustrated in Fig. 20. The reproducibility and operating characteristics of such a counter have been investigated by Davis[39] of this laboratory. As in his work the position and shape of the plateau obtained was found to vary with β -spectral shape but in practice the operating voltage was in the region of 1.6kV and the plateau length 200v.

The source mounts were prepared from VYNS film (thickness about 10 - 15 μ g cm^{-2}) mounted on an aluminium ring 2.6 cm in internal diameter and were coated on one side with about

5 μ g cm^{-2} of gold to render them conducting. To prepare a source, a drop of insulin solution (containing about 1 mg insulin in 10 ml dilute hydrochloric acid) was spread over the central area of the film and dried; this prevented uneven deposition of the active solution which was then applied and evaporated to dryness. This method of source preparation has been fully described by Pate and Yaffe[40].

b) End-window gas flow proportional counter

A diagram of this counter together with the shelf holder for the source mounts is shown in Fig. 18. The cylindrical, hollow counter body was of polished brass through the top of which an anode loop was supported in a Teflon insulator. This anode loop, $\frac{3}{8}$" in diameter and made from Constantan wire (0.001" diameter) was soldered into a fine nickel tube and suspended $\frac{5}{8}$" above the counter window. Connection to the preamplifier was made by the usual Plessey connectors. For normal use the window of this counter was of 1 mg cm^{-2} Melinex film. This is a tough polyester film aluminised on each side and thus having conducting surfaces. The windows were produced by carefully sandwiching a 2" square of the film in the jig shown in Fig. 19 and glueing the supporting ring to the film with a solution of cellulose acetate (Britfix) in amyl acetate. A heavy weight was placed on the ring until the glue had set. On setting the

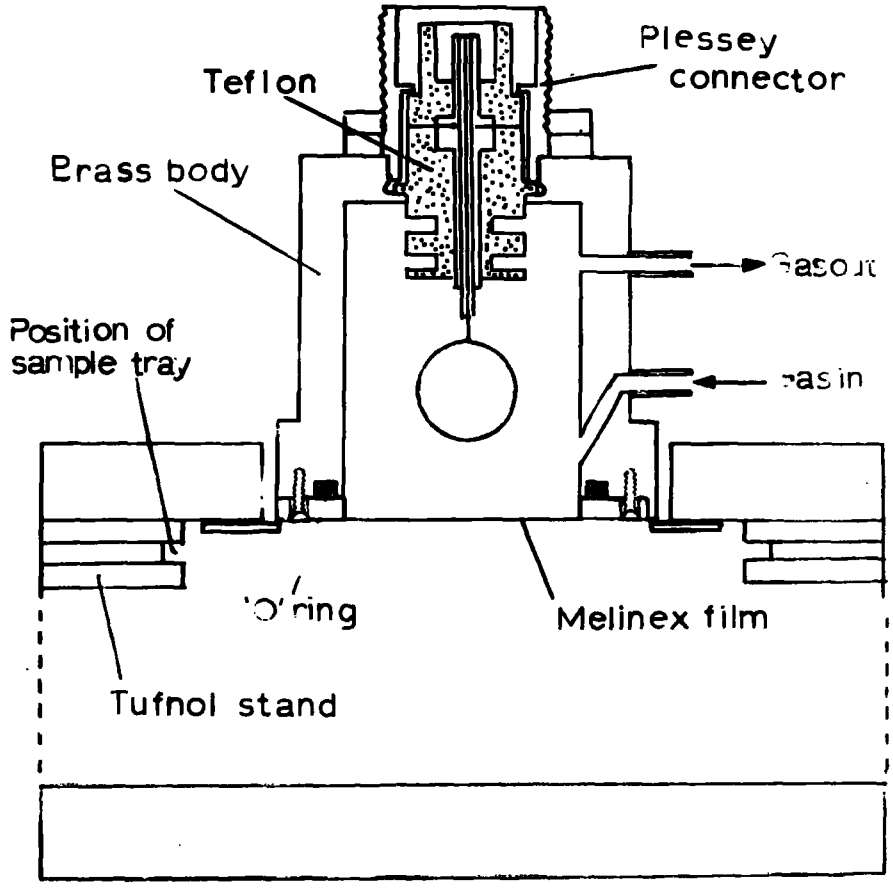

Fig.18.End-window, gas flow proportional counter.

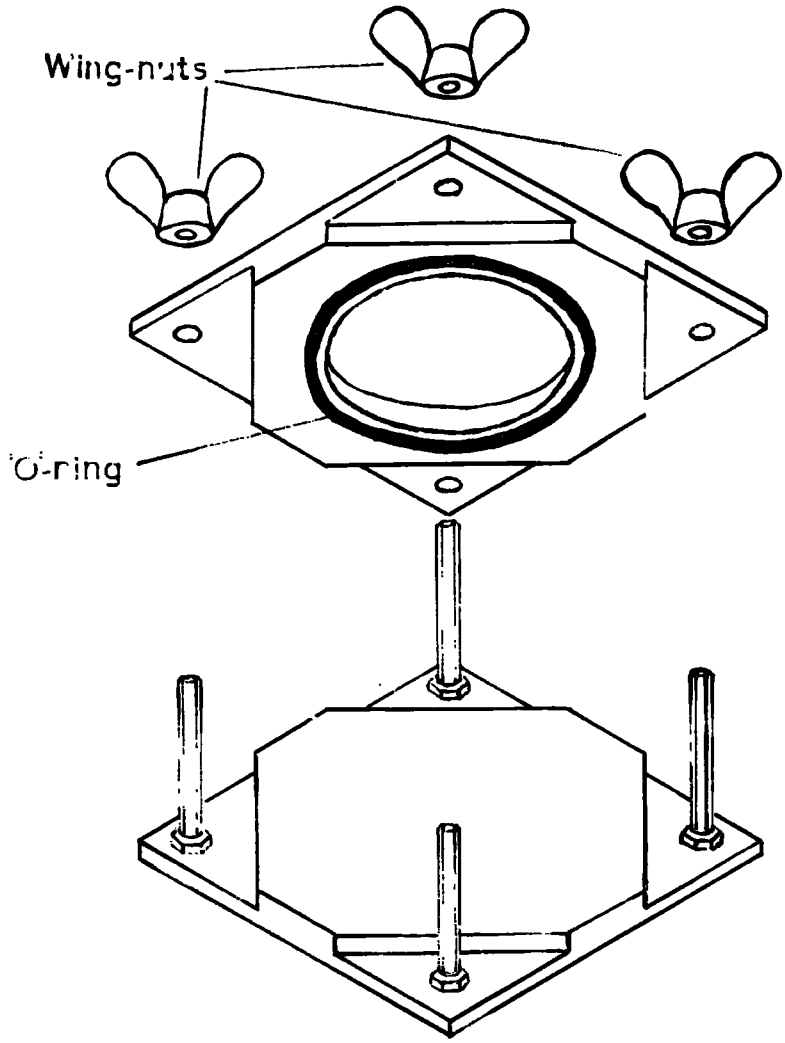

Fig.19. Window jig.

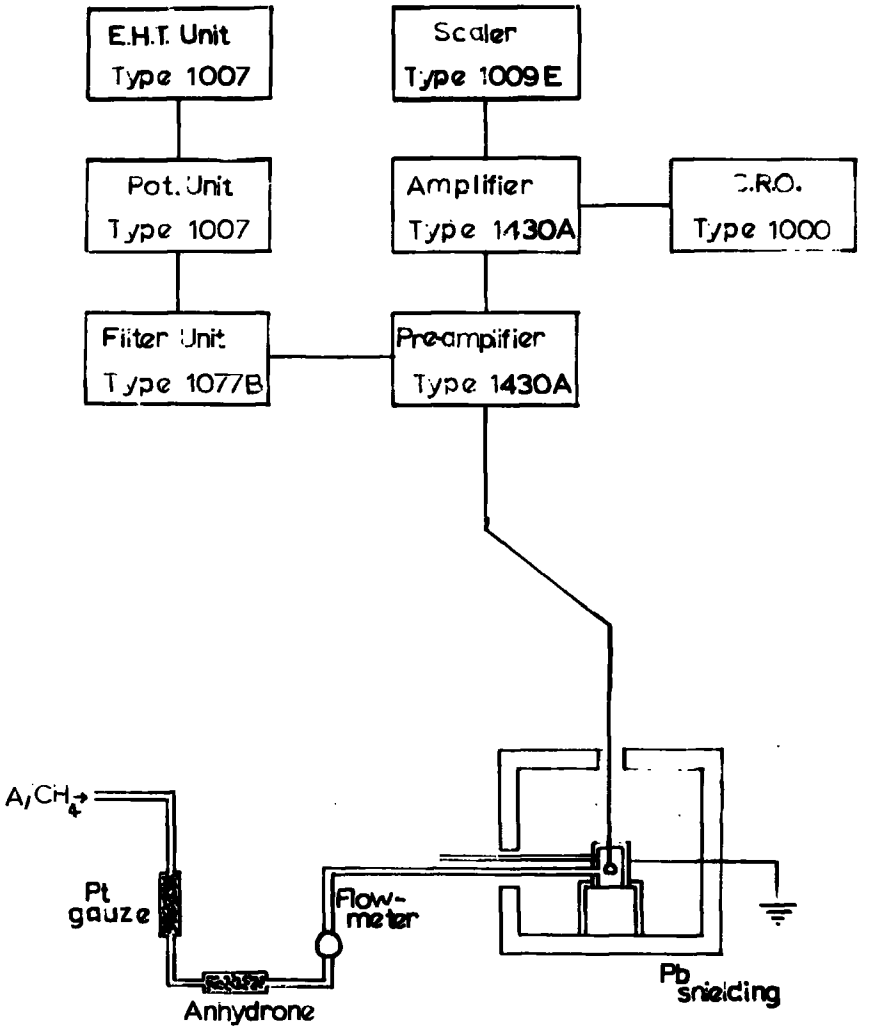

Fig.2 Block diagram of proportional counter electronic and gas flow circuits.

Melinex film was found to shrink slightly thus leaving a window with a taut, unwrinkled surface. Some measurements were made using windows of 3 or 4 layers of VYNS film prepared as described for the 4π films; being so thin (100 $\mu g\ cm^{-2}$) these were very fragile for normal use.

The counter gas was circulated at atmospheric pressure as already described for the 4π counter. The electronics and gas flow arrangement are shown in Fig. 20 in block diagram form. Amplifier and scaler settings for both this and the 4π counter are set out below:-

Amplifier	TYPE 1430 A
with preamplifier type 1430 A	
Differentiation time	0.32 μsec
Integration time	0.32 μsec
Attenuation	10 dB
Scaler	TYPE 1009E
Paralysis time	50 μsec
Discriminator level	15v

The plateau obtained for this counter indicated a working voltage of about 1.8 kV and had a length of 200v. The counter was enclosed in a lead castle with $1\frac{1}{4}$" walls and gave a back ground count rate of 9 to 12 counts per minute.

The shelf holders, made from accurately machined Tufnol strip, were set up on a jig so that the shelf positions could be accurately reproduced if the assembly were dismantled. Work on the reproducibility of this method was carried out by East[41] of this laboratory.

The sources, the preparation of which is described below, were mounted on aluminium planchets (Brilhart Cat. No. 22F.A1, obtained from Nucleonic Accessories, Birmingham) and set in a hole machined in the centre of an aluminium shelf and backed with a square (5 cm x 5 cm) of 1 g cm^{-2} aluminium sheet. This acted as a saturation backscatterer for the source.

c) Preparation of solid sources.

If solid sources were to be counted it was convenient that the form chosen for precipitation and source preparation should also be suitable for the gravimetric determination of

the chemical yield. A standard mounting technique was also necessary to allow relative measurements to be made.

Sources were mounted on glass fibre discs (Whatman GF/A); before use these were washed with water, alchohol and ether (in that order) and dried in a vacuum dessicator. The discs were then mounted on aluminium planchets (described above) and weighed to the nearest 0.01 mg using a Stanton semi-micro balance (Model MCIA).

To prepare a source the weighed disc was supported on sintered polythene in a demountable filter stick. The internal diameter of the stick was standardised at $\frac{5}{8}$" and thus filtration of a slurry of the source material gave a clearly defined area which was reproducible for any source. The source was then washed, dried and weighed as described for the mounts. The balance weights were accurate to $\pm$ 0.05 mg and the source weights were usually between 5 and 40 mg; the chemical yield (assuming that the composition of the precipitate was accurately known) would therefore be determined with an accuracy of about $\pm$1%.

d) Liquid sample Geiger-Müller counter

A calibrated Mullard (MX 124/01) halogen quenched liquid Geiger-Müller counter (Laboratory No.86) of 10 ml capacity

has been used to assay the β-disintegration rates of solutions containing ^{56}Mn obtained from the $^{56}Fe(n,p)^{56}Mn$ reaction which has been used as a reference cross section in this work.

The advantages of using this type of counter for the measurement of the reference activity are that they are simple to operate, the geometry and therefore the efficiency are intrinsic qualities and they do not tie up more sophisticated equipment which might be used to determine the activity of the isotope under investigation. The counter was also used to estimate the disintegration rate of liquid samples of ^{31}Si for which it was not convenient to prepare solid sources.

The tube was operated in conjunction with a 110 A probe unit (No.L97), with which it had been previously calibrated, at a quench pulse time setting of 500 μ sec. The probe had been previously modified to a Mullard specification for use with halogen quenched counters by the insertion of a 2.7 MΩ resistance in series with the input. The counter was found to have a threshold at 340V and a plateau length of some 100 volts; the slope was 0.07%/volt. The working voltage was taken as 400V. The efficiency of the counter was checked periodically with a standard ^{60}Co solution and a ^{137}Cs solid source. It was not found to vary outside

the expected statistics.

e) Crystal Scintillation Counters.

Thallium activated sodium iodide (NaI(Tl)) crystals have been used in this work for the detection of nuclides which emit γ-radiation.

Light quanta from scintillation events caused by the interaction processes of the γ-ray within the crystal fall upon the photosensitive cathode of a photo-multiplier tube placed in optical contact with the crystal. Photoelectrons emitted from this surface are incident upon the first electrode of a dynode chain which causes the signal to be amplified by electron multiplication down the chain. The signal at the output of the photomultiplier may be regarded as proportional to the amount of energy lost by the γ-ray in the crystal. Set out below are the size and type numbers of the three crystals used, together with their photomultiplier tube numbers.

Diameter		Thickness	Nuclear Enterprises Type No.	Photomultiplier (E.M.I.)
3"	x	3"	12/DM-2/12	9531 A
$1\frac{1}{2}$"	x	1"	6 D 4	6097 F
$1\frac{3}{4}$"	x	2" (well-type)	7 F 8	6097 F

Since sodium iodide is hygroscopic the crystals are contained in hermetically sealed aluminium cans (220mg cm^{-2} Al). The relative positions of the crystals inside these cans are shown in Fig. 21. The space between the can wall and the crystal is filled with packing material consisting mainly of aluminium oxide and neoprene which increases the thickness of the window presented to the incident γ-radiation.

The smaller crystals and photomultiplier tubes were mounted in light tight aluminium and brass tubes fabricated in this laboratory, while the 3" crystal formed part of a commercial assembly.

As has already been stated, the output signal from the photomultiplier is proportional to the energy absorbed by the crystal and therefore by linear amplification and pulse height analysis of the signal the complete spectrum of the γ- radiation incident on the crystal may be obtained. A block diagram of the electronic equipment used for γ-spectrometry is shown in Fig. 22.

The amplifier gain and voltage settings depended on the γ-energies of the spectrum under consideration; in general gain settings were in the range X0.5 → x 100 whilst the E.H.T. was set in the region of 600v for the small crystals and 800v for the large crystal.

In general the spectrum of the nuclide to be investigated was first recorded on one of the multichannel pulse height analysers; 100 channel type 1363 B or 512 channel LABEN model A 51 - CT 45. The energies of the photopeaks of the spectrum obtained were identified by comparison with spectra, taken using the same settings, of nuclides with photopeaks of known energy which could be easily recognised; for example ^{22}Na, ^{75}Sb, ^{137}Cs, ^{60}Co, and ^{54}Mn. Published spectra from Crouthamel[42] and Heath[43] were also used for comparison and subsequent identification of the photopeaks.

Having identified the photopeak, the decay of the nuclide was followed by setting the upper and lower gates of a single channel analyser to include this peak and then counting the number of events on a scaler. Alternatively, if the spectra were too complex, the complete spectrum was recorded periodically during the decay using the multichannel analyser and the variation of area under the photopeaks was then used to plot the decay curve.

Sources for the flat crystals were mounted in a similar way to that described for the end-window counter; the planchet containing the source was placed at the centre of an aluminium tray which was slid into a shelf holder attached

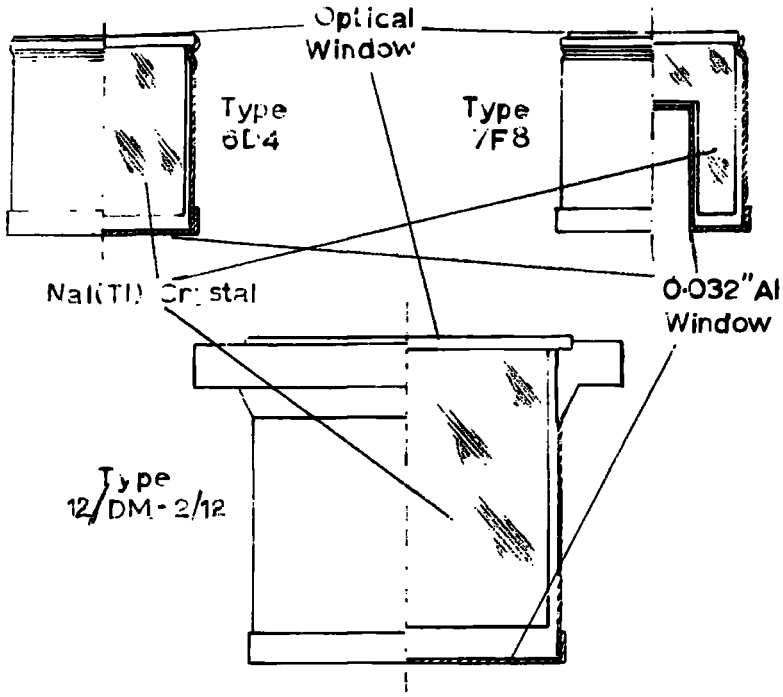

Fig.21. Three types of scintillation crystals used.

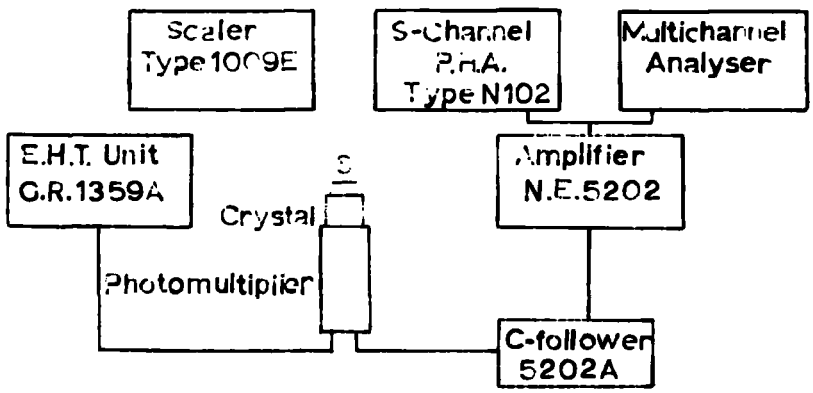

Fig.22. Block diagram of scintillation spectrometer circuit.

to the crystal thus giving a standard, reproducible geometry.

The efficiency of NaI(Tl) crystals for β -particles is not zero and if these were detected they would deform the shape of the γ-spectra. Therefore, sufficient aluminium absorbers were inserted between the source and crystal to prevent any β-particles present from entering the crystal.

Sources for the well crystal were mounted at the bottom of 5ml. semi-micro test tubes which were inserted into a brass cylinder of 1/16" wall (1.03 g cm^{-2}) which in turn was placed inside the well of the crystal. The brass cylinder was used to ensure complete absorption of the β -particles.

The absolute disintegration rates of the sources were determined, where possible, by counting standard sources having photopeaks of similar energy under identical geometrical conditions. Where this was not possible an estimate of the photopeak counting efficiency was made from published data; Crouthamel[42] and Heath[43] for flat crystals and Redon et al[44] for the well crystal.

f) Coincidence counting equipment

During this work $4\pi\beta/\gamma$, end-window β/γ , and γ/γ coincidence methods have been used to determine the absolute disintegration rates of sources and to follow the decay of one nuclide in the presence of others. A sodium iodide crystal was used as the detector for each of the γ -channels.

A block diagram of the electronic equipment is shown in Fig. 23. Outputs from the single channel analysers and proportional counter main amplifier are fed into a 1036 C coincidence unit. The count rate in each of the single channels and the coincidence channel were recorded on scalers.

The settings used on the coincidence unit and the geometrical arrangement of the counters are described in sections where specific nuclides are discussed.

g) Auxiliary Equipment

In measurements involving the determination of short lived nuclides a crystal oscillator timing unit was used to control the length of the irradiation, a pneumatic transfer system, and a camera which was used to record scaler readings.

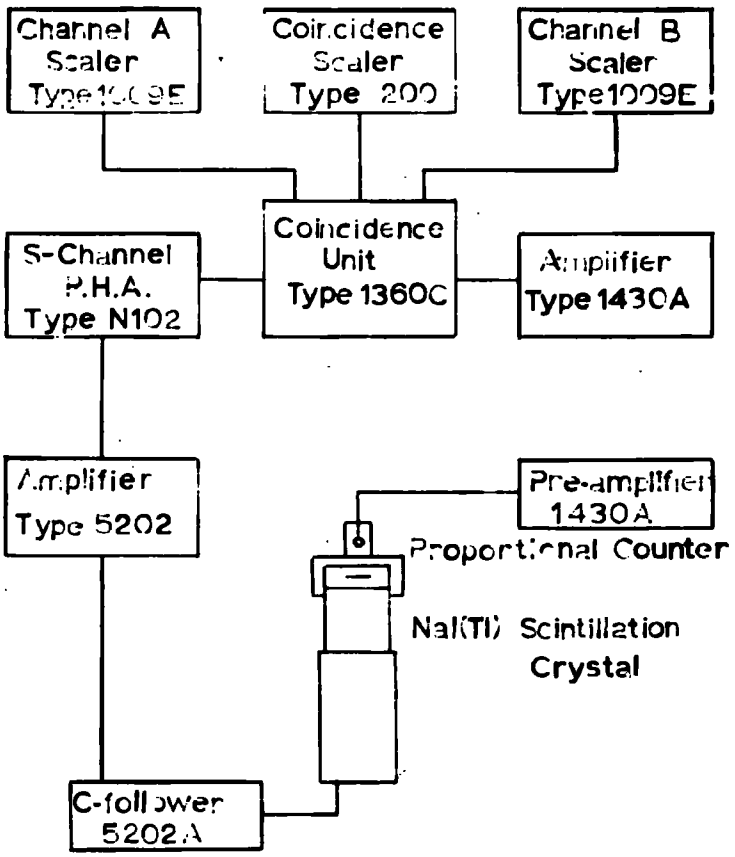

Fig.23. Block diagram of coincidence circuit.

The time for transfer from the irradiation chamber to the counting room was 2.5 seconds.

Part 4. COUNTER CALIBRATIONS

a) Calibration of the liquid Geiger-Müller counter

This counter had been previously calibrated by Martin and Hemingway[45] of this laboratory. The calibration curve and data are presented in Fig. 24 and Table 2. The point for ^{91}Y was determined in the course of the present work by counting a 10 ml aliquot of a solution standardised by $4\pi\beta$ counting. The value for ^{56}Mn in aqueous solution was determined as described in the section on neutron flux standardisation. As can be seen these points appear to fit the previous calibration. The correction to convert the forbidden spectra end-point energy to an allowed equivalent was obtained from the paper by Bayhurst and Prestwood[46].

Table 2

Calibration of liquid counter (No. 86).

Nuclide	Spectral shape	E_{β} max allowed (MeV) (Weighted mean)	Counter eff.(%)
^{204}Tl	1st forbidden	0.860	0.796
^{24}Na	allowed	1.39	5.38
^{89}Sr	1st forbidden	1.55	4.87
^{91}Y	1st forbidden	1.62	5.54
^{32}P	allowed	1.708	6.37
^{42}K	1st forbidden	3.22	11.92
^{56}Mn (in standard acid mixture with 0.5g Fe)	allowed	2.1	7.67
^{56}Mn	allowed	2.1	7.88
^{56}Mn (dil. aq. solution)	allowed	2.1	8.05

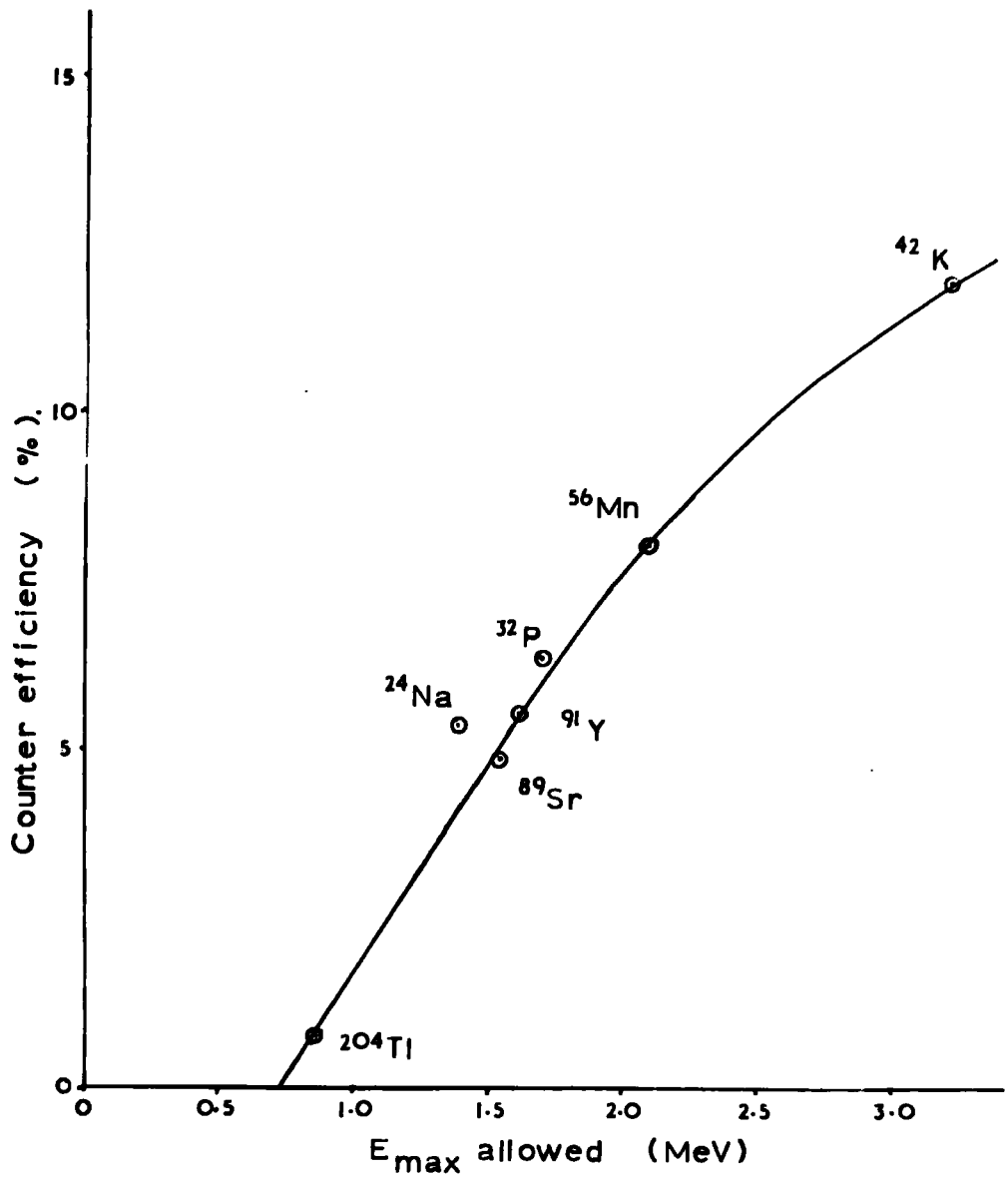

Fig.24.Calibration curve of Geiger-Muller counter.

b) Calibration of the end-window counter

The method of counter calibration proposed by Bayhurst and Prestwood[46], was used here. The method depends on experimentally determining the relationship between the counter efficiency and the average energy of the beta particle. The relationship then eliminates the necessity for making separate corrections for self-absorption, back-scattering, self-focussing etc. for each nuclide.

Carrier-free solutions of high specific activity of the nuclides to be used were obtained either from the Radiochemical Centre, Amersham, or by irradiation of the appropriate targets in a reactor. Samples of each solution were weighed on to prepared VYNS 4π films and their absolute disintegration rates determined by $4\pi\beta$ counting or by $4\pi\beta/\gamma$ coincidence techniques where applicable. A further weighed aliquot of each nuclide was added to a known weight of carrier of the element concerned and precipitated by recommended gravimetric procedures. Sources of varying thickness were then prepared using the standard filter stick method already described. Curves of source weight against counter efficiency were plotted for weights of source of 2 - 50 mg; three of these are shown in Fig. 25. The average β-energy of each nuclide was calculated using

the known maximum energy and a series of graphs given in the original paper[46]; correction was also made for any first forbidden transitions. Curves of average β-energy against efficiency at various source weights were plotted. Two of these, for source weights of 5 and 40 mg are shown in Fig. 26 whilst the complete data is presented in Table 3. From these curves the efficiency of any nuclide for which the maximum β-energy is known can be found. For nuclides emitting more than one β-group the efficiency is found for each group and a weighted mean calculated.

The nuclides used were ^{45}Ca, ^{185}W, ^{131}I, ^{22}Na, ^{198}Au, ^{24}Na, ^{91}Y, ^{90}Y, and ^{42}K. Of these the absolute disintegration rate of ^{22}Na and ^{198}Au were determined by $4\pi\beta/\gamma$ coincidence techniques (to be described in section 5), whilst the rest were determined by $4\pi\beta$ counting. The efficiency obtained for ^{22}Na and ^{24}Na were corrected for γ-rays by estimating this contribution from absorption curves obtained by inserting aluminium absorbers between the source and counter. The corrections were found to be 2 and 2.5% respectively.

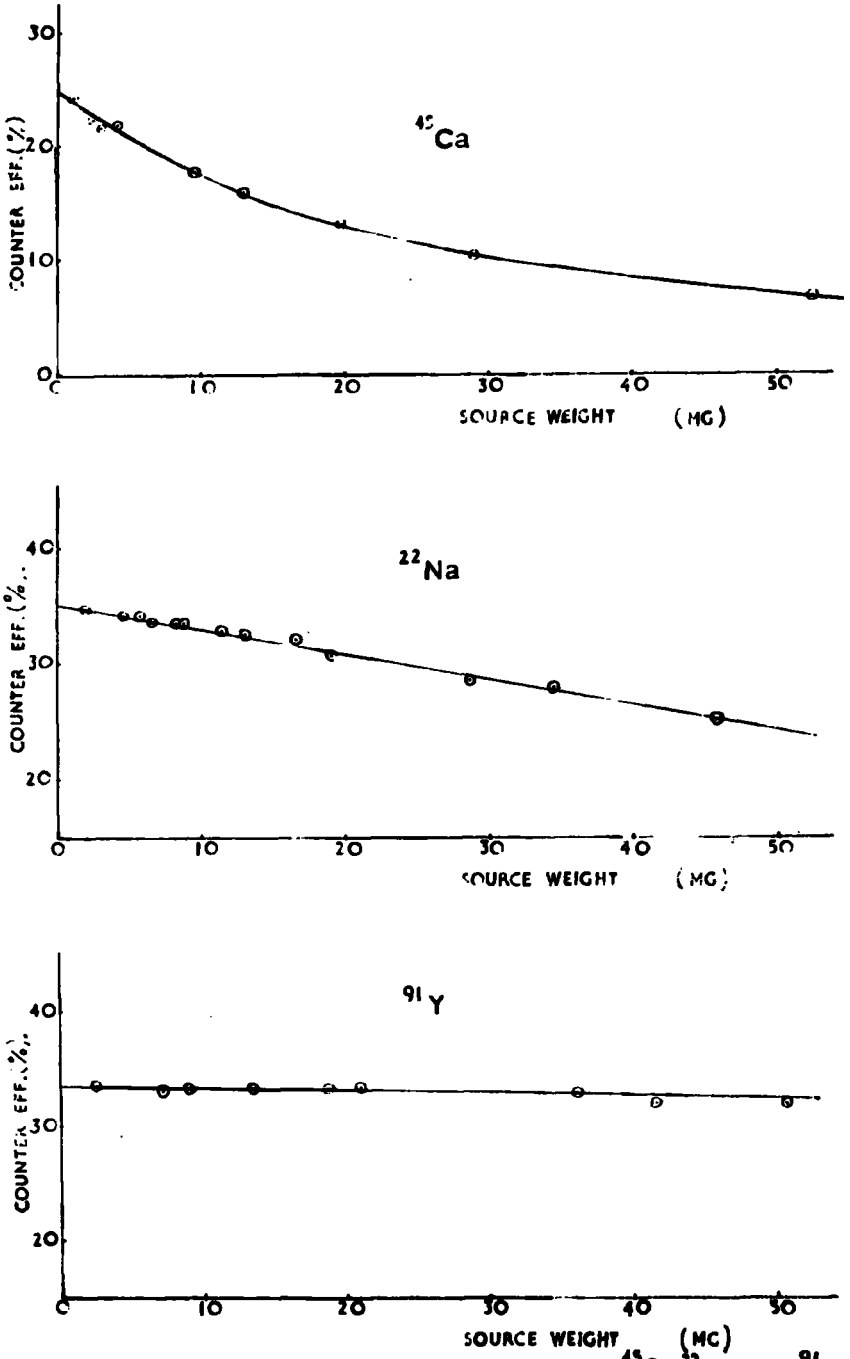

Fig. 25 Counter efficiency for sources of ^{45}Ca, ^{22}Na, and ^{91}Y.

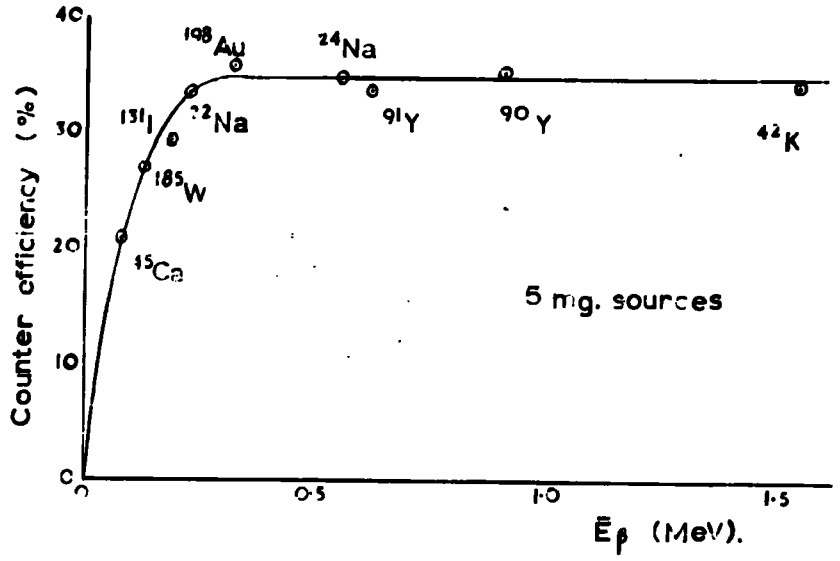

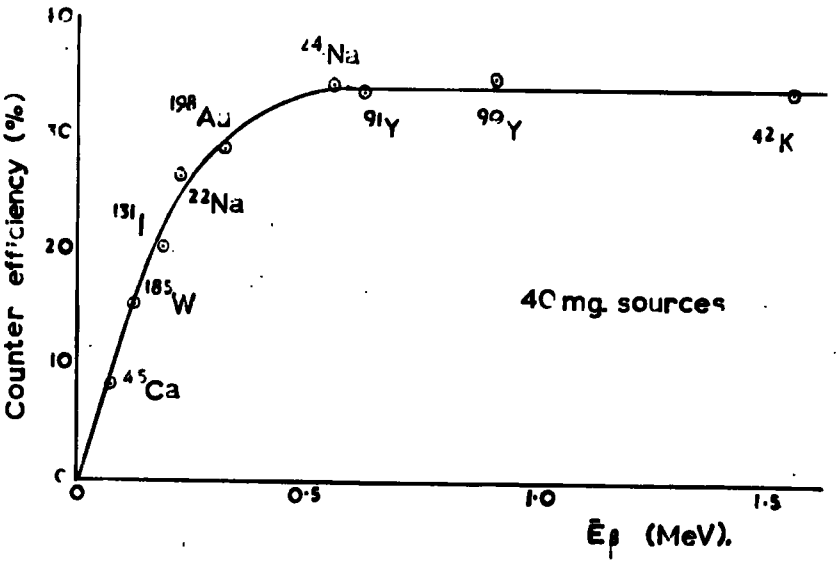

Fig.26. 5mg and 40 mg proportional counter calibration curves.

TABLE 3 Efficiency calibration of end window proportional counter.

Nuclide	Precipitate	E_{max} (Mev)	Spectrum shape	Z	E_{max} allowed (Mev)	$\bar{E}$ (Mev)	Counter efficiency versus source weight 5 mg	10 mg	15 mg	20 mg	25 mg	30 mg	35 mg	40 mg
^{45}Ca	Oxalate	0.254	Allowed	20	0.254	0.076	0.207	0.173	0.148	0.130	0.115	0.102	0.092	0.084
^{185}W	Oxinate	0.428	Allowed	74	0.428	0.127	0.268	0.239	0.217	0.199	0.185	0.172	0.162	0.154
^{131}I	Iodide	0.606	(Complex) allowed	53	0.606	0.188	0.294	0.283	0.270	0.254	0.236	0.219	0.207	0.202
^{22}Na	Chloride	0.542	Allowed (β^+) (-)	11	0.542	0.225	0.333	0.323	0.312	0.304	0.296	0.282	0.271	0.263
^{198}Au	Metal	0.963	(Complex) allowed	79	0.963	0.321	0.359	0.349	0.338	0.328	0.317	0.307	0.296	0.286
^{24}Na	Chloride	1.390	Allowed	11	1.390	0.560	0.347	0.346	0.345	0.345	0.344	0.344	0.343	0.342
^{91}Y	Oxalate	1.537	First	39	1.620	0.620	0.336	0.335	0.333	0.332	0.330	0.329	0.337	0.336
^{90}Y	Oxalate	2.260	First	39	2.260	0.906	0.352	0.351	0.350	0.349	0.349	0.348	0.348	0.347
^{42}K	Tetraphenyl-boron	3.58	(Complex) First	19	3.50	1.55	0.340	0.336	0.336	0.336	0.336	0.336	0.337	0.337

Counter 90 with 1 mg. cm^{-2} Melinex window. Counter stand W.

1 gm. cm^{-2} aluminium backscatterer.

Amplifier 1430A + 1430 head. 10dB. 0.32 μS resolving time
15v discriminator.

Part 5. Coincidence counting.

$4\pi\beta/\gamma$ and end-window β/γ coincidence methods have been used here to determine the absolute disintegration rates of an extended ^{22}Na source used as a standard in irradiations in which reaction products emitting positrons were encounted and also of sources of ^{22}Na and ^{198}Au in the calibration of the end-window proportional counter.

The methods employed were largely those of Campion[47] and Wapstra[48]. The great advantage of this method is that, in principle, absolute disintegration rates may be determined without a prior knowledge of the efficiencies of the counters used. Problems such as the self absorption correction in $4\pi\beta$ counting are therefore avoided.

For extended sources Putman[49] has shown that the method is valid provided that either the β-detector or the γ-detector is equally sensitive to all parts of the source. The absolute disintegration rate is given by

$$N_o = \frac{N_\beta \cdot N_\gamma}{Nc} \cdot \left[\frac{\overline{C_\beta \cdot C_\gamma}}{\bar{C}_\beta \cdot \bar{C}_\gamma} \right], \qquad (1)$$

where N_o is the absolute disintegration rate of the source N_β, N_γ and N_c are the observed counting rates (less background and accidental coincidences) in the β, γ and

coincidence channels respectively, $\bar{C}_\beta$, $\bar{C}_\gamma$, are the means of the individual efficiencies integrated over the source (equal to C_β and C_γ , the effective efficiences) and $\overline{C_\beta . C_\gamma}$ is the mean of the product. If either detector is equally sensitive to all parts of the source the term in brackets reduces to unity. The $4\pi\beta$ counter has been shown to approximately fulfill these conditions[47]. In the end-window β/γ coincidence method, also used here, the source of small diameter ($\prec$ 1 cm) was placed at the centre of the surface of a 3" x 3" NaI(Tl) scintillation crystal and it was assumed that the γ-ray detector was equally sensitive to all parts of the source.

The following expressions were derived by Campion[47] and will simply be quoted here.

a) Correction for accidental coincidence rate.

Since the resolving time of the coincidence mixer is of finite length coincidences may be obtained between two unrelated events when both detectors are less than 100 per cent efficient. The following correction was made for this,

$$Nc = \frac{Nc' - 2\tau_R N_\beta N_\gamma}{1 - \tau_R (N_\beta + N_\gamma)} , \qquad (2)$$

where N_c' is the observed coincidence rate including accidentals but with the background subtracted and τ_R is the resolving time of the mixer. Campion shows that the above expression also applies if N_β and N_γ are replaced by the observed count rate without the background subtracted.

b) Correction for dead time in the single channels

Assuming the dead time of each channel is τ , then

$$N_\beta = No\, C_\beta\, (1 - No\, C_\beta\, \tau),$$

$$N_\gamma = No\, C_\gamma\, (1 - No\, C_\gamma \tau),$$

$$Nc = No\, C_\beta\, C_\gamma \left[1 - \left\{ 1 - (1 - C_\beta)(1 - C_\gamma) \right\} No\tau \right],$$

and therefore

$$\frac{N_\beta\, N_\gamma}{Nc} = No\left[1 - \frac{No\,\tau\, C_\beta\, C_\gamma\, (1 - No\,\tau)}{1 - No\,\tau\,(C_\beta + C_\gamma - C_\beta\, C_\gamma)} \right].$$

Since $No\,\tau$ is in general much less than unity this reduces to

$$\frac{N_\beta\, N_\gamma}{Nc} = No\left[1 - No\tau\, C_\beta\, C_\gamma \right]. \qquad (3)$$

If the dead time of the channels is not equal and $\tau_\beta > \tau_\gamma$

$$\frac{N_\beta\, N_\gamma}{Nc} = No\left[1 - No\, C_\beta\, C_\gamma \tau_\gamma \left\{ \frac{1 - No\,\tau_\beta}{1 - No(\tau_\gamma C_\gamma + \tau_\beta C_\beta - C_\beta C_\gamma \tau_\gamma)} \right\} \right].$$

A similar expression is obtained with β and γ interchanged if $\tau_\gamma > \tau_\beta$. If quadratic terms are neglected equation (3) is obtained. In the special case of the $4\pi\beta$ counter, $C_\beta \rightarrow 1$ and if $\tau_\beta > \tau_\gamma$ the term in curly brackets reduces to unity.

c) Coincidence background due to cosmic rays etc. was subtracted from the observed count rate of the source.

Coincidence unit setting up procedure (1036 C)

The operating settings of the counters to be used were first determined as discussed previously. For the β -channels the coincidence unit discriminator was set at 15 V for the output of the amplifier while for γ -channels a 5V discriminator setting was used for the output from the single channel analysers. Both channels were operated with a paralysis of 5 or 10 μ s.

The delay between the channels was determined by varying the delay settings, with a small value for the coincidence mixer resolving time, until a maximum was obtained in the coincidence rate from the source. Having set the delay the resolving time was now increased until the coincidence rate (excluding accidentals) did not

increase further with increase in resolving time. The resolving time was then set at the minimum value for which saturation was obtained. In general channels 1 and 3 of the coincidence unit were used since the resolving time range is larger than for channels 1 and 2.

The paralysis time of each channel was checked by a double pulse technique using a Dynatron N 107 test set. The values were found to be as indicated. The actual value of the resolving time of the mixer was measured at the various settings by counting the accidental coincidences between the count rates of two independent sources fed into the single channels. The value of the resolving time was then obtained from equation 2 above.

a) Coincidence counting of ^{22}Na and results for the ^{22}Na standard source.

An aqueous solution of ^{22}Na of high specific activity $\leq$ 1 mC mg^{-1} Na as sodium chloride was obtained from the Radiochemical Centre, Amersham. A portion of the original solution was diluted and placed in a polythene capsule. The following series of sources were made.

(i) Point 'solid' cource. A stainless steel planchet was coated with a layer of cellulose acetate leaving a central

spot clear. About 100 mg of the ^{22}Na solution was accurately weighed on to the spot and carefully evaporated. The cellulose acetate served to limit the spread of the liquid and a source 0.7 cm in diameter was formed.

(ii) Extended source. A 2.1 cm diameter glass fibre filter pad was attached to an aluminium planchet by warming a film of polythene on the planchet and then pressing the filter pad onto the polythene. The filter pad was damped with a little water and about 100 mg of the ^{22}Na solution was accurately weighed onto the pad. The solution was spread over the entire surface after which it was carefully evaporated.

(iii) A portion of the ^{22}Na solution was accurately weighed and a known weight of water added thus diluting the original solution about ten times. A series of three ^{22}Na 4π sources were made by weighing 80, 120 and 200 mg of the diluted solution onto previously prepared 4π films. These were also carefully evaporated.

The absolute disintegration rates of the point source and the 4π sources were determined by end-window β/γ coincidence and $4\pi\beta/\gamma$ coincidence techniques described above. Unfortunately one of the 4π sources was damaged

before it could be counted. The sources mounted on planchets were covered and sealed with a layer of Sellotape.

^{22}Na decays by 89.7% positron emission and 10.3% electron capture in coincidence with a 1.28 MeV γ-ray in 100% of the decays. No anisotropy is reported between the positron and the γ-ray[50] .

4$\pi\beta$ / γ coincidence method.

The 4π sources were inserted into a 4π counter which was placed on a 3" x 3" NaI(Tl) γ-ray scintillation crystal. A 200 mg cm^{-2} aluminium sheet was placed between the counters to prevent positrons entering the crystal. The β-channel was delayed by 1μs on the γ-channel and a mixer resolving time of 4μs was necessary. Coincidence measurements were made at two different settings for each pulse height analyser window;(a) including both the 1.28 MeV photopeak and the 1.79 MeV sum peak (discriminator at 1.15 MeV) and (b) including only the 1.79 MeV sum peak (discriminator at 1.64 MeV) as suggested by Campion[47]. The efficiency of the 4π proportional counter to electron capture events was considered to be negligible. The coincidence equations used are:-

a)

$$N_\beta = No\left[\beta C_\beta + (1 - \beta)T_{\beta 1.28} + \beta(1 - C_\beta)(T_{\beta 1.28} + 2\,T_{\beta 0.51})\right]$$

$$N_\gamma = No\; P_{1.28}$$

$$Nc = No\; P_{1.28}\,(\beta C_\beta + \beta(1 - C_\beta)2\,T_{\beta 0.51})$$

$$\frac{N_\beta\; N_\gamma}{Nc} = \frac{No\left[\beta C_\beta + (1 - \beta)T_{\beta 1.28} + \beta(1 - C_\beta)(T_{\beta 1.28} + 2\,T_{\beta 0.51})\right]}{\beta\,(C_\beta\,(1 - 2\,T_{\beta 0.51}) + 2\,T_{\beta 0.51})}$$

where β is the percentage of decays of a nuclide by positron emission to a particular energy level of the daughter (= 0.897 for ^{22}Na).

c_β is the efficiency of the proportional counter to positrons.

$T_{\beta 1.28}$ and $T_{\beta 0.51}$ are the efficiency of the proportional counter for counting 1.28 MeV and 0.51 MeV γ -rays respectively.

$P_{1.28}$ is the efficiency of the scintillation crystal for counting a 1.28 MeV γ-ray in its photopeak (including corrections for absorption in source and absorbers).

A value of 95% was obtained for C_β from counting rates, and from the work of Campion, $T_{\beta 1.28}$ and $T_{\beta 0.51}$ were

estimated to be 1.1% and 0.6% respectively.

On substitution

$$\frac{N_\beta \, N_\gamma}{Nc} = No. \; 1.0015 \; .$$

b) The equations used here are the same as those above except for the substitution

$$N_\gamma = No \; P_{1.28}{}^2 \; P_{0.51} \; ,$$

where $P_{0.51}$ is the efficiency of the crystal for the detection of a 0.51 MeV γ-ray in its photopeak.

β/γ coincidence method

The ^{22}Na point source was counted between an end-window proportional counter and a 3" x 3" γ-ray scintillation crystal. A 240 mg cm^{-2} aluminium absorber was placed between the source and the crystal to prevent positrons entering the crystal. The separation of the proportional counter window and the crystal was 1.8 cm. The β-channel was again delayed by 1 μs and a 4 μs mixer resolving time was required. The crystal was set to count both the 1.28 MeV photopeak and the 1.79 MeV sum peak as described above.

To determine the back ground in the proportional counter due to the 1.28 MeV γ-ray the following procedure was adopted. The source was counted by the proportional counter while sandwiched between two layers of aluminium (240 mg cm^{-2}) to stop the positrons. The count rate is then due to the sum of the 1.28 MeV γ-rays and the annihilation radiation from the two plates. The source was now inverted and counted with only one 240 mg cm^{-2} aluminium plate on the counter side of the source. (The crystal had been removed). The count rate was now the sum of the 1.28 MeV γ-ray and the annihilation radiation from one plate. Neglecting γ-ray coincidences and γ-ray attenuation in the aluminium, the count rate from the 1.28 MeV γ-rays passing through the counter was obtained by subtraction. 10% of these γ-rays have no coincident positron and therefore contribute to the γ background. Of the remainder about 1/3 will be counted in coincidence with positrons in the proportional counter; the efficiency of the proportional counter for β-particles for the source distance used was about 33%. Thus 70% of the 1.28 MeV γ-ray count from the aluminium sandwich count will contribute to the β channel count rate in coincidence measurements. The coincidence equation derived above (for $4\pi\beta/\gamma$ (a)) will also apply here but the correction for the 1.28 MeV γ-ray

TABLE 4 Determination of the absolute disintegration rate of the 2.1 cm diam. ^{22}Na source.

Source	Wt. of standard solution (mg)	Date of Measurement	Method	N_β (c.p.m.)	N_γ (c.p.m.)	N_c' (c.p.m.)	N_c (c.p.m.)	N_o (d.p.m.)	N_o at zero time x 10^{-4}	d.p.m./mg standard solution x 10^{-3}	Mean
4π 1	12.94	24/5/63	4πβ/γ a	36,890	1208	1035	1032	4.32	4.32	3.34	
		3/2/64	4πβ/γ b	30030	106.0	100.6	99.9	3.54	4.26	3.29	
		4/2/64	4πβ/γ a	30050	1089.0	922.2	917.9	2.56	4.28	3.31	
4π 2	22.40	25/5/63	4πβ/γ a	64090	2198	1880	1871	7.52	7.52	3.36	3.41
		7/6/63	β/γ	14850	3574	687.9	681.7	7.79	7.87	3.51	±0.03
'Point Source'	96.3	27/5/63	β/γ	73120	16490	3667	3540	34.2	34.3	3.56	
		7/6/63	β/γ	69860	15770	3460	3342	33.1	33.4	3.47	
		11/2/64	β/γ	59990	12620	2856	2776	27.3	33.1	3.44	
		10/3/65	β/γ	35056	9599	1664	1644	20.5	33.2	3.45	

Weight of the extended 2.1 cm diam. source in 130.4 mg.

Activity on 24/5/63 = $4.45 \pm 0.04 \times 10^5$ d.p.m.

The half life of ^{22}Na was taken as 2.58 years.

The 4 μ S resolving time setting of the coincidence mixer was 3.52 μS.

count in the β -channel was subtracted. It amounted to some 1% of the β-channel count rate.

The result of these determinations are given in Table 4. The $4\pi\beta/\gamma$ method appears to give a result about 5% lower than the β/γ method. Within the errors the $4\pi\beta/\gamma$ methods (a) and (b) give the same value. The mean of all the results has been taken in calculating the specific activity of the initial ^{22}Na solution. The error from weighing and counting statistics has been estimated to be $\pm$ 2%.

The computed activity for the 2.1 cm diameter ^{22}Na source is therefore $4.45 \pm 0.09 \times 10^5$ d.p.m. on 24.5.63.

b) Coincidence counting of ^{198}Au

Similar $4\pi\beta/\gamma$ measurements to those described above were made to determine the activity of 4π sources of ^{22}Na and ^{198}Au for use in calibrations of the end-window counters.

In 99% of its decays ^{198}Au emits a negatron group of maximum energy 0.962 MeV followed by a γ-ray of 0.412 MeV. In the other 1% a negatron group of 0.287 MeV maximum energy is followed by a 1.087 MeV γ-ray in 18% of the events, and

in the other 82% by a cascade of an 0.675 MeV and an 0.412 MeV γ-rays. The decay directly to the ground state of ^{198}Hg which occurs in 0.025% of the cases was considered to be negligible. The γ-ray channel was set to count the 0.412 MeV photopeak (0.310 - 0.515 MeV) and the β-channel was again delayed by 1 μ s. The coincidence mixer resolving time required was 2 μ s. Since ^{198}Au decays by 100% β -particle emission it was considered that the following coincidence equations could be used without significant error.

$$N_\beta = No\ C_\beta$$

$$N_\gamma = No\ P_{0.412}$$

$$Nc = No\ C_\beta P_{0.412}$$

Where $P_{0.412}$ is the efficiency of counting the 0.412 MeV γ-ray in the photopeak.

No correction was made for the angular correlation between the β-particles and γ-rays in this nuclide since the β -particles were detected with almost 100% efficiency.

CHAPTER 3

Methods of Calculation

Part 1. Correction for the variation of neutron flux during an irradiation

The cross sections reported here have been measured either by the associated particle method, or relative to that of a reference reaction, usually $^{56}Fe(n,p)^{56}Mn$. In the first method the flux through the sample is determined directly, while in the second it is assumed that both the sample and reference element are exposed to the same flux. The radioactive products induced in the sample and in the reference element decay during the irradiation, at different rates, and correction must be made for this.

As mentioned in Chapter 2 the neutron generator does not produce a steady neutron flux and allowance must be made for this also.

Consider an irradiation of duration T. Resultant activities are plotted and the activities at time t_o, the end of the irradiation, are determined by extrapolation.

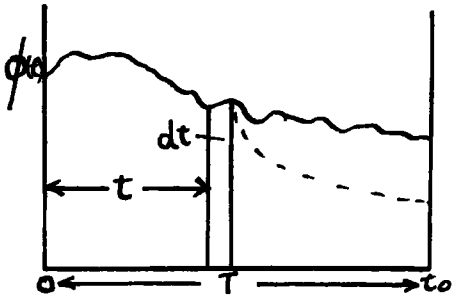

Variation of neutron flux with time during the course of an irradiation.

a) A stable nuclide, 1, is activated during the irradiation, producing a radioactive nuclide, 2. The radioactive nuclide, 2, subsequently decays to a stable nuclide at a rate determined by its disintegration constant, λ .

$$\text{i.e.} \quad 1 \xrightarrow{(n,x)} 2 \xrightarrow[\lambda]{\beta} \text{stable}$$

The nuclide, 2, is produced throughout the irradiation at an irregular rate given by the expression

$$\frac{dN_2}{dt} = N_1 \cdot \sigma_{12} \cdot \phi(t) ,$$

where, $\frac{dN_2}{dt}$ is the rate of production of 2.

N_1 is the number of nuclei of 1 exposed to the neutron flux.

σ_{12} is the cross section for the reaction $1 \xrightarrow{(n,x)} 2$.

ϕ (t) is the neutron flux as a function of time.

During the short interval, dt, the number of nuclei of 2 which are produced is $dN_2 = N_1 \cdot \sigma_{12} \cdot \phi(t).dt.$ and these decay exponentially so that at the end of the irradiation, time to, the number remaining is

$$dN_2(to) = N_1 \cdot \sigma_{12} \cdot \phi(t) \cdot e^{-\lambda(T - t)} \cdot dt.$$

The value of ϕ t at any instant is not known absolutely, but its variation is proportional to the variation in the counting rate of the neutron monitor, I(t).

$$\text{i.e.} \qquad \phi(t) = I(t) / \eta$$

where, η is the factor relating flux at the sample position to the counting rate of the neutron monitor (determined in the associated particle method).

Thus:

$$N_2(to) = \frac{N_1 \cdot \sigma_{12}}{\eta} \int_{t = o}^{t = to} I(t) \cdot e^{-\lambda(T - t)} \cdot dt.$$

The integral is conveniently replaced by the summation

$$\Sigma (I \cdot e^{-\lambda(T - t)}) \cdot \delta t \quad \text{(abbreviated to } S_2)$$

so long as δ t is small compared to the half life of the nuclide 2.

Then:

$$N_2(to) = \frac{N_1 \cdot \sigma_{12} \; S_2}{\eta} .$$

A similar expression applies to every nuclear reaction

occuring during the irradiation and, if

$$1_r \longrightarrow 2_r \xrightarrow[\lambda_r]{\beta} \text{stable}$$

represents the reference reaction,

$$\frac{N_2(to)}{N_{2_r}(to)} = \frac{N_1 \cdot \sigma_{12} \cdot S_2}{N_{1r} \cdot \sigma_{12r} \cdot S_{2r}}$$

the unknown factor, η , cancelling between the two expressions, provided both sample and reference substance are exposed to the same flux.

The activities of resultant nuclides at time t_o , the end of the irradiation, are determined by extrapolation of their decay curves. Then, since $Ao = C. \lambda . No$,

$$\frac{Ao\ (2)}{Ao\ (2r)} = \frac{C_2 \cdot \lambda \cdot N_1 \cdot \sigma_{12} \cdot S_2}{C_{2r} \cdot \lambda_r \cdot N_{1r} \cdot \sigma_{12r} \cdot S_{2r}} \qquad (1)$$

where, C_2 and C_{2r} are the detection coefficients for the respective nuclides.

b) In some cases, it was required to measure the relative cross-sections for the independent production of a pair of nuclear isomers.

A stable nuclide, 1, is activated during an irradiation, producing both the metastable and ground states of a radioactive nuclide, 2. Allowance must be made for the formation of ground state nuclei via the metastable during the course of the irradiation. The process can be represented:

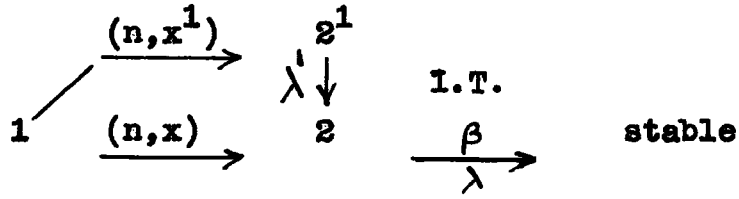

The total number of nuclei of 2^1 present at the end of the irradiation is given by

$$N_2^1(to) = \frac{N_1 \cdot \sigma_{12}^1 \cdot}{\eta} \sum (I \cdot e^{-\lambda^1 (T - t)}) \cdot \delta t. \qquad (2)$$

$$= \frac{N_1 \cdot \sigma_{12}^1 \cdot S_2^1}{\eta} .$$

The total number of nuclei of 2 present at the end of the irradiation is given by

$$N_2(to) = \frac{N_1 \cdot \sigma_{12}}{\eta} \cdot \Sigma (I \cdot e^{-\lambda(T - t)}) \delta t + N$$

$$= \frac{N_1 \cdot \sigma_{12} \cdot S_2}{\eta} + N ,$$

where, N is the number of nuclei of 2 formed via the metastable state 2^1, during the course of the irradiation.

The rate of formation of 2 via 2^1 is given by

$$\frac{dN}{dt} = N_2^1 \cdot \lambda^1 - N\lambda .$$

Then:

$$N = \frac{N_1 \cdot \sigma_{12}^1}{\eta} \cdot \frac{\lambda^1}{\lambda - \lambda^1} \cdot \Sigma I(e^{-\lambda^1(T - t)} - e^{-\lambda(T - t)}) \delta t \qquad (3)$$

$$= \frac{N_1 \cdot \sigma_{12}^1}{\eta} \cdot \frac{\lambda^1}{\lambda - \lambda^1} \cdot (S_2^1 - S_2) ,$$

and the total number of nuclei of 2 present at the end of

the irradiation is

$$\frac{N_1}{\eta}\left[\sigma_{12}^{1} \cdot \frac{\lambda^1}{\lambda-\lambda^1}\cdot(S_2^{1} - S_2) + \sigma_{12}\, S_2\right]. \qquad (4)$$

$$\frac{N_2^1}{N_2} = \frac{\sigma_{12}^{1} \cdot S_2^{1}}{\sigma_{12}^{1} \cdot \frac{\lambda^1}{\lambda-\lambda^1}\,(S_2^{1} - S_2) + \sigma_{12}\, S_2}.$$

c) A similar case to that discussed in b) is when a reaction product decays to an active daughter which itself is formed directly in a reaction. The process can be represented:

$$1^1 \xrightarrow{(n,y)} 2^1$$

$$\lambda^1 \downarrow \beta$$

$$1 \xrightarrow{(n,x)} 2 \xrightarrow[\lambda]{\beta} \text{stable}$$

$N_1 \sigma_{12}^{1}$ in equation 2 and 3 of b) is then replaced by $N_1^1 \sigma_{1\,2}^{1\,1}$, and the total number of nuclei of 2 present at

Part 2 Straight-line

A semilog plot of
species yields a strai
species present with s
than a factor of 2) it
the composite decay by
are similar (less than
stripping is often dif
of the decay curve fro

A method of overc
plot[51] (or a 'Bunney']

Consider a decay
components 1 and 2 of
λ_2. The total activ

$$A = /$$

By multiplying bo

$$A\ e^{\lambda_1 t} = /$$

As stated λ_1 and

the end of irradiation is

$$\frac{1}{\eta}\left[N_1^1\ \sigma_{1'2'}\ \frac{\lambda^1}{\lambda - \lambda^1}\ (S_{2'} - S_2) + N_1 \sigma_{12}\ S_2\right]. \qquad (5)$$

to pa

activ

plot

$Ae^{+\lambda t}$

as a function of t, a plot of $Ae^{\lambda_1 t}$ versus $e^{(\lambda_1 - \lambda_2)t}$ is a straight line with intercept A_1^0 and slope A_2^0, the initial activities of components 1 and 2.

The above method only applies to independent components but an analogous method for use with parent-daughter growth-decay curves has been recently pointed out by Buchanan[53].

The net (background-subtracted) counting rate of a parent-daughter mixture is the sum of the counting rate due to the parent activity, the daughter activity present initially, and the daughter activity grown from the parent.

I

nuclid

A_p^o an

of the

$$A = A_p^o e^{-\lambda_p t} + A_d^o e^{-\lambda_d t} + A_p^o \left(\frac{C_d}{C_p}\right)\left(\frac{\lambda_d}{\lambda_d - \lambda_p}\right)\left(e^{-\lambda_p t} - e^{-\lambda_d t}\right),$$

or rearranging

$$A = A_p^o e^{-\lambda_p t}\left[1 + \left(\frac{C_d}{C_p}\right)\left(\frac{\lambda_d}{\lambda_d - \lambda_p}\right)\right] + e^{-\lambda_d t}\left[A_d^o - A_p^o \left(\frac{C_d}{C_p}\right)\left(\frac{\lambda_d}{\lambda_d - \lambda_p}\right)\right].$$

and

D

In these equations, A is the net observed counting rate, C is the counting efficiency, t is the elapsed time, superscript 0 designates an activity at t = 0, subscript p refers

anisotropy corrections are additive here for both particles a better arrangement would have been to accept and count particles in the same direction where the corrections would have largely cancelled.

If α particles are counted at an angle ϕ to the incident deuteron beam direction by a detector which subtends a solid angle $\Delta\Omega_\alpha$ at the target, the total number of neutrons produced per α-particle incident on the target is given by

$$N = \left(\frac{4\pi}{\Delta\Omega_\alpha}\right) R_\alpha ,$$

where R_α is an anisotropy factor whose value depends on ϕ and on the incident deuteron energy. In Fig. 27 are shown values of R_α for thick targets obtained from the work of Ruby and Crawford[57]. For the present conditions R_α was taken to be 1.028. The relationship, $\left(\frac{dw'}{dw}\right)$, between the neutron centre of mass solid angle (w') and laboratory solid angle (w) was obtained from the data of Benveniste and Zenger[54] and is shown in Fig. 28 for various laboratory angles and incident deuteron energies. A value of 1.05 was taken for $\left(\frac{dw'}{dw}\right)$ for irradiations made here in the forward

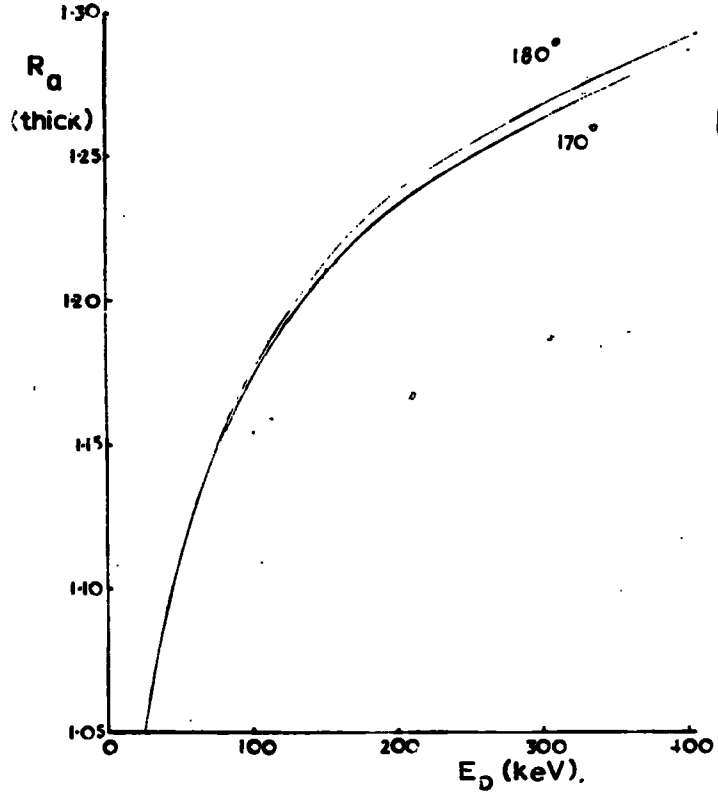

Fig.27 Neutron yield curves.(Ruby and Crawford).

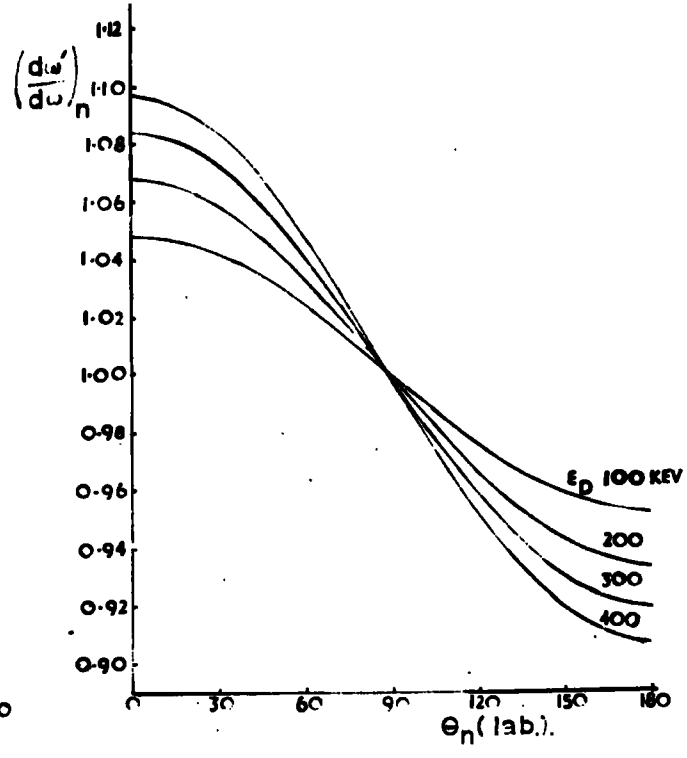

Fig.28 Ratio between the neutron C.O.M. and Lab. solid angles.(Benveniste & Zenger).

direction since most of the neutrons will be produced in the resonance region of the excitation function.

The mean neutron path length through the actual foil was also calculated; the expression used was derived as follows. In Fig. 29, let the diameter of the foil be R, the thickness d, and the distance from the disc to the point source S,D. Since D $>$ R and $>>$ d, edge effects of the disc were considered to be negligible.

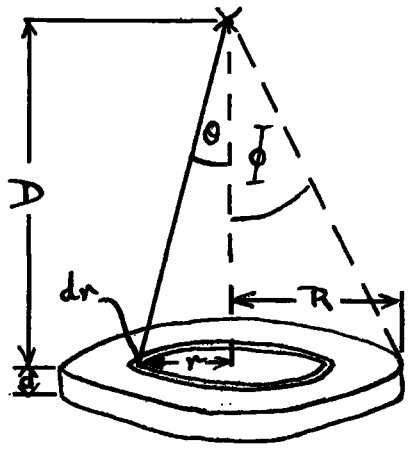

Fig. 29

Consider an annulus of the disc with radius r and width dr

Area of annulus = $2\pi r.dr.$

Apparent thickness of disc to neutron incident at an angle θ = $\frac{d}{\cos\theta}$.

The apparent volume of the annulus = $\frac{d}{\cos\theta} \cdot 2\pi r.dr.$

But $r = D \tan\theta$,

and $\frac{dr}{d\theta} = D \sec^2\theta$.

The apparent volume of whole disc (where ϕ is the semi-angle of the cone subtended by the disc at the target)

$$= \int_0^{\phi} \frac{d.2\pi r}{\cos\theta} \cdot D \tan\theta \cdot D \sec^2\theta \cdot d\theta .$$

The mean thickness of the disc to incident neutrons

$$= \frac{d. \int_0^{\phi} (\cos\theta)^{-4} \sin\theta \, d\theta}{\int_0^{\phi} (\cos\theta)^{-3} \sin\theta \, d\theta}$$

$$= \frac{2}{3} d \left[\frac{(\cos\phi)^{-3} - 1}{(\cos\phi)^{-2} - 1} \right] .$$

In general this correction added about 1% to the foil thickness.

The deuteron beam contained D_2^+ ions which were seen

from the α-recoil spectrum to contribute 15% to the total neutrons produced. Correction was made assuming that the reacting deuterons were incident at 70 keV which gave a correction of -1.6% on the calculated neutron yield in the forward direction.

Tritium decays to ^{3}He by β-decay with a 12.26y half-life and since the reaction $^{3}He + {}^{2}H = {}^{4}He + {}^{1}H$ gives rise to α-particles of similar energy to those from the DT process, errors could arise here. At 140 keV the cross section has been shown by Wandel et al.[58] to have a value of 80mb, while that for the DT reaction is 5000 mb; further, the ^{3}He contained in the targets is 10% or less of the ^{3}H content, therefore contributions from this reaction were considered to be negligible.

Protons from the D,D process were easily discriminated against with the ORTEC counter and the reactions studied by this method had threshold energies above the 3 MeV energy of these neutrons.

The error of this method is estimated to be 5%, arising mainly from uncertainties in the distribution of tritium in the target as mentioned above. The solid angles were measured to an accuracy of 1%.

b) D,D process

Irradiations here were, in general, carried out at 90° to the incident deuteron beam to reduce to a minimum the spread in neutron energy caused by the spread in the energy of the reacting deuterons (0 - 400 keV).

As was stated in Chapter 2 it was more convenient to count protons associated with the competing $^{2}H(d,p)\ ^{3}H$ reaction rather than the low energy ^{3}He particles associated with the neutrons produced in the $^{2}H(d,n)\ ^{3}He$ process. Thus if the proton detector subtended a solid angle $\Delta\Omega_p$ at the target the number of neutrons produced per proton counted is,

$$N = \left(\frac{4\pi}{\Delta\Omega_p}\right) R_p \left(\frac{Y_{d,n}}{Y_{d,p}}\right),$$

where R_p is the proton anisotropy factor and $(Y_{d,n}/Y_{d,p})$ is the ratio of the total neutron to proton yield. Values of these parameters were obtained from Ruby and Crawford[57] and are plotted in Fig. 30. In calculations the distribution of deuterium is assumed to be uniform. Deuterium in fact is being continuously replaced and will diffuse throughout the layer.

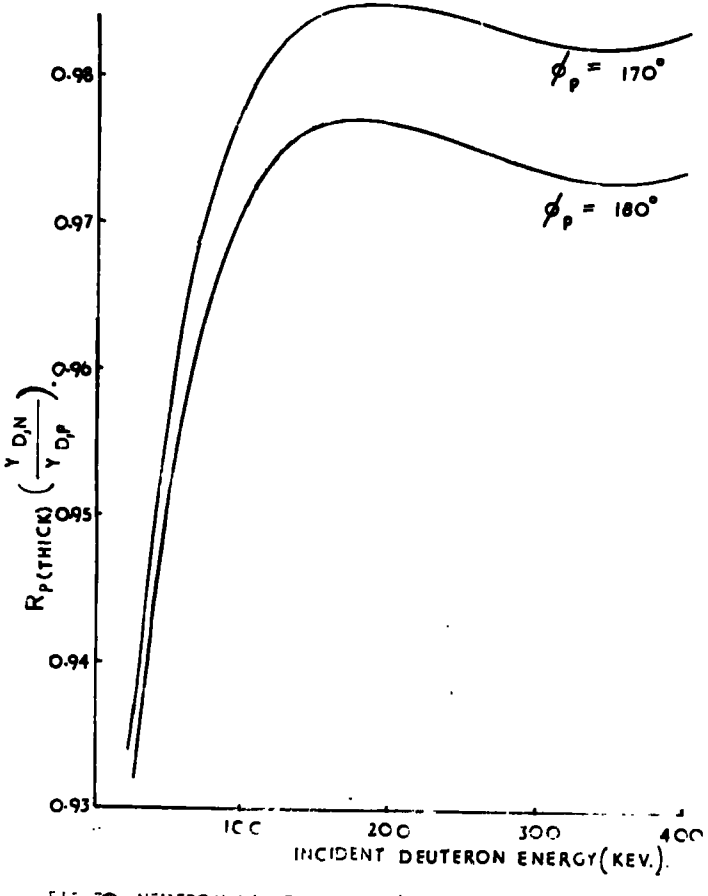

FIG. 30. NEUTRON YIELD CURVES (RUBY & CRAWFORD).

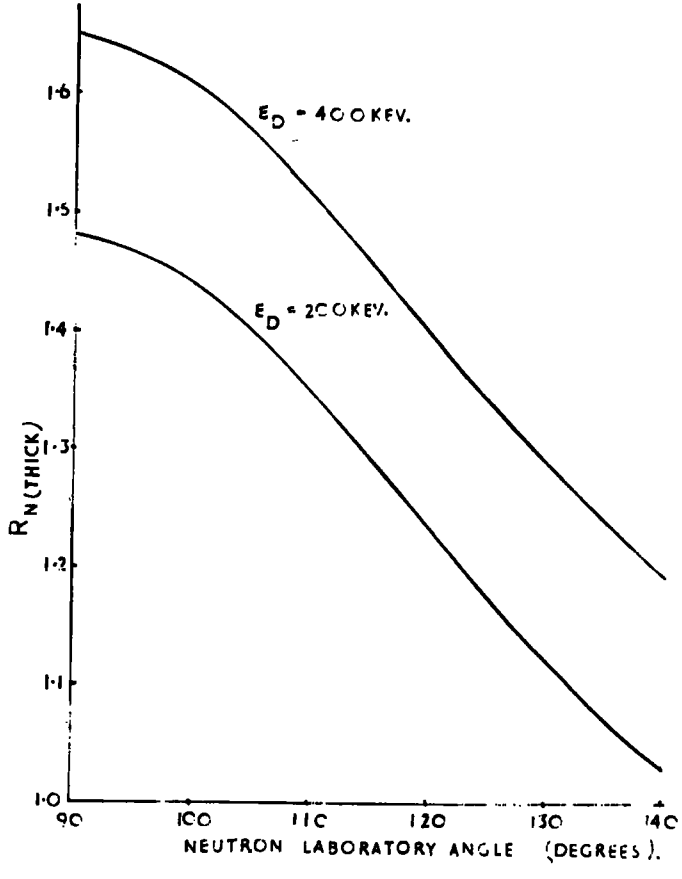

FIG. 31. CALCULATED NEUTRON YIELD.

Preston et al.[30] have shown that both branches of the DD process are anisotropic (to different extents) in the centre of mass system. They obtained an anisotropy dependence in the centre of mass system of the form

$$\frac{d\sigma(\theta)}{d\omega'} = \frac{d\sigma(90^\circ)}{d\omega'} \left[1 + A \cos^2\theta + B \cos^4\theta \right]$$

$$\simeq \frac{d\sigma(90^\circ)}{d\omega'} \left[1 + (A + B) \cos^2\theta \right],$$

where ω' is the solid angle in the centre of mass system (ω being the corresponding angle in the laboratory system), θ is the particle centre of mass angle and A and B are anisotropy constants. Values of A and B measured by Preston et al[30] at five different incident deuteron energies are plotted in Fig. 32. By drawing smooth curves through these points values of the sum (A + B) were estimated at intermediate energies, Fig. 33. Using the data of Tuck[59] for the total cross section the differential cross section at 90° was calculated from

$$\frac{d\sigma(90^\circ)}{d\omega^1} = \frac{\sigma}{\left[1 + (A + B)\cos^2\theta \right] d\omega^1}$$

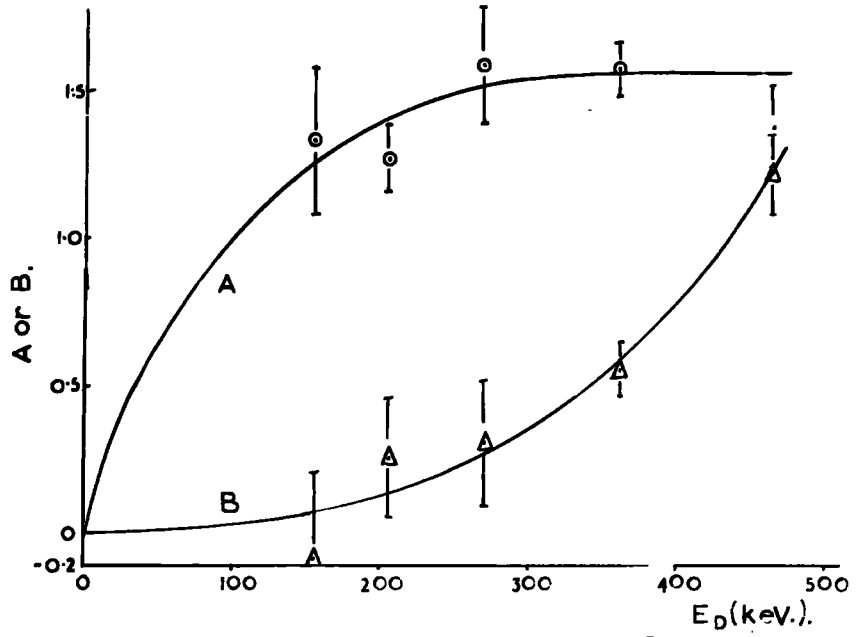

Fig. 32. Anisotropy constants for the D(d,n)^{3}He reaction, (Preston et al.).

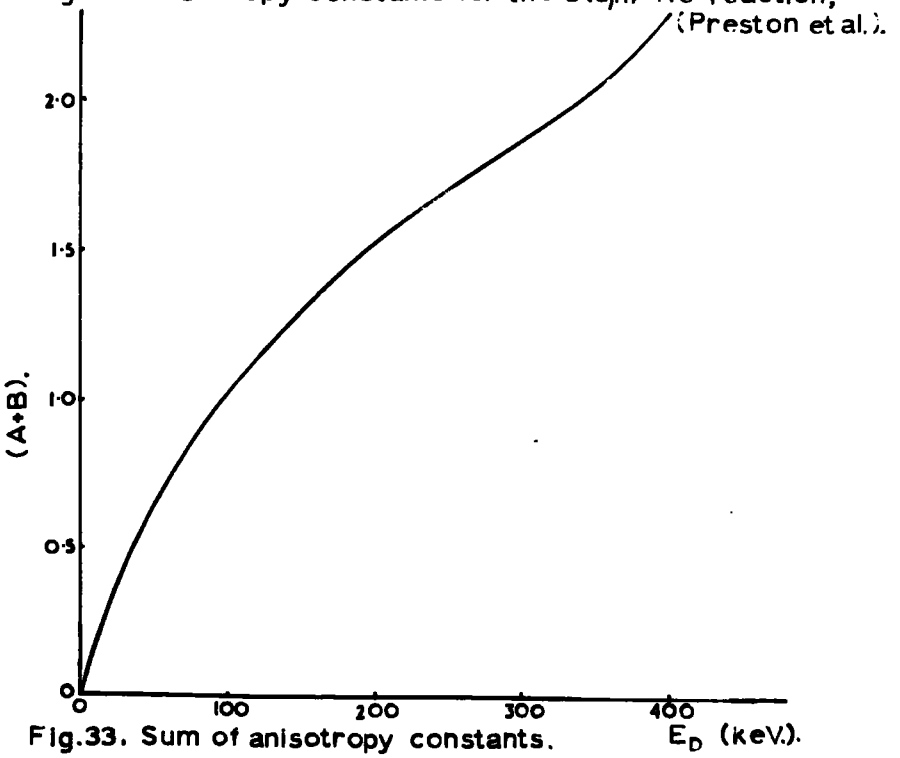

Fig. 33. Sum of anisotropy constants.

$$= \frac{\sigma}{4\pi\left[1 + \frac{1}{3}(A + B)\right]} .$$

Since the total cross section values for the D,D process rise almost linearly with incident deuteron energy in the range 0 – 400 keV, the incident deuteron energy was divided into eight 50 keV intervals and the values of $\frac{d\sigma(\theta)}{d\omega'}$ at 5° intervals from 90° - 140° were calculated for the mean of each energy interval. A plot of $\frac{d\sigma(\theta)}{d\omega'}$ against θ was then made for each mean energy and values corresponding to angles of 90° - 140° at 10° intervals in the laboratory system were interpolated. The values for each laboratory angle (ϕ) were then added together and their average ($\frac{d\bar{\sigma}(\phi)}{d\omega}$) calculated. The mean value for each laboratory angle was then divided into the mean total differential cross section to obtain the value of R_n (thick) for each laboratory angle for an incident deuteron energy of 400 keV.

$$R_n \text{ (thick) } \phi = \left(\frac{\left(\frac{\bar{\sigma}}{4\pi}\right)}{\left(\frac{d\bar{\sigma}}{d\omega}\right)_\phi} \right)_{0 - 400 \text{ keV.}}$$

A similar calculation was made for an incident energy of 200 keV to enable the contribution from D_2^+ ions to be made. The curves of R_n (thick) versus laboratory angle are shown in Fig. 31.

Samples irradiated at 90° were in the form of thin, narrow foils or as powder in narrow tubes arranged around the circumference of the target. The mean angle $\bar{\phi}$ and distance $\bar{R}$ of the sample from the target was calculated. The total neutron flux through the sample is then given by $N/(4\pi \bar{R}^2 . Rn(\bar{\phi}))$ neutrons cm^{-2}.

Chapter 4

Part 1.

Determination of the cross-sections of the nuclear reactions $^{56}Fe(n,p)^{56}Mn$ and $^{63}Cu(n,2n)^{62}Cu$ by the associated particle method.

Both the reactions,

$^{56}Fe(n,p)^{56}Mn$ ($t_{\frac{1}{2}}$ = 155 ± 1m)(Q = -2.926 MeV) and

$^{63}Cu(n,2n)^{62}Cu$ ($t_{\frac{1}{2}}$ = 9.9 ± 0.1m)(Q = -10.838 MeV),

have been widely used as reference reactions when comparative measurements have been made. Unfortunately the scatter in the published values, (see the compilation of Liskein and Paulsen[17]) is large, and therefore in the present work these cross-sections were measured absolutely by the associated particle method. All Q values quoted have been taken from Everling et al[61].

Experimental procedures.

a) Irradiation. Discs of iron (see Appendix A) and copper (Hopkin and Williams ltd., AnalaR grade), 2.1 cm in diameter, were irradiated 5 cm below the target in a light polythene holder. In this position the activating neutrons were almost monoenergetic, since, because of the resonance in the DT reaction, over 80 per cent lie within the energy range 14.8 ± 0.1 MeV with the incident deuteron energy of 145 KeV. In

four of seven runs, each of 30 - 60 minutes duration, and with tritium targets of different ages, the iron and copper were irradiated together in the form of a sandwich, and the ratio of the values of the cross-sections obtained (Table 5). Polystyrene discs, 13 mg cm^{-2} thick, were placed between the metals to prevent transfer of recoil nuclei between adjacent layers. The diameters of the foils and their separation from the tritium target segment were accurately measured so that the solid angle subtended at the sample could be calculated. The arrangement of the solid state counter, used to count the recoil α-particles from the DT reaction, has been previously described in Chapter 2.

b) Counting techniques.

(i) ^{56}Mn. The iron discs were dissolved in the standard acid mixture and counted in the liquid sample G.M. counter as described in Appendix A.

(ii) ^{62}Cu. ^{62}Cu emits positrons in 97.92% of its decays, and therefore the irradiated copper discs were sandwiched between aluminium plates thick enough to stop the positrons, and the resulting annihilation radiation was detected in coincidence by two $1\frac{1}{2}$" x 1" NaI(Tl) scintillation crystals, 4.5 cm apart, set on the 0.51 MeV photopeak. The coincidence count obtained was compared with that from a

standard ^{22}Na source, with the same dimensions, counted under exactly similar conditions.

Both channels were operated with a paralysis time of 5μs while the resolving time of the coincidence mixer was set at 2μs . The coincidence unit settings had been previously determined with the ^{22}Na source, and count rates were corrected for paralysis of single channels and the coincidence mixer, backgrounds, and random coincidences as described in Chapter 2.

The 9.9m decay of ^{62}Cu was corrected for the small contribution from 12.84h ^{64}Cu(which arises from the reaction $^{65}Cu(n,2n)$) by graphical curve stripping. Equations for the corrections to annihilation radiation coincidences for the nuclides are shown below, that for ^{22}Na being corrected for the contribution from the 1.28 MeV γ-ray, while the γ-rays occurring in only 0.5% of the ^{62}Cu decays were regarded as negligible. Values of the efficiencies used in calculations were taken from the data of Crotthamel[42] and absorption corrections were obtained from Davisson and Evans[62]. The following symbols are used in the expressions.

N_1 = observed count rate in channel 1(c.p.m).

No = actual disintegration rate of a source (d.p.m).

P_1 = probability of counting γ_1 in its photopeak and including corrections for absorption in the source and

absorbers.

T_1 = probability of γ_1 being counted by any absorption process (again absorption correction being made).

T_1^2 = probability of part of the spectrum of γ_1 being within the photopeak of γ_2.

β = percentage of decays of a nuclide by positron emission to a particular energy level of the daughter product.

$\frac{\omega}{4\pi}$ = the solid angle subtended by the source at a crystal.

^{22}Na.

0.51 MeV channels.

$$N_1 = N_2 = No\left[2\beta_1 P_{0.51}(1-T_{1.28})+\beta_1 T_{1.28}^{0.51}(1-2(T_{0.51}-P_{0.51}))+\beta_1 T_{1.28}^{0.51}\right].$$

Coincidence channel

$$N_{12} = No\left[2.\beta_1 (P_{0.51})^2 \frac{4\pi}{\omega}(1-T_{1.28})+T_{1.28}^{0.51}(1-(T_{0.51}-P_{0.51})\frac{4\pi}{\omega})2.\ {}_1P_{0.51}\right].$$

$$\beta_1 = 0.897.$$

^{62}Cu.

Coincidence channel

$$N_{12} = No\left[2.\beta_2 (P_{0.51})^2 \ \frac{4\pi}{\omega}\right].$$

$$\beta_2 = 0.9792.$$

The ratio between the counting efficiencies ($^{22}Na/62_{Cu}$)

$$= 0.993 \cdot \beta_1 / \beta_2$$

$$= 0.908.$$

The corrections indicated in Chapter 3 were applied in calculations of the cross-sections for the neutron flux obtained by the associated particle method.

Results and comparison with other work.

The measured values of the cross-sections together with the corrections made are shown in Tables 5 and 6.

The mean value of 98.3 ± 2.4 mb. at 14.8 ± 0.1 MeV for the $^{56}Fe(n,p)^{56}Mn$ reaction cross-section agrees well with that of 96.7 ± 4 mb obtained by Hemingway et al[25]. of this laboratory using helium measuring techniques. The only common factor between the two determinations was the liquid sample G.M. tubes which were calibrated together and used under identical conditions.

The disparity in the published values[17] may be partly explained by the fact that the energy of the neutrons used is not always clearly stated; the excitation function for the reaction determined by Terrel and Holm[63], Bormann et al.[64], and Santry and Butler[65] indicates a smooth variation with neutron energy, with a maximum at about 13.6 MeV. The

majority of the measurements lie within the range 80 - 120 mb and thus the value obtained here would appear to be at the centre of this distribution.

Chittenden et al.[66] have measured the combined cross-section for the reaction $^{57}Fe(n,np + n,d)^{56}Mn$ and obtained a value of 6.1 ± 2.6 mb at 14.8 MeV. The correction for the production of ^{56}Mn from ^{57}Fe in natural iron is therefore only 0.12%, which will not effect the result here since it is within the experimental error.

The scatter for the values of the cross-section for $^{63}Cu(n,2n)^{62}Cu$ is again large; at 14.5 Me V the values range between 482 ± 72 mb (Paul and Clarke[7]) and 647 ± 80 mb (Brolley et al.[67]). The value of 550 ± 6 mb at 14.8 MeV obtained here is in agreement with the recent work of Grimeland et al.[68] of 548 ± 10 mb at 14.8 MeV, and also with that of 550 ± 30 mb at 14.77 MeV which Glover et al.[69] took as the average of their own work and that of Ferguson and Thompson[70]. The excitation functions obtained by these last two groups show the cross-section rising smoothly in this energy region and thus values around 500 mb measured by several workers at 14.1 MeV would indicate a somewhat higher value at 14.8 MeV.

Estimation of error.

The errors quoted above were the standard errors of the

means of the values obtained; the actual errors are estimated as follows:- (1) Determination of neutron flux 5% (2) Calibration of the standard ^{22}Na source and liquid sample G.M. tube 2% (3) Counting statistics, ^{56}Mn, 1% and ^{62}Cu 2%. These give a total error of $\pm$ 5.5% for the $^{56}Fe(n,p)^{56}Mn$ cross-section and $\pm$ 6% for that of $^{63}Cu(n,2n)^{62}Cu$.

Run No.	No. of target nuclei $\times \frac{10^3}{N}$	Mean neutron path length $\times \frac{1}{d}$	Ao obs (c/m)	Ao count (d/m) $\times 10^{-4}$	S_α $\times 10^{-5}$	Ω_α (steread) $\times 10^6$	Ω_n (steread)	Sn $\times 10^{-10}$	Target and previous use (hours)	Cross section (mb)	Mean (mb)	$\frac{^{63}Cu(n,2n)\sigma}{^{56}Fe(n,p)\sigma}$	Mean Ratio
494	7.170	1.010	975	1.53	5.287	3.02	0.1277	2.789	1.5C	97.6		–	
502	7.172	1.010	888	1.39	4.599	3.02	0.1277	2.428	3.0C	102.2		–	
542	6.945	1.011	355	0.555	1.895	2.92	0.1202	0.9736	1.3A	104.5	98.3	5.27	5.71
554	7.092	1.011	758	1.19	3.942	3.02	0.1277	2.114	3.0C	102.9	±2.4	5.29	±0.08
600	7.077	1.010	709	1.11	4.547	3.33	0.1291	2.236	11.0E	91.3		6.04	
658	7.170	1.010	600	0.939	3.458	3.02	0.1277	1.855	7.5C	91.4		6.24	

Table 5. Results for the $^{56}Fe(n,p)^{56}Mn$ reaction.

R_α = 1.208, $(\frac{d\omega^1}{d\omega})_n$ = 1.05, D_2^+ corrtn. = 0.984, $\lambda^{56}Mn$ = 0.004472min^{-1}

N = Avogadro's No., Counter eff. for ^{56}Mn = 0.0767 Chemical Yield = 0.8333.

Run No.	No. of target nuclei $\times \frac{10^2}{N}$	Mean neutron path length $\times \frac{1}{d}$	Counting eff. (%)	Ao obs. (c/m)	Ao corrt. (d/m)	S_α $\times 10^{-4}$	Ω_α (sterad) $\times 10^6$	Ω_n (sterad)	S_n $\times 10^{-9}$	Target and previous use (hours)	Cross section (mb)	Mean (mb)
Table 6. Results for the $^{63}Cu(n,2n)^{62}Cu$ reaction.												
530	0.6959	1.014	0.321	635	1.98	5.531	2.92	0.1852	4.449	0.9A	535	
542	1.038	1.011	0.305	890	2.92	8.079	2.92	0.1202	4.151	1.3A	551	550 ± 6
554	1.381	1.010	0.299	2680	8.97	18.41	3.02	0.1277	9.876	3.0C	544	
600	1.381	1.010	0.289	2520	8.71	19.27	3.33	0.1291	9.374	11.0E	551	
658	1.381	1.010	0.283	1350	4.77	9.341	3.02	0.1277	5.010	7.5C	570	

$\lambda^{62}Cu = 0.07002 \ min^{-1}$.

Part 2.

Irradiation of ^{54}Fe.

Pure iron foil and granules, as normally used for the $^{56}Fe(n,p)\ ^{56}Mn$ reference reaction, were irradiated in order to check the value of 0.6 ± 0.1 mb obtained by Chittenden et al[66]. for the cross-section of the $^{54}Fe(n,t)^{52m}Mn$ reaction. A search was made for activity resulting from the $^{54}Fe(n,t)\ ^{52g}Mn$ reaction and an upper limit for the cross-section of this reaction was estimated.

The reactions studied were:-

$^{54}Fe(n,t)^{52m}Mn$ ($t_{\frac{1}{2}}$ = 21m) (Q = -12.795 MeV)

$^{54}Fe(n,t)^{52g}Mn$ ($t_{\frac{1}{2}}$ = 5.7d) (Q = -12.412 MeV)

$^{54}Fe(n,p)^{54}Mn$ ($t_{\frac{1}{2}}$ = 314d) (Q = +0.094 MeV)

$^{54}Fe(n,2n)^{53}Fe$ ($t_{\frac{1}{2}}$ = 8.9±0.1m) (Q = -13.620 MeV)

Half-life values (except that measured for ^{53}Fe) were taken from the Nuclear Data Sheets[71].

Experimental procedures.

In all the irradiations carried out, the cross-sections were measured relative to the $^{56}Fe(n,p)^{56}Mn$ reaction by dissolving the whole or part of the sample in the standard acid

solution, and counting the ^{56}Mn activity in a liquid sample G.M. tube. All samples were irradiated close up to the D,T target thus giving a neutron bombarding energy of 14.7 ± 0.5 MeV.

a) $^{54}Fe(n,t)^{52m}Mn$ and $^{54}Fe(n,2n)^{53}Fe$ reactions.

In a preliminary bombardment, iron granules were irradiated for 30 minutes, and then placed between two γ-ray scintillation crystals set on the 0.51 MeV photopeak and also connected in coincidence. The decay was followed and γ-ray spectra were taken from time to time on the Laben multichannel analyser. The coincidence channel revealed both an 8.9m activity and a 155m activity, but no 21m ^{52m}Mn. By using spectrum handling equipment, associated with the multichannel analyser, photopeaks ascribed to ^{54}Mn, ^{56}Mn and ^{53}Fe were observed, but none characteristic of ^{52m}Mn could be seen.

^{52m}Mn emits positrons in 92% of its decays (1% electron capture). These are in coincidence with a 1.434 MeV γ-ray to the ground state of ^{52}Cr. It was considered therefore, that by counting coincidence between two γ-ray scintillation crystals, one set on the 1.434 MeV photopeak and the other on the 0.511 MeV photopeak, the ^{52m}Mn activity would be counted preferentially in the coincidence channel.

Two irradiations were carried out; one in which a 2.1 cm

diameter iron foil (0.5g) and another in which 1 g of iron granules were irradiated close up to the target for 20 minutes. The samples were then sandwiched between aluminium plates to ensure annihilation of the positrons, and counted between a 3" x 3" and a $1\frac{1}{2}$" x 1" γ-ray scintillation crystal. The separation between the source and the can of the large and small crystal was 0.4 and 0.5 cm. respectively.

The large crystal was set to count the 1.434 MeV photopeak while the other was set on the 0.51 MeV photopeak. Both channels had a dead time of 10μs and the resolving time of the coincidence mixer was 0.3μs. This, and the delay between the two channels, was again previously determined using a ^{22}Na source since the decay scheme of the nuclide is similar to that of ^{52m}Mn. The decay of the sample was followed as described for 500 minutes.

The single and coincidence channels all showed a weak short lived component and a strong contribution from 155m ^{56}Mn. Unfortunately the large statistical scatter of the readings from the coincidence channel made these results unusable. Straight line plot analysis applied to both of the single channels, however, revealed a 20 minute component in the 1.434 MeV channel and a 9 minute component from the 0.511 MeV channel. The counting efficiences of the channels were determined by comparison of calculated efficiences (found

using the data of Crouthamel[42] and the absorption curves of Davisson and Evans[62]) with the experimental efficiency obtained for a standard ^{22}Na source counted under similar conditions. The threshold settings of the large crystal were reduced to include the 1.28 MeV photopeak of ^{22}Na.

Below are set out the 0.51 MeV and 1.434 MeV γ-ray channel equations for ^{53}Fe and ^{52m}Mn respectively. The corresponding equations for ^{22}Na together with the notation used have been previously described in Part 1 of this chapter.

0.51 MeV channel

^{53}Fe

$$N = No\Big[\, 2.\beta_1.\, P_{0.51} + 2.\beta_2.\, P_{0.51}\,(1 - T_{0.383})$$

$$+(2.\beta_3.\alpha_1.\, P_{0.51}\,(1 - T_{1.298}) + \beta_3.\alpha_1.\, T^{0.51}_{1.298}(1 - 2(T_{0.51} - P_{0.51}))$$

$$+(2.\beta_3.\alpha_2.\, P_{0.51}\,(1 - T_{0.915})(1 - T_{0.383})$$

$$+\beta_3.\alpha_2.\, T^{0.51}_{0.915}\,(1 - T_{0.383})(1 - 2(T_{0.51} - P_{0.51}))\Big]\,,$$

$$\beta_1 = 0.495, \qquad \beta_2 = 0.37, \qquad \beta_3 = 0.11$$

$$\alpha_1 = 0.45, \qquad \alpha_2 = 0.55.$$

where α is the percentage of decays from an energy level via a particular γ-ray.

The calculated efficiency for ^{53}Fe from comparison with ^{22}Na was 0.0625.

1.434 Mev channel

^{52m}Mn

$$N = No\left[\delta_1 P_{1.434}(1 - 2 T_{0.51}\beta_1) + (\delta_2 P_{1.434}(1 - T_{1.51})(1 - 2 T_{0.51}\frac{\beta_2}{\delta_2}) + (\delta_3 P_{1.434}(1 - T_{0.7})(1 - T_{1.02})\right]$$

$\beta_1 = 0.92, \quad \beta_2 = 0.015$

$\delta_1 = 0.93, \quad \delta_2 = 0.02, \quad \delta_3 = 0.03$

where δ is the percentage of decays of a nuclide by positron emission and electron capture events to a particular energy level of the daughter product.

The calculated efficiency for ^{52m}Mn from comparison with ^{22}Na was 0.0405.

b) $^{54}Fe(n,t)^{52g}Mn$ and $^{54}Fe(n,p)^{54}Mn$.

After the decay of ^{56}Mn, the long lived activities which remain in a manganese source prepared from iron irradiated with 14 MeV neutrons are ^{52g}Mn (5.7d) and ^{54}Mn (314d). Since ^{52g}Mn emits positrons in 29% of its decays, the remaining 71% being electron capture events, while ^{54}Mn decays entirely by

electron capture, under an end-window counter the former will be counted with the greater efficiency.

Two runs were carried out in which about 2.5g of iron granules were irradiated close to the target for 90 minutes. After an irradiation the granules were thoroughly mixed and 0.5g taken for use as the monitor. The remainder were treated as described below.

Carrier solutions.

Manganese and chromium carrier solutions were prepared by dissolving 'AnalaR' grade $MnCl_2 . 4 H_2O$ and $CrCl_3 . 6 H_2O$ in water to give concentrations of about 5 mg ml^{-1}.

Isolation of manganese.

Step 1. The irradiated iron granules were placed in a beaker together with 2 ml of each of the carrier solutions, and dissolved on heating with concentrated hydrochloric and nitric acids.

Step 2. A few drops of hydrogen peroxide were added to ensure complete oxidation of the iron to iron (III) and the solution was evaporated to a small volume. It was then made up to 30 ml and adjusted to 8N in hydrochloric acid.

Step 3. Four extractions with di-isopropyl ether (previously equilibrated with 8N hydrochloric acid) were carried

out to remove the iron. On testing with potassium thiocyanate the aqueous phase was found to be free of iron. The organic phase was discarded.

Step 4. The aqueous phase was heated on a water bath to remove ether and then evaporated to reduce the volume. Sodium hydroxide was added to the hot solution followed by hydrogen peroxide to precipitate manganese dioxide.

Step 5. The manganese dioxide was washed with water, dissolved in concentrated nitric acid and hydrogen peroxide, and reprecipitated from a boiling solution on the addition of excess potassium chlorate. The precipitate was washed and mounted on a glass filter pad in the usual way.

Counting techniques.

The manganese sources were counted under an end-window proportional counter and the decay followed for several weeks. No component with a half-life of 5.7d was observed, the only activities present being those of ^{56}Mn (155m) and ^{54}Mn (314d). A typical decay curve is shown in Fig. 34. The efficiency of the counter for ^{52g}Mn and ^{54}Mn was calculated using the method of Bayhurst and Prestwood[46] and an upper limit was estimated for the cross-section of the reaction $^{54}Fe(n,t)^{52g}Mn$ together with an estimate of the value of the cross-section for the

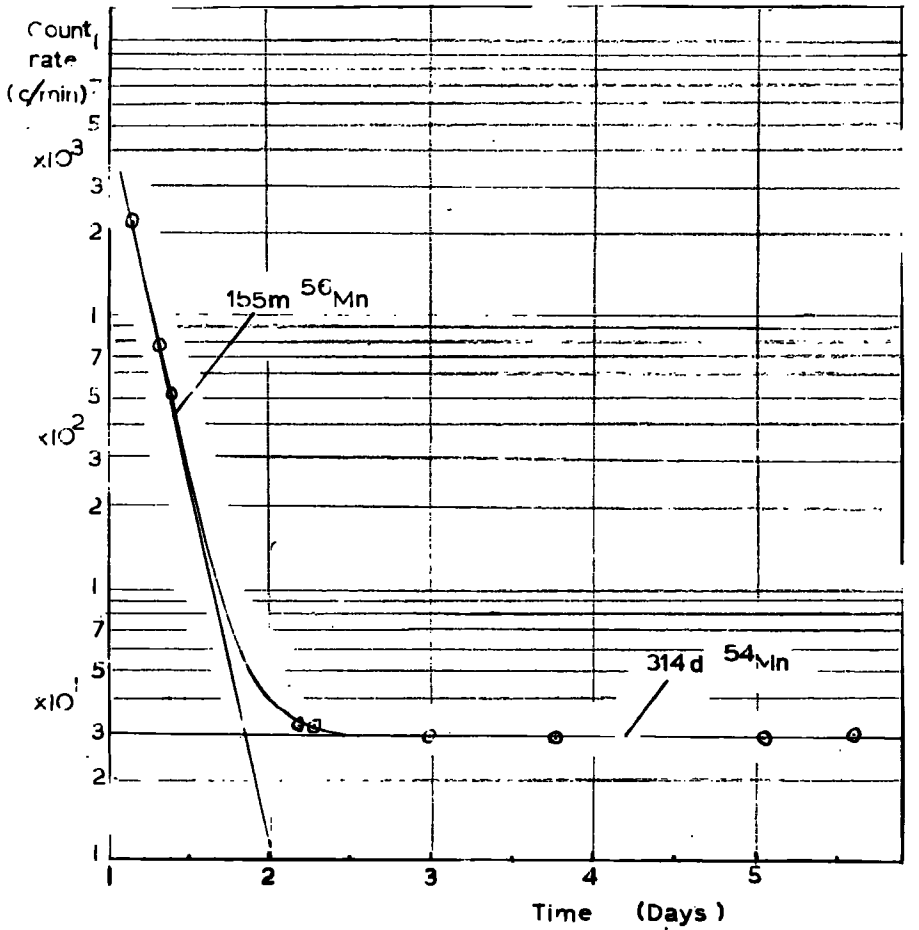

Fig. 34. Decay curve of manganese activity.

reaction $^{54}Fe(n,p)^{54}Mn$.

Results and comparison with other work.

The values of the cross-sections measured are presented in Tables 7 to 11. The value obtained for the $^{54}Fe(n,t)^{52m}Mn$ cross-section of 2.66 ± 0.42 mb is higher than, but of the same order as, that found by Chittenden et al[66] of 0.6 ± 0.1 mb. These workers irradiated $^{54}Fe_2O_3$ (96.66% ^{54}Fe) and followed the decay of the resulting activities on an end-window proportional counter.

Other values reported in the literature are some two orders of magnitude smaller. Baerg and Bowes[72] found an upper limit of 75 μb at 14 MeV for the reaction leading to the ground state while Heinrich and Tanner[22], using tritium measuring techniques, obtained a value of 120 μb at 16 MeV for the combined reaction to both states. These are lower than the upper limit for the cross-section of the reaction leading to the ground state of ^{52}Mn (estimated as $\leq$ 0.31 mb).

The spins of the excited and ground states of ^{52}Mn are 2 and 6 respectively and therefore it is surprising that the lower spin state appears to have the higher cross-section.

Possible explanations for the discrepancy are poor counting statistics (the count rate of ^{52m}Mn was less than 5%

of the background count rate of ^{56}Mn), or a contribution from the activity of ^{53}Fe. The decay scheme of ^{53}Fe from the Nuclear Data Sheets[71] includes a low percentage of high energy γ-rays which might have been detected inthe 1.430 MeV channel. However, standard γ-ray spectra[43] of ^{53}Fe do not show photopeaks corresponding to these γ-rays.

A straight line plot analysis of the decay curves was carried out using both 9 minute and 21 minute half-lives corresponding to ^{53}Fe and ^{52m}Mn; a typical pair is shown in Fig. 35 and Fig. 36. The curved portion of the curve obtained when the 9 minute half-life was used indicates that this value is too short while that obtained with the 21 minute half-life is reasonably straight. This would indicate that only a very small proportion of the count rate attributed to ^{52m}Mn can be due to ^{53}Fe.

The large negative Q values for the (n,nd) reactions eliminate any contribution from this process at this energy.

The value for the ^{54}Fe(n,2n)^{53}Fe cross-section of 8.90 $\pm$ 0.03 mb obtained here is supported by other workers; Depray et al.[74] (7 $\pm$ 0.7 mb at 15 MeV.), Chittenden et al.[66] (7.9 $\pm$ 0.8 mb at 14.8 MeV), Allan[75] (10 $\pm$ 4 mb), Neuert and Pollehn[76] (11 $\pm$ 1.5 mb) and Carles[77] (10 $\pm$ 5.6 mb) all at 14 MeV. The value of 14.4 $\pm$ 0.3 mb at 15 MeV obtained by Rayburn[78] appears to be rather high.

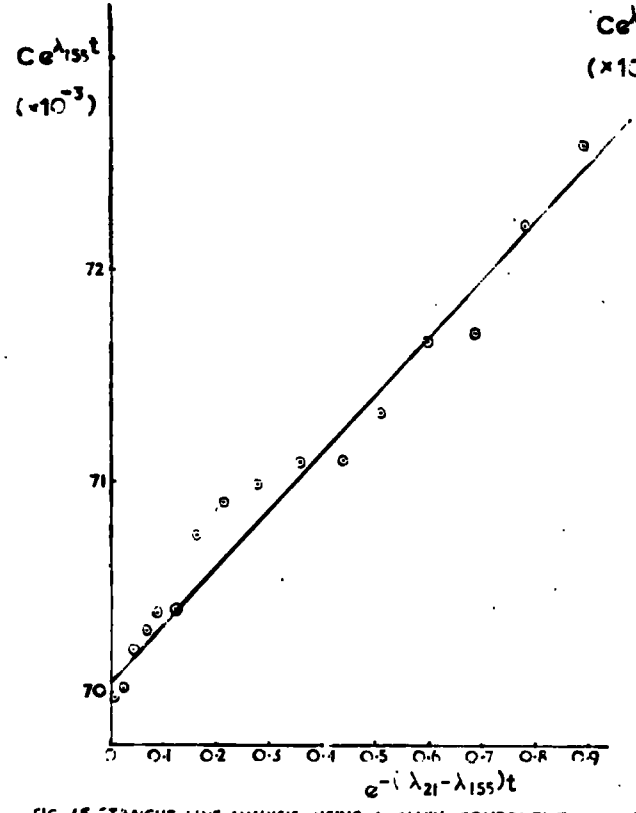

FIG. 35 STRAIGHT LINE ANALYSIS USING A 21 MIN. COMPONENT.

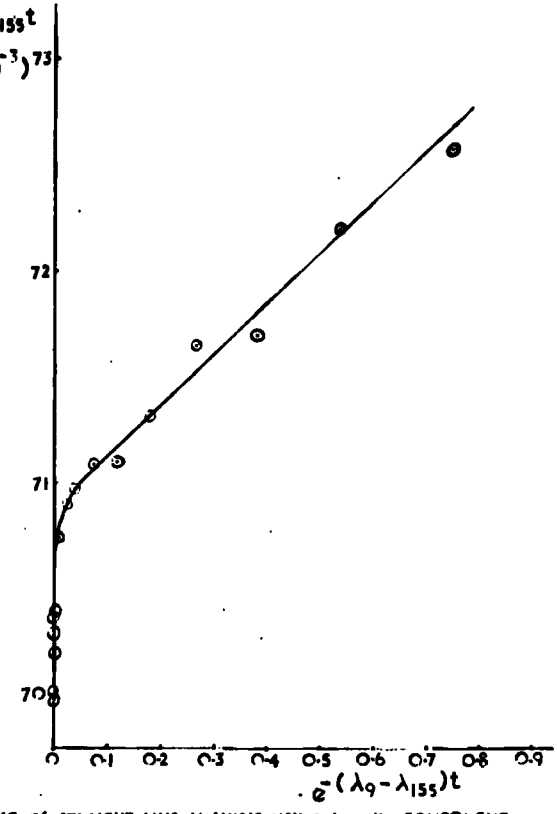

FIG. 36 STRAIGHT LINE ANALYSIS USING A 9 MIN. COMPONENT.

The rough estimate of 371 ± 40 mb for the value of the $^{54}Fe(n,p)^{54}Mn$ cross-section is in approximate agreement with the values of Allan[79] (382 ± 13 mb at 14 MeV) and March and Morton[80] (376 ± 50 mb at 13.5 MeV) both using nuclear emulsion techniques. The direct measurements of Storey et al[81] gave 333 ± 67 mb at 14 MeV and 561 ± 112 mb at 15.7 MeV. The values of Pollehn and Neuert[77] (254 ± 28 mb at 14.1 MeV), Cross et al.[82] (310 ± 25 mb at 14.5 MeV) and Martin and Martin[83] (291 ± 18 mb at 14.7 MeV), all measured using activation techniques, are lower than that obtained here.

Estimation of errors.

The reactions were measured relative to a value of the $^{56}Fe(n,p)^{56}Mn$ cross-section which had an estimated error of ± 5.5%. In the case of the $^{54}Fe(n,t)^{52m}Mn$ cross-section errors of up to ± 15% were possible from the graphical analysis of the decay data excluding the effect of any contaminating activity as mentioned above. The error in the estimation of the efficiency of the 1.484 MeV γ-channel should not be more than ± 10%. The error on this value should not therefore be more than ± 20%.

No 5.7d activity from the decay of the ground state of ^{52}Mn was observed and the upper limit for the cross-section quoted has an estimated error of ± 50%.

The ^{53}Fe activity from the $^{54}Fe(n,2n)^{53}Fe$ reaction was measured relative to a standard ^{22}Na source. The error in the standardisation of this source was $\pm$ 2% and the total error in the comparison should not be more than $\pm$ 5%. The graphical analysis made should have an error of less than 2%. This gives a total of $\pm$ 7% for the cross-section.

The value of the cross-section for the $^{54}Fe(n,p)^{54}Mn$ may be in error by up to 50% arising from the weak intensity of the activity, (only twice background), and the estimation of the efficiency of the proportional counter for the γ-rays of ^{54}Mn.

Irrad No.	No. of target nuclei x N^{-1}	Chemical Yield (%)	Counter Eff.	Ao Obs. (c.p.m.)	Ao correct (d.p.m.)	S x 10^{-6}	Measured cross section (mb)	Mean

Table 7. Data for reference reaction $^{56}Fe(n\ p)^{56}Mn$.

K71	7.036×10^{-3}	83.33	0.0767	3.36×10^{5}	5.26×10^{6}	3.60		
K74	1.674×10^{-2}	39.42	0.0767	1.99×10^{5}	6.60×10^{6}	1.51		
K77	3.290×10^{-2}	11.12	0.0767	2.75×10^{5}	3.23×10^{7}	4.49		
K78	3.356×10^{-2}	0.9782	0.080	1.81×10^{4}	2.31×10^{7}	3.20		

N is Avogardro's No. $\lambda Mn^{56} = 0.004472\ min^{-1}$ $Fe^{56}(n,p)Mn^{56} = 98.3$ mb

Table 8. Results for $^{54}Fe(n,t)^{52m}Mn$.

K71	4.483×10^{-4}	100	0.041	1,790	4.37×10^{4}	2.79	2.24	
K74	1.067×10^{-3}	100	0.041	2,690	6.56×10^{4}	1.14	3.08	2.66 ± 0.42

$\lambda Mn^{52m} = 0.03301\ min^{-1}$

Table 9. Results for $^{54}Fe(n,2n)^{53}Fe$.

K71	4.483×10^{-4}	100	0.0625	1.80×10^{4}	2.88×10^{5}	1.95	8.92	
K74	1.067×10^{-3}	100	0.0621	2.13×10^{4}	3.43×10^{5}	0.781	8.87	8.90 ± 0.03

$\lambda^{53}Fe = 0.07789\ min^{-1}$

Irrad. No.	No. of target nuclei x N^{-1}	Chemical Yield (%)	Counter eff.	Ao. obs. (c.p.m.)	Ao. correct (d.p.m.)	S x 10^{-6}	Measured cross section (mb)	Mean
Table 10. Results for $^{54}Fe(n,t)^{52g}Mn$.								
K77	2.096×10^{-3}	86.7	0.10	< 10	< 115	5.45	< 0.24	< 0.31
K78	2.138×10^{-3}	76.3	0.10	< 10	< 130	3.89	< 0.38	
$\lambda\ ^{52g}Mn = 0.00008445\ min^{-1}$.								
Table 11. Results for $^{54}Fe(n,p)^{54}Mn$.								
K77	2.096×10^{-3}	86.7	0.015	38	4400	5.47	331	371 ± 40
K78	2.138×10^{-3}	76.3	0.015	30	3932	3.91	412	
$\lambda\ ^{54}Mn = 1.533 \times 10^{-5}\ min^{-1}$.								

Part 3.

Irradiation of oxygen, nitrogen and fluorine.

The reactions studied were:-

^{14}N (n,2n) ^{13}N ($t_{\frac{1}{2}}$ = 10.0 ± 0.1m) Q = -10.553 MeV.

^{19}F (n,2n) ^{18}F ($t_{\frac{1}{2}}$ = 110 ± 3m) Q = -10.442 MeV.

^{16}O (n,p) ^{16}N ($t_{\frac{1}{2}}$ = 7.35s) Q = -9.626 MeV.

The half lives of ^{13}N and ^{18}F were measured, the values obtained being shown above; all the decay schemes and the half life of ^{16}N, were taken from the Nuclear Data Sheets[71].

An accurate knowledge of the values of cross-sections of nuclear reactions induced by neutrons in oxygen and nitrogen is required in nuclear reactor technology. The more important of these in this field are ^{16}O (n,p) ^{16}N and ^{14}N (n,2n) ^{13}N, both of which have been measured here.

Since ^{16}N has a short half-life coupled with a complex decay scheme it was decided to compare the count rates obtained from ^{13}N and ^{16}N on irradiation of a foil containing both nitrogen and oxygen. By irradiating and counting different thicknesses the actual ratios of activities should be obtained by extrapolation to zero thickness of foil, and thus the relative values of the cross-sections could be cal-

culated. The ^{14}N (n,2n) ^{13}N cross-section was first measured relative to the ^{56}Fe (n,p)^{56}Mn reaction, a value for the $^{19}F(n,2n)^{18}F$ cross-section being arrived at in the process.

Foils of cellulose nitrate of thicknesses 0.003", 0.004" and 0.005" were obtained from B.X. Plastics Ltd., and sent to the Microanalytical Laboratories, Oxford, for analysis of hydrogen, carbon and nitrogen. The result of the analysis is shown in Table 12, the values for oxygen being obtained by difference. The mean values for the three samples were used in calculations.

Table 12. Analysis of cellulose nitrate foil.

Foil thickness (0.001")	% content C	H	N	O
3	39.06	4.93	8.48	47.53
4	39.98	5.12	8.54	46.36
5	39.73	5.11	8.56	46.60
Mean	39.59±0.28	5.05±0.06	8.53±0.03	46.83±0.40

Measurement of $^{14}N(n,2n)^{13}N$ and $^{19}F(n,2n)^{18}F$ reaction cross-sections.

Although ^{13}N is a pure positron emitter (100% β^+), the low activity obtained from the irradiation of cellulose nitrate prevented a direct comparison with a standard ^{22}Na source, by

counting annihilation γ-ray coincidences. ^{18}F was therefore used as a secondary standard, since this is also a pure positron emitter (97% β^+, 3% E.C.), and can be obtained in high activities from the $^{19}F(n,2n)^{18}F$ reaction.

Direct comparison of ^{13}N and ^{18}F activities was made on a single scintillation crystal set to count the annihilation photopeak, the strength of the ^{18}F source being determined relative to a standard ^{22}Na source by coincidence techniques.

Experimental procedures.

Discs of cellulose nitrate, Teflon ($(C_2 F_4)_n$), and iron, 2.1 cm in diameter were irradiated as a stacked foil 2.5 cm below the target block in a light polythene holder. The energy of the activating neutrons was taken as 14.8 $\pm$ 0.1 MeV. Seven irradiations of 30 minutes duration were made.

After the irradiation the iron discs were dissolved in dilute hydrochloric acid and made up to 25 ml of which 10 ml was counted in a calibrated liquid sample G.M. tube as described in Appendix A.

The cellulose nitrate discs were sandwiched between aluminium absorbers and placed 0.5 cm from a 1½" x 1" NaI(Tl) scintillation crystal spectrometer set on the 0.51 MeV photopeak. The decay of ^{13}N was followed for 6 half-lives, after

which the discs of cellulose nitrate were replaced by one of Teflon, and the ^{18}F from this counted under identical conditions. No activities other than ^{13}N and ^{18}F were observed in the sources.

The Teflon disc and absorbers were subsequently counted between two $1\frac{1}{2}$" x 1" scintillation crystals both set on the 0.51 MeV photopeak, their separation being 4.2 cm. Comparison was made with the coincidence rate of a standard ^{22}Na source, counted under identical conditions. The delay and mixer resolving time of the coincidence unit were previously determined using the ^{22}Na source.

Correction was made to the coincidence rates for background, random coincidences, and single channel and mixer dead time as described in Chapter 2. The coincidence equation for ^{18}F is identical with that for ^{62}Cu, except for the substition of the value of β_2 (here 0.97), as is set out together with the equation for ^{22}Na, in Part 1 of this Chapter. The measured ratio between the counting efficiences ($^{22}Na/^{18}F$) was 0.916.

Results and comparison with other work.

The values of the cross-sections measured are shown in Tables 13 to 15. In calculating the mean value for the

$^{14}N(n,2n)^{13}N$ cross-section the value of 8.98 mb from irradiation 3 has been ignored since it is more than five standard deviations from the mean of the remainder of the set. No explanation can be offered to cover this disparity.

Table 16 shows the values for cross-sections found in the literature together with those of the present work; 7.42 ± 0.47 mb for $^{14}N(n,2n)^{13}N$ and 52.1 ± 3.3 mb for $^{19}F(n,2n)^{18}F$. From the reported excitation function of both reactions[90] the value of the cross-sections can be seen to rise rapidly over the neutron energy range 14 - 15 MeV; care is therefore necessary in quoting neutron energies. Both values for the cross-sections measured here lie towards the centre of the scatter of quoted values (some of these having large errors) and agree closely with the work of Rayburn[79] who used similar techniques. His values were measured relative to 503 mb for the $^{63}Cu(n,2n)^{62}Cu$ cross-section at 14.4 MeV which is lower than that indicated by the present value of 550 mb at 14.8 MeV. A somewhat higher value for both cross-sections would therefore be expected on extrapolation to 14.8 MeV. The ratio of the cross-sections agrees within the errors with that found by Rayburn[79] and Cevolani and Petralia[24].

Estimation of errors.

The errors quoted in Tables 14 and 15 are standard errors

of the means of the results. The actual errors were estimated as follows:- (1) $^{56}Fe(n,p)^{56}Mn$ reference cross-section 5.5%; (2) standard ^{22}Na source 2%; (3) graphical decay analysis 1%; (4) nitrogen content of the sample 0.5%. This gives a total error of $\pm$ 6.3% for both cross-section values.

Irrad. No.	No. of target Nuclei $\times \frac{10^3}{N}$	Ao obs. c.p.m.	Ao corrt. d.p.m. $\times 10^{-4}$	S $\times 10^{-5}$

Table 13. Data for the reference reaction $^{56}Fe(n,p)^{56}Mn$.

1	6.996	2110	6.53	10.83
2	7.060	1110	3.43	5.015
3	7.070	5050	15.6	18.70
4	7.060	2100	6.49	7.484
5	7.047	730	2.26	2.888
6	7.080	706	2.18	2.550
7	7.031	1180	3.65	4.192

$^{56}Fe(n,p)^{56}Mn$ σ = 98.3 mb. N = Avogardro's No.

Counter Efficiency = 0.0767 x 1.055 = 0.0809

Dilution factor = 0.4 $\lambda^{56}Mn$ = 0.004472 min^{-1}

Irrad. No.	No. of target nuclei $\times \frac{10^3}{N}$	Counter eff. (%)	Ao obs. c.p.m.	Ao corrt. d.p.m.	S $\times 10^{-5}$	Measured cross section (mb)	Mean

Table 14. Results for the $^{14}N(n,2n)\ ^{13}N$ reaction.

1	3.807	6.53	1140	1.74×10^4	4.525	7.40	
2	3.806	6.54	652	9.97×10^3	2.163	7.93	
3	3.809	6.88	2930	4.26×10^4	6.694	(8.98)	7.42 $\pm$0.13
4	3.808	7.08	1230	1.74×10^4	3.304	7.14	
5	3.780	7.20	414	5.75×10^3	1.222	7.11	
6	3.780	7.19	368	5.12×10^3	0.9310	7.64	
7	3.778	7.30	731	1.00×10^4	1.862	7.29	

$$\lambda^{13}N = 0.06932 \text{ min}^{-1}$$

Table 15. Result s for the $^{19}F(n,2n)\ ^{18}F$ reaction.

1	35.46	0.152	371	2.44×10^5	10.55	53.8	
2	35.46	0.158	201	1.27×10^4	4.887	53.7	
3	35.46	0.154	855	5.55×10^5	18.14	51.9	52.1 $\pm$ 0.6
4	35.46	0.157	353	2.25×10^5	7.297	50.3	
5	35.45	0.159	131	8.24×10^4	2.813	52.9	
6	35.46	0.159	123	7.74×10^4	2.467	52.0	
7	35.45	0.160	203	1.26×10^5	4.089	49.8	

$$\lambda^{18}F = 0.006189 \text{ min}^{-1}$$

Table 16. Collected values of cross-sections for the $^{14}N(n,2n)^{13}N$ and $^{19}F(n,2n)^{18}F$ reactions.

$^{14}N(n,2n)^{13}N$ σ (mb)	$^{19}F(n,2n)^{18}F$ σ (mb)	Neutron energy (MeV)	Ratio $\frac{\sigma_F}{\sigma_N}$	Reference
3.4 ± 1	–	14.0	–	Dudley et al.[84].
5.4 ± 0.46	38.9 ± 2.3	14.1	7.2	Cevolani and Petralia[24].
5 ± 1	43 ± 4	14.3	8.6	Heertze et al.[85].
5 ± 1	60 ± 20	14.0	12.0	Brill et al.[86].
5.67 ± 0.85	60.6 ± 18.2	14.7	10.7	Paul and Clarke[7].
5.18 ± 0.6	–	13.77	–	Ferguson[70].
8.69 ± 0.9	–	14.74	–	Ferguson[70].
7.41 ± 0.59	51.9 ± 3.7	14.4	7.0	Rayburn[79].
–	56 ± 7	14.18	–	Picard and Williamson[88].
–	66 ± 15	14.5	–	Williamson[89].
8.38 ± 0.17	–	14.8	–	Grimeland et al.[68].
6.3 ± 0.4	41.2 ± 2.2	14.1	6.6	Bormann et al.[90].
8.7 ± 0.7	60.2 ± 2.2	15.2	6.9	Bormann et al.[90].
19 ± 10	62 ± 9	14.1	3.3	Ashby et al.[91].
7.42 ± 0.47	52.1 ± 3.3	14.8	7.0	Present work.

B. Measurement of the $^{16}O(n,p)\ ^{16}N$ reaction cross-section.

Experimental procedures.

Various thicknesses of cellulose nitrate in the form of 2.1 cm diameter discs were irradiated for ten minute periods 1.5 cm below the target block. This arrangement gave an effective activating neutron energy of 14.8 ± 0.1 MeV. After irradiation they were transported by pneumatic tube to the counting room. The total time for transfer and for placing the discs under a counter was 10 seconds.

The discs were supported on a 1 mg cm^{-2} Mylar film stretched over a 5 cm diameter hole cut in a normal source shelf and counted between two opposing end-window proportional counters connected in parallel. These had previously been selected as having the same operating voltage. Since the counters were fitted with thin (100 μ g cm^{-2}) VYNS windows, and together subtended a solid angle of 3.3 π steradians it was assumed that backscattering effects would be eliminated and any decay scheme coincidence effects minimised.

During an irradiation the variations in the neutron flux were followed using the ORTEC solid state counter (since this was more stable than the plastic scintillation neutron monitor); counts were fed to a scaler and recorded at short time intervals by a camera operated by a quartz crystal timer. Eight one

minute time intervals were followed by twenty of six seconds. The camera operated in 1.2 seconds during which time the scaler was stopped. It was assumed in calculations that the neutron flux remained constant over each complete cycle of the camera.

The activity of the ^{16}N and ^{13}N detected on the twin proportional counters was similarly recorded by the camera with periods of six seconds initially, then increasing gradually to six minutes.

The decay data were analysed by the straight line plot method with the aid of an Elliott 803 computer; the programme used was kindly lent by Professor G. R. Martin.

Twenty four irradiations were carried out at six different thicknesses.

In order to obtain some indications of any trend in the variation of the measured value of the ^{16}O cross-section due to absorption of the radiations of ^{16}N and ^{13}N in the source and supports the following absorption measurements were made.

^{16}N. It was inconvenient to carry out absorption measurements on ^{16}N directly because of its short half life. Therefore experiments were made on ^{42}K which, like ^{16}N, decays with the emission of some β-particles of high maximum energy. The

mean β -particle energies are ^{16}N, 2.75 MeV and ^{42}K, 1.55 MeV.

A solution containing ^{42}K was evaporated on a 1 mg cm^{-2} Mylar film supported on a 4π -ring and counted between the twin proportional counters with and without sheets of cellulose nitrate placed on either side. Correction was made for the decay of ^{42}K ($t_{\frac{1}{2}}$ = 12.45 h) during the measurement. The source (3.96 mg cm^{-2}), support (1 mg cm^{-2}) and air gap (0.6 mg cm^{-2}) gave a mean thickness of 3.1 mg cm^{-2} to the β-particles at zero added absorber thickness.

^{13}N. A suspension of dicyanamide ($C_2H_4N_4$) in benzene was evaporated at the centre of a Mylar film supported on a Perspex '4π -ring'. The dicyanamide was 'fixed' with a drop of cellulose nitrate dissolved in acetone. The sample was irradiated for periods of 20 minutes and counted between the two proportional counters as described above. No activity with a half life other than that of 10 minutes corresponding to ^{13}N was observed. The source (2.4 mg cm^{-2}), support (1 mg cm^{-2}) and air gap (0.6 mg cm^{-2}) gave a mean thickness of 2.3 mg cm^{-2} to the βparticles at zero added absorber thickness.

The absorption curves obtained are shown in Fig. 37a, the values having been normalized to 100% at zero absorption. Fig. 37b. shows the variation of the ratio of ^{13}N absorption to ^{42}K absorption with foil thickness.

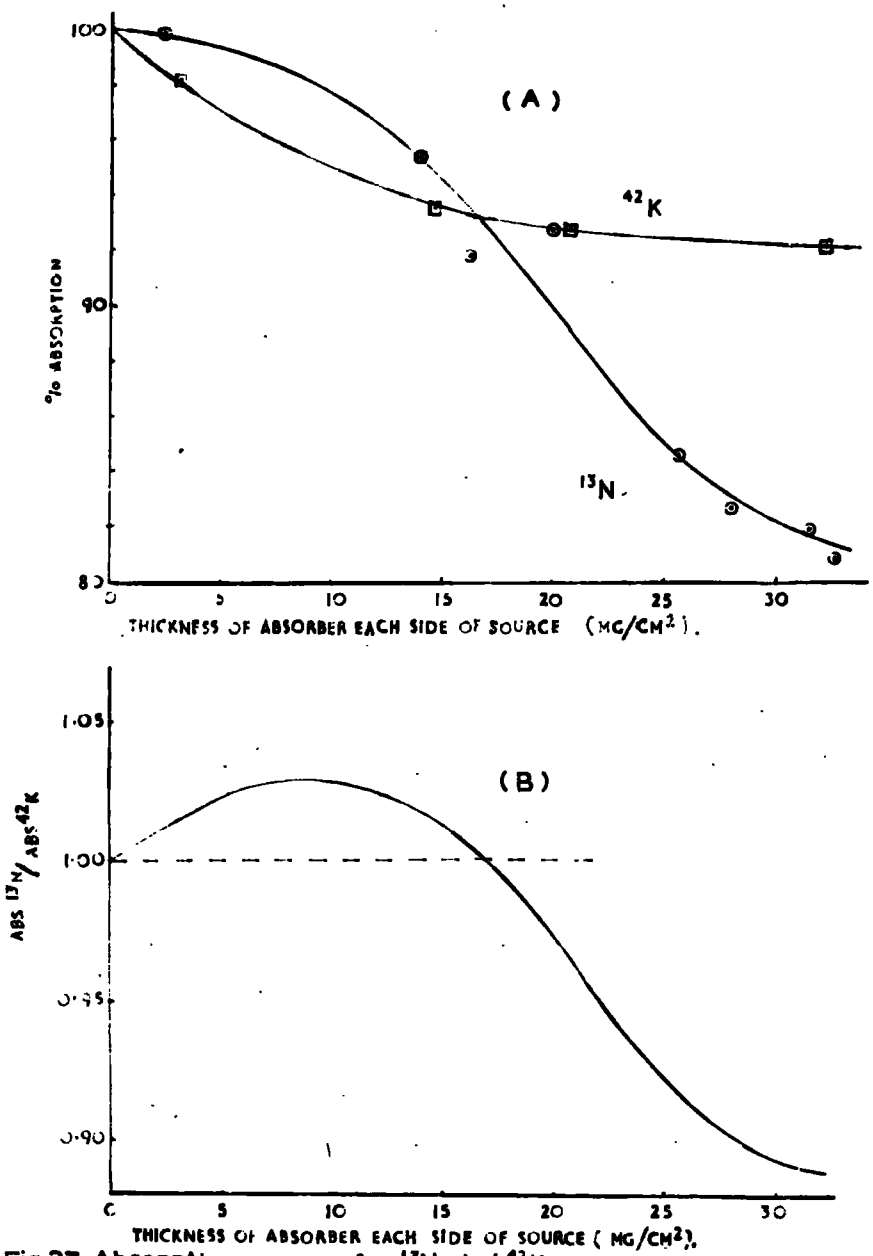

Fig.37. Absorption curves for ^{13}N and ^{42}K.

Results and comparison with other work.

In Table 17 are presented the results of measurements of the $^{16}O(n,p)^{16}N$ cross-section relative to the $^{14}N(n,2n)^{13}N$ reaction cross-section at six different target foil thicknesses. The mean value obtained at each thickness has been plotted against foil thickness in Fig. 38. The trend in the variation of the apparent cross-section with target thickness was assumed to be linear and a straight line through the points was drawn from a least squares analysis of the values.

The continuous energy distribution of β^+-particles from a positron emitter, such as ^{13}N, has a smaller proportion of particles in the low energy region of the spectrum compared with that of negatron emitters such as ^{16}N. At these absorber thicknesses therefore, a higher proportion of β -particles from ^{16}N are stopped than from ^{13}N. This is shown in the relative absorption curves for ^{42}K and ^{13}N (Fig. 37b); the ratio shows a variation of 3% from 0 to 18 mg cm^{-2} absorber thickness. From these considerations, at the target foil thicknesses used, the slope of the variation of apparent cross-section with foil thickness would be expected to be negative and have a value of a few per cent. The slope of the line was found to be -1.3%. The extrapolated value of the cross-section at zero thickness of the foil was 36.2 $\pm$ 0.4 mb.

The excitation function for this cross-section obtained

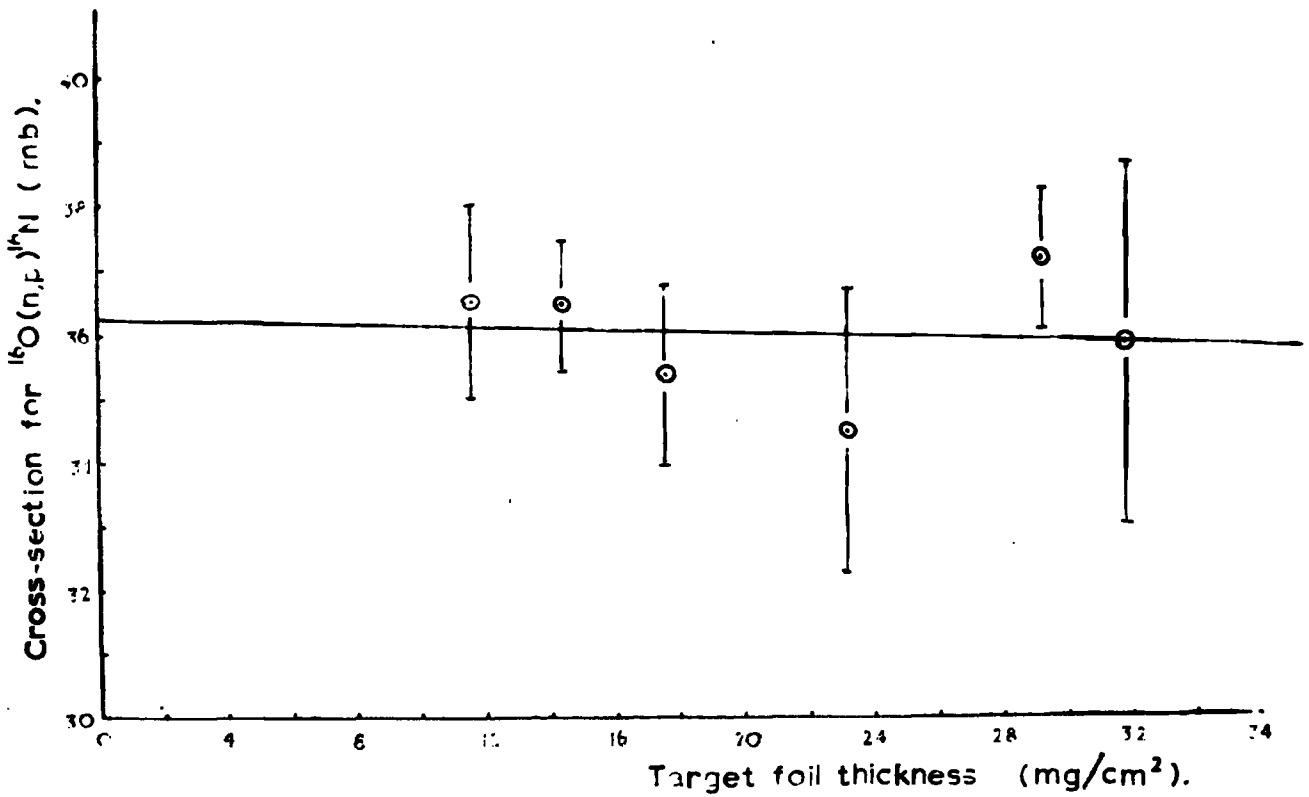

Fig. 38. Variation of measured cross-section with target foil thickness.

by Seeman and Moore[92] and De Juren et al.[93] show peaks at neutron energies of 11.8 MeV, 13.7 MeV, 15.1 MeV and 17 MeV with a trough between 14 and 15 MeV. At 14.8 MeV the value obtained here is in fair agreement with both these workers, De Juren et al.[93] (33.29 ± 2.4 mb at 14.76 MeV), Seeman and Moore[92] (32.8 ± 1.4 at 14.84 ± 1.4 MeV) and also with that of Kantele and Gardner[94] (38.2 ± 5 mb at 14.7 MeV) all using activation methods. Lillie[95], using cloud chamber techniques, obtained a value of 35 mb at 14.1 MeV. The earlier measurements of Paul and Clarke[7] (49.0 ± 2.5 mb at 14.5 MeV) and Martin[96] (89 ± 30 mb at 14 MeV) are significantly higher.

Estimation of errors.

The errors quoted in Table 17 are standard errors of the mean of each set of values. The actual error has been estimated as follows:- (1) Counting statistics not more than ± 5% (2) Graphical extrapolation ± 2% (3) Oxygen and nitrogen content of foils ± 1% (4) Estimated error in the $^{14}N(n,2n)^{13}N$ reference reaction ± 6.3%. This gives a total error of ± 8.5%.

Irrad. No.	Foil thickness mg cm^{-2}	Ao obs. ^{16}N c.p.s.	S ^{16}N	Ao obs. ^{13}N c.p.s.	S ^{13}N x 10^{-5}	Measured cross section (mb)	Mean of set

Table 17. Results for the $^{16}O(n,p)^{16}N$ reaction cross-section.

419	11.58	306	4411	6.25	1.796	37.7	
574		362	2314	5.04	0.7096	41.6	
580		634	4511	14.3	1.902	33.3	36.5
634		194	1474	5.43	0.7672	35.0	± 1.5
648		159	1605	3.92	0.6874	32.9	
420	14.44	483	4370	10.5	1.833	36.6	
562		656	3599	12.3	1.375	38.5	
572		444	2564	9.74	1.028	34.5	36.4
576		743	4187	14.3	1.650	38.7	± 1.0
579		720	4360	18.0	1.965	34.0	
421	17.64	533	4058	12.2	1.784	36.2	
581		1140	5233	22.0	1.868	35.0	
633		567	2521	11.7	1.049	38.2	35.3 ± 1.4
649		287	1609	6.23	0.5910	31.9	
427	23.20	395	3228	8.72	1.322	35.0	
619		483	1739	11.4	0.8216	38.0	34.5
646		307	1497	8.71	0.6833	30.3	± 2.2
429	29.20	567	3725	13.2	1.577	34.5	
560		1360	3615	22.4	1.198	37.8	
618		1060	2934	20.0	1.101	37.4	37.1 ± 1.1
647		681	2162	12.3	0.7999	38.8	

428	31.80	511	3285	12.0	1.386	33.9	
620		793	2009	12.3	0.6871	41.6	35.8
645		474	1558	12.8	0.7113	32.1	$\pm$ 2.8

Ref. cross-section $^{14}N(n,2n)^{13}N$ = 7.42 $\pm$ 0.47 mb.

$\lambda^{13}N$ = 1.155 x 10^{-3} $sec.^{-1}$ $\lambda^{16}N$ = 9.432 x 10^{-2} $sec.^{-1}$

Extrapolated value of $^{16}O(n,p)^{16}N$ cross-section at zero thickness = 36.2 $\pm$ 0.4 mb.

Part 4.

Irradiation of Calcium.

Calcium was irradiated with 14 MeV neutrons in an attempt to measure the cross-section for the reaction $^{40}Ca(n,t)\ ^{38}K$ previously reported by Baerg and Bowes[72] to have an upper limit of 20 μ b. The reactions studied were;

$^{40}Ca(n,t)\ ^{38}K$	($t_{\frac{1}{2}}$ = 7.7m)	Q = -12.933 MeV.
$^{42}Ca(n,p)\ ^{42}K$	($t_{\frac{1}{2}}$ = 12.5 $\pm$ 0.1h)	Q = -2.747 MeV.
$^{43}Ca(n,p)\ ^{43}K$	($t_{\frac{1}{2}}$ = 22.4h)	Q = -1.034 MeV.
$^{44}Ca(n,p)\ ^{44}K$	($t_{\frac{1}{2}}$ = 22.2 $\pm$ 0.2m)	Q = -5.320 MeV.
$^{48}Ca(n,2n)\ ^{47}Ca$	($t_{\frac{1}{2}}$ = 4.7d)	Q = -9.928 MeV.

The half lives for ^{42}K and ^{44}K are measured values the others being taken from the Nuclear Data Sheets.[61]

Experimental procedures.

Preliminary irradiations (K92, K94) were made in which 1.5g quantities of AnalaR grade (Hopkins and Williams Ltd.) calcium carbonate were irradiated. The specification for this chemical gave the impurity from sodium and potassium as less than 0.05%, but this was found to be sufficient for ^{38}K activity, arising from the reaction $^{39}K(n,2n)^{38}K$ on the con-

taminating potassium, to mask that from the $^{40}Ca(n,t)\ ^{38}K$ reaction. Granular calcium metal of 99.9% purity was obtained from Koch-Light Ltd. (Batch No. 36236), the chemical specification of which indicated it to be free from potassium. Four irradiations were made with 0.5g samples of this material placed close up to the D,T target for durations of 8 - 20 minutes.

All cross-sections were measured relative to the $^{56}Fe(n,p)\ ^{56}Mn$ cross-section as previously described. The samples were sandwiched between two 2.0 cm diameter discs of iron foil; the latter being wrapped in polythene to prevent transfer of recoil products (9 m ^{53}Fe could possibly interfere in the detection of 8 m ^{38}K especially since both are positron emitters). The whole sample was contained in a polythene capsule and irradiated close to the target. The separation of the foils was 0.3 cm, while the distance between the first foil and the target segment was 0.3 cm. This arrangement gave a neutron bombarding energy of 14.7 $\pm$ 0.5 MeV with deuterons of 220 keV energy incident on the target.

The iron foils were weighed and enough pure iron was added to bring up the weight to 1 g. It was then dissolved in 40 ml of the standard acid mixture and made up to 500 ml with distilled water; this was then equivalent to the 250 ml dilution of Appendix A. A correction was made to the obser-

ved activity of the iron, to obtain the neutron flux at the position of the calcium, by applying the foil/granule ratio also determined as described in Appendix A.

Preparation of carrier solution.

A suitable carrier solution for potassium was made by dissolving KCl in water. The solution contained about 2.5 mg ml^{-1} of carrier.

Separation of potassium.

Step 1. The calcium carbonate or metal was placed in a conical flask containing 2 ml of potassium carrier solution with a few mg each of $FeCl_3$ and $NaNO_3$ to act as hold-back carriers for iron (^{54}Fe) and nitrogen (^{13}N possibly arising from the $^{14}N(n,2n)^{13}N$ reaction on atmospheric nitrogen). 3 ml of 6N hydrochloric acid were added, and the solution boiled to ensure complete dissolution, chemical exchange and the removal of any argon formed from (n, α) reactions on calcium.

Step 2. The solution was diluted with 150 ml of ice-cold water to make it less than 0.1 N in hydrochloric acid and 15 ml of 6% sodium tetraphenylboron solution added to precipitate the potassium[97].

Step 3. The precipitate was carefully washed with water, acetone and ether and mounted on a pre-weighed glass filter disc in the usual way. The time for this procedure was about 10 minutes.

Separation of calcium.

Step 1. The filtrate from the potassium procedure was boiled down to reduce the volume and made just neutral with the addition of dilute sodium hydroxide solution.

Step 2. Excess oxalic acid solution was added to precipitate the calcium which was then washed and dried at 80°C. The calcium oxalate was then packed into a semi-micro test tube and counted in a well type NaI(T1) scintillation crystal.

Counting techniques.

^{38}K was the only possible positron emitter in the potassium sources. Therefore, in an attempt to distinguish any activity of ^{38}K from the other potassium activities present, the potassium source was placed between two NaI(T1) γ-ray scintillation crystals both set on the annihilation photopeaks. Coincidences between the two crystals were counted using a coincidence unit, the setting of delay and mixer resolving time (0.3 μs) being previously determined with the aid of a ^{22}Na source. Aluminium plates were placed on each side, and,

to obtain maximum counter efficiency, the crystals were arranged to touch the aluminium plates; their separation was then 1.2 cm.

To obtain the absolute counting efficiency direct comparison was made with the coincidence rate from a standard ^{22}Na source counted under identical conditions. The decay schemes of ^{22}Na and ^{38}K being regarded as sufficiently similar, no corrections were made in comparing the coincidence rates other than for the percentage of positron emission. Corrections were made to the coincidence rate for the single channels paralysis time, the resolving time of the mixer and random coincidences in the usual way. The coincidence decay was followed as described for 500 minutes.

The activities of ^{42}K, ^{43}K and ^{44}K were measured by counting the potassium source under an end-window proportional counter. Those of ^{42}K and ^{44}K were determined by the usual curve stripping while that of ^{43}K was found by straight line analysis of the decay data using the method outlined in Chapter 3. The counter efficiency for ^{42}K had been obtained directly from the calibration runs of ^{42}K, while those for ^{43}K and ^{44}K were estimated by the method of Bayhurst and Prestwood[46].

In one irradiation (K101) the initial activity of ^{44}K was estimated from the single channels of the γ-ray scintillators

by direct comparison with later irradiations (K102, K104, K106).

The initial activity of ^{48}Ca in the calcium sources was estimated by counting the source on a well-type scintillation crystal set on the 1.30 MeV photopeak (>1.15 MeV). The source was placed inside a brass walled cylinder of 1.03 g cm^{-2} thickness to prevent any β-particles entering the crystal. The counting efficiency was estimated from the work of Redon et al.[44] and Crouthamel[42] whilst γ-ray absorption data was taken from Davisson and Evans[62].

The equation used to determine the efficiency is shown below; the notation is described in Part 1 of this Chapter.

^{47}Ca

$$N = No\,\beta_1\left[\beta_2 \cdot P_{1.30} + \beta_3 \cdot P_{0.8} \cdot P_{0.5}\right]$$

$$\beta_1 = 0.82, \quad \beta_2 = 0.93, \quad \beta_3 = 0.07.$$

The calculated efficiency is 0.0257.

Results and comparison with other work.

In Tables 18 to 23 are presented the results of measurements on the cross-sections.

The value of 5.8 ± 1.1 μb for the $^{40}Ca(n,t)^{38}K$ reaction

is based on the first one or two points of the initial part of the decay curve observed in the coincidence channel which lay above a line of 22.3 m slope drawn through the remainder. A typical curve is shown in Fig. 39. Previous values of this cross-section are $<$ 0.1 mb (Weigold and Glover[98]) and $<$ 0.02 mb (Baerg and Bowes[72]). Khurana and Govil[99] quote a value of 20 $\pm$ 4 mb which must be regarded as extremely high.

The value of 148 $\pm$ 7 mb for the $^{42}Ca(n,p)^{42}K$ reaction agrees with that of 140 $\pm$ 45 mb by Hille[100], and lies between the values of 120 $\pm$ 12 mb by Cohen[101] and 160 $\pm$ 30 mb by Levkovskii[102], and is therefore well supported.

No previous measurement has been found for the $^{43}Ca(n,p)^{43}K$ reaction and the value here of 100.2 $\pm$ 3.7 mb would seem reasonable compared with its neighbours.

40.4 $\pm$ 1.5 mb for the $^{44}Ca(n,p)^{44}K$ cross-section again agrees fairly well with the values of Hille[100], 25 $\pm$ 12 mb, and Levkovskii[102], 37 + 7 mb, but again that quoted by Khurana and Govil[99] (91 $\pm$ 20 mb) is much higher.

The value of 868 $\pm$ 67 mb for the $^{48}Ca(n,2n)^{47}Ca$ cross-section agrees within the errors with the two previous measurements, 1070 $\pm$ 360 mb (Hille[100]) and 920 $\pm$ 184 mb (Hillman[103]) the errors on all of these being rather large.

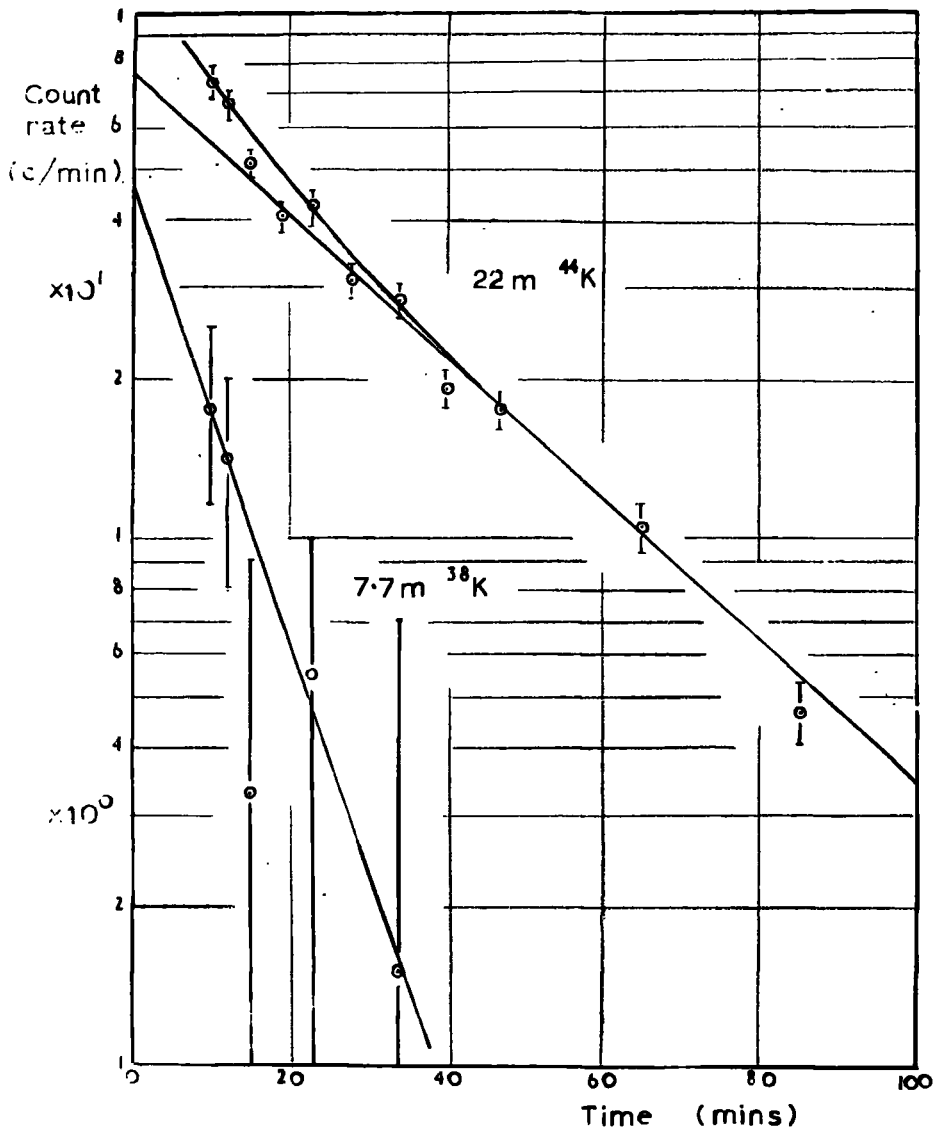

Fig. 39. Decay curve of short-lived potassium activities.

Estimation of errors.

The errors in the values quoted above were standard errors of the mean of the results.

The main error in the $^{40}Ca(n,t)^{38}K$ reaction arises in the estimation of the initial activity which may be in error by as much as $\pm$ 50% on such poor data and thus a value of $6 \pm 3 \mu b$ is quoted.

For the $^{42}Ca(n,p)$ and $^{44}Ca(n,p)$ cross-sections, an error of $\pm$ 1% is estimated from the graphical determination of the initial activity, while the calibration of the proportional counter is $\pm$ 3%. The error in weighing and in the volumetric ware are both less than 1%. The reference cross-section error has previously been quoted as 5.5%, which gives a total error of $\pm$ 6.5% for these cross-sections.

The activity of ^{43}K was low, and the error in the initial activity is estimated to be $\pm$ 5%. The remaining errors are as those quoted above and give a total error of $\pm$ 8% for this cross-section.

The error in the ^{47}Ca activity again arises from the very low count rates (of the order of only twice background initially), and also from the estimation of the counter efficiency. Both of these have been taken to be $\pm$ 10% which, with the other errors quoted above, give a total of $\pm$ 15%.

Irrad. No.	No target nuclei x N^{-1}	Ao obs. c.p.m.	Ao corrt. d.p.m.	S

Table 18. Data for the reference reaction $^{56}Fe(n,p)^{56}Mn$.

K92	1.412×10^{-2}	7.65×10^{3}	4.56×10^{6}	2.062×10^{6}
K94	1.387×10^{-2}	5.25×10^{3}	3.13×10^{6}	9.204×10^{5}
K101	1.385×10^{-2}	1.70×10^{4}	1.01×10^{7}	3.059×10^{6}
K102	1.414×10^{-2}	1.37×10^{4}	8.16×10^{6}	2.314×10^{6}
K104	1.424×10^{-2}	5.53×10^{4}	3.29×10^{6}	9.831×10^{5}
K106	1.297×10^{-2}	5.70×10^{3}	3.40×10^{6}	1.057×10^{6}

N is Avogardro's No., $\sigma^{56}Fe(n,p)^{56}Mn$ = 98.3 mb.

$t_{\frac{1}{2}}$ ^{56}Mn = 155m., $\lambda^{56}Mn$ = 0.004472 min^{-1}.

Counter Eff. ^{56}Mn = 0.080, Dilution factor = 0.02,
Ratio foil/granules = 1.049.

Irrad. No.	No. target nuclei x N^{-1}	Chem. Yield (%)	Counter Eff.	Ao obs. c.p.m.	Ao corrt. d.p.m.	S	Measured cross-section (mb)	Mean

Table 19. Results of the $^{40}Ca(n,t)^{38}K$ reaction.

K101	1.155×10^{-2}	66.93	0.0225	54	3.6×10^{3}	1.494×10^{6}	4.3 μb	
K102	1.316×10^{-2}	18.44	0.0223	31	7.5×10^{3}	1.367×10^{6}	8.2 μb	5.8
K104	1.314×10^{-2}	65.41	0.0225	47	3.2×10^{3}	7.159×10^{5}	7.0 μb	± 1.1 μb
K106	1.404×10^{-2}	38.41	0.0233	19	2.1×10^{3}	7.854×10^{5}	3.7 μb	

$\lambda^{38}K = 0.090026 \text{ min}^{-1}$

Table 20. Results of the $^{42}Ca(n,p)^{42}K$ reaction.

K92	7.057×10^{-5}	86.07	0.337	1990	6.86×10^{3}	2.132×10^{6}	139	
K94	6.264×10^{-5}	58.11	0.337	820	4.19×10^{3}	9.612×10^{5}	135	
K101	7.623×10^{-5}	66.93	0.337	4680	2.08×10^{4}	3.166×10^{6}	172	
K102	8.685×10^{-5}	18.44	0.336	930	1.50×10^{4}	2.371×10^{6}	139	148
K104	8.671×10^{-5}	65.41	0.337	1460	6.62×10^{3}	9.970×10^{5}	155	± 7 mb.
K106	9.263×10^{-5}	38.41	0.336	1000	7.75×10^{3}	1.071×10^{6}	150	

$\lambda^{42}K = 0.0009243 \text{ min}^{-1}$

Irrad. No.	No target nuclei x N^{-1}	Chem. Yield (%)	Counter Eff.	Ao obs. c.p.m.	Ao corrt. d.p.m.	S	Measured cross-section (mb)	Mean

Table 21. Results of the $^{43}Ca(n,p)^{43}K$ reaction.

K92	1.599×10^{-5}	86.07	0.264	155	682	2.139×10^{6}	108.0	
K94	1.419×10^{-5}	58.11	0.292	70	413	9.654×10^{5}	104.4	
K101	1.727×10^{-5}	66.93	0.285	368	1928	3.177×10^{6}	105.4	
K102	1.968×10^{-5}	18.44	0.326	84	1400	2.377×10^{6}	101.8	100.2 ± 3.7 mb
K104	1.964×10^{-5}	65.41	0.286	100	534	9.984×10^{5}	98.3	
K106	2.099×10^{-5}	38.41	0.310	65	546	1.072×10^{6}	83.0	

$\lambda^{43}K = 0.0005181 \text{ min}^{-1}$

Table 22. Results of the $^{44}Ca(n,p)^{44}K$ reaction.

K101	2.454×10^{-4}	66.93	0.0347 *	1.01×10^{4}	4.35×10^{5}	2.388×10^{6}	44.0	
K102	2.795×10^{-4}	18.44	0.305	2.14×10^{4}	3.80×10^{5}	1.941×10^{6}	39.7	
K104	2.791×10^{-4}	65.41	0.296	3.27×10^{4}	1.69×10^{5}	8.873×10^{5}	41.1	40.4 ± 1.5 mb
K106	2.982×10^{-4}	38.41	0.302	2.14×10^{4}	1.85×10^{5}	9.604×10^{5}	36.8	

$\lambda^{44}K = 0.03109 \text{ min}^{-1}$

* Scintillation counting, efficiency estimated from comparison with K102, K104, K106.

Table 23. Results of the $^{48}Ca(n,2n)^{47}Ca$ reaction.

K104	2.207×10^{-5}	100	0.0257	29	1130	1.001×10^{6}	934	
K106	2.659×10^{-5}	100	0.0257	34	1320	1.074×10^{6}	801	868 ± 67 mb

$\lambda^{47}Ca = 0.0001024 \text{ min}^{-1}$

Part 5.

Irradiation of Selenium.

A study of the literature showed that little work had been done on the measurement of neutron induced reactions of selenium at 14 MeV. Since selenium has adjacent stable isotopes, it was considered to be of some interest to investigate whether the Levkovskii[10] trend holds for the reactions of this element.

Samples of selenium dioxide were irradiated close up to the D,T target; the reactions studied were:-

$^{74}Se(n,2n)^{73m}Se$ ($t_{\frac{1}{2}}$ = 44 ± 3m) → $^{73}As(t_{\frac{1}{2}} = 79d)$ (Q= ———)

$(n,2n)^{73g}Se$ ($t_{\frac{1}{2}}$ = 7.1 ± 0.1h) → " " " (Q= -12.040MeV)

$^{76}Se(n,2n)^{75}Se$ ($t_{\frac{1}{2}}$ = 120d) (Q= -11.126MeV)

$^{82}Se(n,2n)^{81m}Se$ ($t_{\frac{1}{2}}$ = 59 ± 1m) (Q= -9.190MeV)

$(n,2n)^{81g}Se$ ($t_{\frac{1}{2}}$ = 18.6m) (Q= -9.190MeV)

$^{76}Se(n,p)^{76}As$ ($t_{\frac{1}{2}}$ = 26.5h) (Q= -2.187MeV)

$^{77}Se(n,p)^{77}As$ ($t_{\frac{1}{2}}$ = 38.7h) (Q= +0.099MeV)

$^{78}Se(n,p)^{78m}As$ ($t_{\frac{1}{2}}$ = 5.5 ± 1m) (Q= -3.320MeV)

$^{78}Se(n,\alpha)^{75}Ge$ ($t_{\frac{1}{2}}$ = 82 ± 1m) (Q= +0.526MeV)

$^{80}Se(n,\alpha)^{77}Ge$ ($t_{\frac{1}{2}}$ = 11.3h) → $^{77}As(t_{\frac{1}{2}} = 38.7h)$ (Q=-0.970MeV)

$^{82}Se(n,\alpha)^{79}Ge$ ($t_{\frac{1}{2}} \leq$ 1m) → $^{79}As(t_{\frac{1}{2}}$ = 9.0 ± 0.1m) →

$^{79}Se(t_{\frac{1}{2}}$ = 3.9m) (Q= ———)

The resultant species were chemically separated and counted under an end-window proportional counter or on a NaI(T1) scintillation spectrometer. Since selenium has six stable isotopes and many of the reaction products have active daughters, the decay of each source was still complex after chemical separation; it was therefore necessary to use the values of the half-lives from the Nuclear Data Sheets[61] and to analyse the decays by means of straight line plots (as described in Chapter 3). The only information[104] found in the literature on ^{79}Ge stated that this nuclide decayed by β^- emission with a half-life of less than one minute. A value of one minute was used in the present calculations.

Experimental procedures.

1 g quantities of 99.999% pure selenium dioxide, obtained from Koch-Right Ltd. (batch No. 16626), were sandwiched between two 2.0 cm diameter discs of iron foil, which were wrapped in polythene to prevent transfer of recoil products; 9 m ^{53}Fe could possibly interfere in the detection of 9m ^{79}As. The whole sample was contained in a polythene capsule and irradiated close to the target. The separation of the foils was 0.3 cm, while the distance of the front foil from the target segment was 0.3 cm. This arrangement gave a neutron bombarding energy of 14.7 $\pm$ 0.5 MeV with deuterons of 220 keV energy incident on the target.

The irradiated iron foils were treated as previously described for the irradiation of calcium; corrections were again made to the observed activity to obtain the neutron flux at the position of the selenium dioxide, by applying the foil/granule ratio of Appendix A.

Preparation and standardisation of the carrier solutions.

A suitable As(III) solution was prepared by dissolving As_2O_3 in dilute NaOH, and a Ge (IV) solution by dissolving germanium metal in a solution of NaOH and H_2O_2. Both solutions contained about 5 mg ml^{-1} of carrier.

The As(III) solution was standardised by titration against a standard KIO_3 solution in the presence of HCl and CCl_4.[105] The Ge(IV) solution was determined gravimetrically by precipitation of GeS_2 by H_2S in 6N HCl.

Separation of selenium.

Step 1. The irradiated SeO_2 was added to 2 ml each of the As(III) and Ge(IV) carrier solutions and dissolved on heating.

Step 2. 4 ml concentrated HCl was added and selenium precipitated as element by the addition of excess hydrazine hydrate. This precipitate was centrifuged off, and the time

after the end of the irradiation noted. The supernate was retained.

Step 3. The precipitate was dissolved in the minimum amount of HNO_3, evaporated almost to dryness, and diluted with 6N HCl.

Step 4. The selenium was reprecipitated with SO_2 water, and washed with dilute SO_2 water, alcohol and ether. A small portion was mounted on a weighed glass filter pad, dried, and counted under an end-window proportional counter. The remainder was dried, placed in a semimicro test tube, and counted in a well-type NaI(Tl) scintillation crystal.

Separation of arsenic.

Step 1. To the supernate from step 2 in the selenium procedure was added 0.5g of NaH_2PO_2 and the solution boiled until the arsenic precipitate coagulated. Again the time after the end of the irradiation was noted. The supernate was retained.

Step 2. The precipitate was mounted on a glass filter pad, washed with water, alcohol and ether, dried and counted. The time taken to reach this point was 12m after the end of the irradiation.

Separation of Germanium.

Step 1. More NaH_2PO_2 was added to the supernate from step 1 in the arsenic procedure, and the mixture boiled to ensure the complete removal of arsenic. If necessary the solution was filtered.

Step 2. Germanium sulphide was precipitated by passing H_2S through the filtrate.

Step 3. The precipitate was dissolved in 6N KOH and boiled. The solution was made 6N in HCl and H_2S again passed to precipitate GeS_2. This was mounted on a glass filter pad, washed with water, alcohol and ether, dried, and counted.

Standardisation of arsenic precipitate.

Since finely divided arsenic could be oxidised in air the arsenic sources were determined titrimetrically using Volhard's method[105].

Step 1. Each source was dissolved in HNO_3, and NaOH added until the solution was just alkaline to phenolphthalein; dilute acetic acid was then added dropwise to neutralise the solution.

Step 2. Excess silver nitrate solution was added, the solution stirred, and the precipitate allowed to settle in the

dark. The solution was filtered on a porosity 4 sintered crucible and washed with cold water to remove excess silver nitrate.

Step 3. The Ag_2AsO_4 was dissolved in 1N HNO_3 and the solution filtered. The remaining precipitate was washed with 1N and 0.5N HNO_3 and the washings added to the filtrate.

Step 4. This solution was then titrated against a standard KCNS solution using saturated ferric alum solution as indicator.

Counting techniques.

i. Selenium. The selenium sources mounted on glass filter pads were counted under an end-window proportional counter. From these sources the initial count rates of ^{81}Se and ^{81m}Se were determined. An 18.6m activity of ^{81}Se was not actually observed in the gross decay curve but when the initial part of the 59m decay was plotted it was found to be slightly concave towards the origin indicating the growth of the activity of the ground state from the isomeric state. A straight line plot analysis (described in Chapter 3) revealed the initial activity of both states.

The initial activities of ^{73}Se and ^{73m}Se were determined relative to a standard ^{22}Na source of exactly similar geometry

mounted in a semimicro test tube by counting the 0.511 MeV annihilation photopeaks. The sources were placed inside a brass cylinder having 1g cm^{-2} walls to ensure complete annihilation of positrons at the sources and to prevent β-particles entering the crystal. Corrections were made for sum events as indicated below.

The initial activity of ^{75}Se was estimated by setting the window of the single channel analyser on the 0.402 MeV photopeak and calculating the counter efficiency from the published data of Redon[44] and Crouthamel[42].

The equations used to calculate the counter efficiencies of the various nuclides are set out below. The notation and equation for ^{22}Na have previously been described in part 1 of this Chapter.

^{73m}Se.

The isomeric state of ^{73}Se decays directly to ^{73}As without passing through its ground state. The second excited state of ^{73}As has a half-life of 6μS and therefore since the clipping time of the NE 5202 main amplifier used here is 1.2μS, only some 13% of the decays from this state can be detected in coincidence with the annihilation radiation from the preceding positron decay. ^{73}As decays entirely by electron capture to ^{73}Ge with a half-life of 79 days, and therefore any contribution

to the counting rate from this nuclide was considered to be negligible. No activity with a 79 day half-life was detected in the sources. The efficiency equation used is:-

$$N = No(2\,P_{0.51}(1 - T_{0.51})(1 - 0.13\,T_{0.359})(1 - 0.13\,T_{0.066}))$$

The counter efficiency calculated on comparison with that measured for ^{22}Na is 0.304.

^{73}Se.

Since some 98.9% of the decays from the ground state of ^{73}Se also pass through the 6 μS second excited state of ^{73}As a similar correction to that outlined above has been made here.

$$N = No(2.\beta_1.P_{0.51}(1 - T_{0.51})(1 - 0.13\,T_{0.359})(1 - 0.13\,T_{0.066}) + 2.\beta_2 . P_{0.51}(1 - T_{0.51})(1 - T_{0.066}).$$

$$\beta_1 = 0.699, \qquad \beta_2 = 0.007.$$

The counter efficiency calculated on comparison with that measured for ^{22}Na is 0.212.

^{75}Se.

This nuclide decays entirely by electron capture to various excited states of ^{75}As. The single channel analyser was set at 0.402 MeV to count the photopeak and sum peak at this energy.

The γ-ray cascades decaying via the 0.305 MeV level of ^{75}As, which has a half-life of 17 ms, were considered not to contribute to the sum peak.

$$N = No((\alpha_1.\beta_1 P_{0.402}) + \alpha_2.\beta_1.P_{0.136}(\alpha_3 P_{0.265} + \alpha_4.P_{0.066}P_{0.199})$$

$$+ \alpha_5.\beta_1.P_{0.121}(\alpha_6 P_{0.280} + \alpha_7.P_{0.081}.P_{0.199})$$

$\alpha_1 = 0.20$, $\alpha_2 = 0.54$, $\alpha_3 = 0.97$, $\alpha_4 = 0.03$, $\alpha_5 = 0.18$,

$\alpha_6 = 0.987$, $\alpha_7 = 0.013$.

$\beta_1 = 0.76$.

The calculated counter efficiency is 0.078.

ii. Arsenic sources.

The arsenic sources were counted under an end-window counter and also on a 3" x 3" NaI(Tl) scintillation spectrometer. From the decay curves followed on the end-window counter the initial activities of $^{76,77,78}As$ and $^{79}As(^{79}Ge)$ were determined.

The scintillation spectrometer was used to search for the isomeric state of ^{78}As found by Nemilov[106] but not confirmed by Fritze[107]. This state was reported to decay to the ground state with a half-life of 6m on emitting a γ-ray of 0.5 MeV. A weak component of 5.5 $\pm$ 1m half-life of energy between 0.40

and 0.57 MeV was observed in the two runs in which this was investigated, so adding to the evidence for the existence of this state. A γ-ray spectrum of the source taken on a multichannel analyser did not, however, reveal a peak at 0.5 MeV. Fig. 40 shows one of the decay curves.

In the calculation of the $^{77}Se(n,p)^{77}As$ cross-section an allowance was made for the contribution to the observed ^{77}As activity of that arising as a result of the decay of ^{77}Ge before the separation of arsenic (the method of calculation is described in Chapter 3). The $^{82}Se(n,\alpha)^{79}Ge$ cross-section was calculated, as is also outlined in Chapter 3, using the data from the decay of the daughter product, ^{79}As, which in turn was corrected for the decay of its own daughter, ^{79m}Se. It was assumed that all the ^{79}Ge formed had decayed to ^{79}As before arsenic was separated from the germanium fraction (about 10m after the end of an irradiation).

iii. Germanium sources.

These sources were counted only on an end-window proportional counter; from their decay the initial activities of ^{75}Ge and $^{77}Ge(^{77}As)$ were determined.

Results and comparison with other work.

The results for the cross-sections of the reactions studied

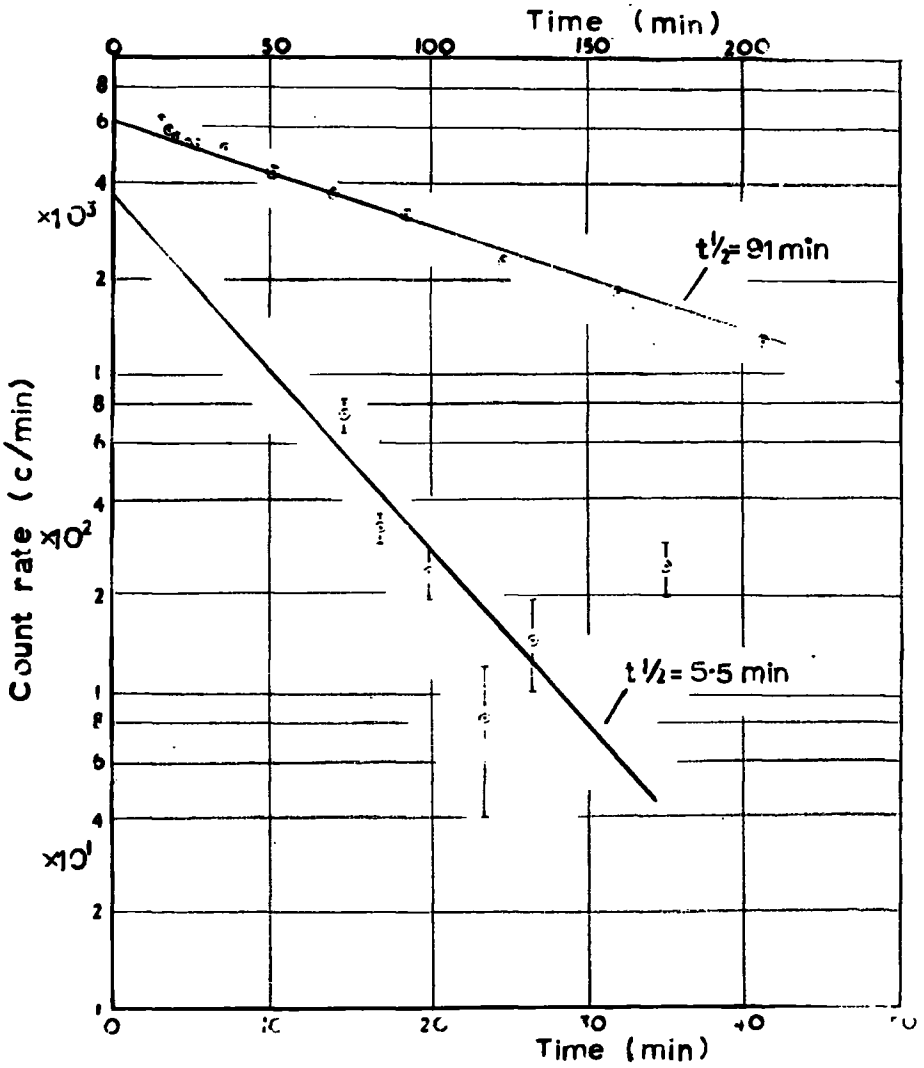

Fig.40. Resolution of ^{79m}As component from the decay curve.

are presented in Tables 24 to 36. Table 24 shows the values for the $^{56}Fe(n,p)^{56}Mn$ reference reaction.

Of the (n,2n) measurements made here, only those on ^{74}Se and ^{82}Se have been previously reported. Rayburn[78] obtained a value of 383 ± 31 mb for the $^{74}Se(n,2n)^{73g}Se$ reaction cross-section, and 48.7 ± 8.0 mb for the cross-section of the reaction leading to the excited state. Both of these are lower than the values obtained here of 458 ± 19 mb and 167 ± 7 mb respectively. The methods used were similar in that annihilation radiation coincidences were counted under standard conditions. In the case of ^{82}Se, cross-sections of 860 ± 170 mb (excited state) and 485 ± 95 mb (ground state) were obtained. Paul and Clarke[7] found a value of 1500 ± 500 mb and Mangal and Khurana[108] a value of 1600 ± 100 mb for the reaction going to the 57 m excited state. The latter workers did not observe any 18m decay to the ground state, and quote an upper limit of 100 mb for this cross-section, which gives an unusually high isomeric ratio (high spin state/ total spin) of 0.9. As mentioned earlier the 18m decay of the ground state was not observed directly in the present work, but was infered from the slight curvature in the 57m decay of the excited state. The isomeric ratio obtained here was 0.6 which is a more usual value.

No value for the $^{76}Se(n,2n)^{75}Se$ reaction cross-section has been found in the literature to compare with that obtained here

of 2850 ± 144 mb.

A cross-section of 58.8 ± 5.1 mb was measured for the $^{76}Se(n,p)^{76}As$ reaction. The only other determination is that of Cohen[101], of 16.5 mb for fission spectrum neutrons, which Chatterjee[14] has estimated to be approximately equivalent to 90 mb at 14 MeV. Cohen[101] did not observe, and therefore did not correct for, the 39h activity resulting from the $^{77}Se(n,p)^{77}As$ reaction, which could have increased his observed count rate for the 26h ^{76}As activity.

The value of the $^{77}Se(n,p)^{77}As$ cross-section (44.7 ± 5.5 mb) agrees with the only other measurement, that of Paul and Clarke[7] (45 ± 23 mb). No previous values have been reported for the $^{78}Se(n,p)^{78}As$ and ^{78m}As reactions; those obtained here were 20.6 ± 0.7 mb and 16.3 ± 6.5 mb respectively.

Again no values are reported in the literature for the $^{78}Se(n,\alpha)^{75}Ge$ reaction (6.35 ± 0.18 mb). Paul and Clarke[7] found 38 ± 16 mb at 14.5 MeV for the $^{80}Se(n,\alpha)^{77}Ge$ reaction as compared with 2.26 ± 0.15 mb obtained here. No chemical separations were carried out by these workers, and therefore errors may have arisen in analysing the complex decay curves obtained; 11.3h ^{77}Ge decays to 40h ^{77}As which is also produced, as they observed, from the $^{77}Se(n,p)^{77}As$ reaction. In addition 26h ^{76}As which would also be present is not mentioned in their article.

The other (n,α) cross-section measured here is that for $^{82}Se(n,\alpha)^{79}Ge$ (6.47 ± 0.50 mb); the initial ^{79}Ge activity was estimated from the ^{79}As daughter activity as described above. Cohen et al[109] measured the cross-section for the $^{80}Se(n,np + d)^{79}As$ reaction and obtained an upper limit of 0.8 ± 0.3 mb; any contribution from the $^{82}Se(n,\alpha)^{79}As$ reaction appears to have been ignored. Assuming that their observed activity was due to this process, their results give a value of 4.5 mb for the (n,α) cross-section which is of the magnitude of that obtained here.

Estimation of errors.

The errors quoted above are standard errors of the means of the results obtained. All the cross-section values quoted are relative to the $^{56}Fe(n,p)^{56}Mn$ reference cross-section which has an estimated error of not more than ± 5.5%. The estimation of proportional counter efficiences should be within ± 3% while the estimated efficiences for γ-ray scintillation counting may be as large as ± 10%. For ^{78m}As and ^{81g}Se errors arise from the analysis of the decay curves; these may be as much as 30% for ^{78m}As and ± 10% for ^{81g}Se. For the other species the error should not exceed 5% and is thus indicated by the standard errors of the mean.

Some of the reactions studied here have positive or small

negative Q values and therefore the reactions may be energetically possible at the 3 MeV D,D neutron energy. Since the proportion of D,D to D,T neutrons is less than 3%, and the values of the cross-section drop off with energy, contributions from this source were considered to be negligible.

Irrad. No.	No. of target nuclei	Ao obs.	Ao corrt.	S
		c.p.m.	d.p.m.	
	$\times 10^{2}/N$	$\times 10^{-3}$	$\times 10^{-6}$	$\times 10^{-6}$
K118	1.315	9.15	5.45	2.322
K122	1.262	2.62	1.56	0.7247
K128	1.244	4.92	2.93	1.248
K133	1.275	5.12	3.05	1.110
K136	1.292	3.82	2.28	0.9882

Table 24. Data for the reference reaction $^{56}Fe(n,p)^{56}Mn$.

N is Avogadro's No. $t_{\frac{1}{2}}\ ^{56}Mn = 155$ min.

$\sigma\ ^{56}Fe(n,p)^{56}Mn = 98.3$ mb. $\lambda^{56}Mn = 0.004472\ min^{-1}$

Counter efficiency $^{56}Mn = 0.080$. Foil/Granules = 1.049.

Dilution factor $^{56}Mn = 0.02$.

Irrad. No.	No. of target nuclei x 10^5/N	Chemical Yield (%)	Counter Eff.	Ao observed (c.p.m.)	Ao correct. (d.p.m.)	S x 10^{-6}	Measured cross-section (mb)	Mean (mb)

Table 25. Results of the $^{74}Se(n,2n)^{73m}Se$ reaction.

K118	4.455	100	0.304	2.56×10^4	8.42×10^4	1.786	165	
K122	2.523	100	0.304	5.40×10^3	1.78×10^4	0.6191	185	
K133	6.071	100	0.304	2.31×10^4	7.60×10^4	1.056	153	167 ± 7
K136	5.853	100	0.304	1.78×10^4	5.86×10^4	0.9447	165	

$\lambda^{73m}Se = 0.01575 \text{ min}^{-1}$

Table 26. Results of the $^{74}Se(n,2n)^{73g}Se$ reaction.

K118	4.455	100	0.212	6080	2.87×10^4	2.489	391	
K122	2.523	100	0.212	1210	5.71×10^3	0.7550	473	
K128	3.004	100	0.212	2580	1.22×10^4	1.260	459	458 ± 19
K133	6.071	100	0.212	5300	2.50×10^4	1.124	458	
K136	5.853	100	0.212	4200	1.98×10^4	1.001	511	

$\lambda^{73}Se = 0.001627 \text{ min}^{-1}$

Table 27. Results of the $^{76}Se(n,2n)^{75}Se$ reaction.

K118	46.19	100	0.078	354	4540	2.592	2320	
K122	26.20	100	0.078	754	965	0.7731	3060	
K128	31.14	100	0.078	164	2100	1.267	3080	2850 ± 144
K133	62.94	100	0.078	305	3910	1.132	2780	
K136	60.68	100	0.078	233	2980	1.006	3000	

$\lambda^{75}Se = 0.4012 \times 10^{-5} \text{ min}^{-1}$

Irrad. No.	No. of target nuclei $\times 10^5/N$	Chemical Yield (%)	Counter Eff.	Ao obs. (c.p.m.)	Ao correct. (d.p.m.)	S $\times 10^{-6}$	Measured cross-section (mb)	Mean (mb)
Table 28. Results of the $^{82}Se(n,2n)^{81m}Se$ reaction.								
K133	0.4050	100	0.215	3.73×10^3	1.73×10^4	1.075	689	860 ± 170
K136	4.004	100	0.099	1.86×10^4	1.89×10^5	0.9598	1030	
$\lambda^{81m}Se = 0.011749\ min^{-1}$								
Table 29. Results of the $^{82}Se(n,2n)^{81g}Se$ reaction.								
K133	0.4050	100	0.356	1.12×10^4	3.14×10^4	0.9580	391	489 ± 95
K136	4.004	100	0.337	1.16×10^5	3.45×10^5	0.8651	586	
$\lambda^{81g}Se = 0.038511\ min^{-1}$								
Table 30. Results of the $^{76}Se(n,p)^{76}As$ reaction.								
K118	79.96	63.39	0.337	4470	1.41×10^4	2.563	57.6	58.8 ± 5.1
K122	75.67	47.33	0.353	1110	6.64×10^3	0.7682	67.4	
K128	77.78	75.37	0.335	2630	1.04×10^4	1.265	56.4	
K133	74.82	87.92	0.343	2280	7.56×10^3	1.130	41.8	
K136	72.57	100	0.341	3120	9.12×10^3	1.003	70.7	
$\lambda^{76}As = 0.00043597\ min^{-1}$								

Irrad. No.	No. of target nuclei $\times \frac{10^3}{N}$	Chemical Yield (%)	Counter Eff.	Ao obs. (c.p.m.)	Ao correct. (d.p.m.)	S $\times 10^{-6}$	Measured cross-section (mb)	Mean (mb)
Table 31. Results of $^{77}Se(n,p)^{77}As$ reaction.								
K118	0.6720	63.39	0.247	1540	9830	2.573	46.3	
K122	0.6359	47.33	0.328	420	2710	0.7697	47.3	
K128	0.6537	75.37	0.305	1530	6650	1.266	62.4	44.7
K133	0.6288	87.92	0.316	2170	7820	1.130	30.4	± 5.5
K136	0.6099	100	0.311	860	2770	1.005	37.0	
	$\lambda^{77}As = 0.00029854\ min^{-1}$							
Table 32. Results of $^{78}Se(n,p)^{78}As$ reaction.								
K118	2.085	63.39	0.343	6.20×10^4	1.92×10^5	2.149	20.3	
K122	1.973	47.33	0.356	1.42×10^4	8.43×10^4	0.6922	20.6	
K128	2.028	75.37	0.341	4.48×10^4	1.74×10^5	1.234	21.0	20.6
K133	1.951	87.92	0.346	4.57×10^4	1.50×10^5	1.094	18.6	± 0.7
K136	1.892	100	0.344	3.78×10^4	1.30×10^5	0.9754	22.5	
	$\lambda^{78}As = 0.0077022\ min^{-1}$							
Table 33. Results of $^{78}Se(n,p)^{78m}As$ reaction.								
K128	2.028	75.37	0.128	3600	3.7×10^4	0.4189	22.8	16.3
K133	1.951	87.92	0.128	1600	1.4×10^4	0.3404	9.81	± 6.5
	$\lambda^{78m}As = 0.12604\ min^{-1}$							

Irrad. No.	No. of target nuclei $\times \frac{10^3}{N}$	Chemical Yield (%)	Counter Eff.	Ao obs. (c.p.m.)	Ao correct. (d.p.m.)	S $\times 10^{-6}$	Measured cross-section (mb)	Mean (mb)
Table 34. Results of $^{78}Se(n,\alpha)^{75}Ge$ reaction.								
K118	2.085	13.32	0.355	4770	1.01×10^5	2.111	6.66	
K133	1.951	19.52	0.355	3850	5.56×10^4	1.090	6.29	6.35
K136	1.892	34.19	0.342	4650	3.85×10^4	0.9725	6.09	$\pm$0.18
	$\lambda^{75}Ge = 0.0084537\ min^{-1}$							
Table 35. Results of $^{80}Se(n,\alpha)^{77}Ge$ reaction.								
K118	4.417	13.32	0.361	543	1.93×10^4	2.526	2.43	
K133	4.133	19.52	0.360	394	5.60×10^3	1.127	2.40	2.26
K136	4.008	34.19	0.358	400	3.27×10^3	1.002	1.96	$\pm$0.15
	$\lambda^{77}Ge = 0.0010224\ min^{-1}$							
Table 36. Results of $^{82}Se(n,\alpha)^{79}Ge \rightarrow {}^{79}As$ reaction.								
K122	0.7710	47.32	0.356 (0.200) *	1.86×10^4	5.54×10^4	0.02032 (0.3008) †	7.61	
K128	0.7925	75.37	0.341 (0.144)	4.51×10^4	1.60×10^5	0.1994 (1.263)	6.92	6.47
K133	0.7623	87.92	0.346 (0.167	3.68×10^4	1.12×10^5	0.1765 (0.8192)	5.36	$\pm$0.50
K136	0.7394	100	0.344 (0.171)	3.56×10^4	8.75×10^5	0.1907 (0.7517)	5.99	

* The values here are for ^{79}As, those in brackets for ^{79m}Se.

† The values in brackets are for ^{79}As.

$\lambda^{79}As = 0.077022\ min^{-1}$. $\lambda^{79}Ge = 0.6932\ min^{-1}$.

Part 6.

Irradiation of indium metal at 2.5 MeV.

a). Investigation of the contribution to the induced activity from background neutrons.

Many of the nuclear reactions induced at 2 MeV are also energetically possible with thermal and epithermal neutrons. The effect of scattered neutrons of degraded energy must therefore be considered when measuring cross-sections at this energy. The contribution to the activity induced in indium foil from the reaction $^{115}In(n,\gamma)^{116m}In$, by background neutrons was investigated by two methods.

In the first, comparison was made between the activity induced in foils irradiated with and without wrappings of cadmium sheet, to act as a slow neutron shield. In the second, the variation with distance from the target of the activity induced in unshielded foils was studied.

Experimental procedures.

(i) The indium foil in the form of a narrow strip, encircling the target at a radius of 2.23 cm, was positioned to accept neutrons at about 90^{o} to the incident deuteron beam direction. The thin walled target block described in Chapter 2 was used here to reduce the scattering material near the sample. The

foil was irradiated with and without cadmium sheet. The direct neutron flux was monitored using the associated particle method by counting protons, and the ^{116m}In activity was counted on a NaI(T1) scintillation crystal set on the 1.27 MeV photo-peak. The results obtained are shown in Table 37.

(ii) Sixteen squares of indium foil were irradiated on a cone at 105° to the direction of the deuteron beam by placing four squares at each of four distances from the target centre. Each square of a set of four was spaced at 90° intervals to the others round the cone, and arranged so that it did not screen any other square from the target. Again the direct neutron flux was monitored by counting protons, and the induced activity detected on a scintillation crystal. The results are shown in Table 38.

Table 37. Variation of induced activity with thickness of cadmium shield.

Thickness of cadmium shield (mg cm^{-2})	Position of shield	Normalised specific activity (c/m/g/proton)
—	—	1
330	outside and inside	0.733
660	" "	0.704
990	" "	0.681
660	outside	0.791
660	inside	0.826

Table 38. Variation of induced activity with distance from target.

Target distance R, (cm)	$\frac{1}{R^2}$ (cm^{-2})	Normalised specific activity (c/m/g/proton)
2.55	0.154	1
3.05	0.108	0.861
4.05	0.061	0.702
5.05	0.039	0.620

From Table 37 it is seen that the activity induced by background neutrons is some 30% of that from direct neutrons at the position of the foil, and also that 330 mg cm^{-2} of cadmium is sufficient to absorb the majority of these neutrons. The figures for the cadmium shield on the inside or outside of the foil indicate that a large percentage of low energy neutrons arise from within the target itself as well as from the surrounding walls.

A plot of the values from Table 38, of specific activity versus the square of the reciprocal of the target distance (Fig 41), gives a fairly straight line indicating that the inverse square law is obeyed.

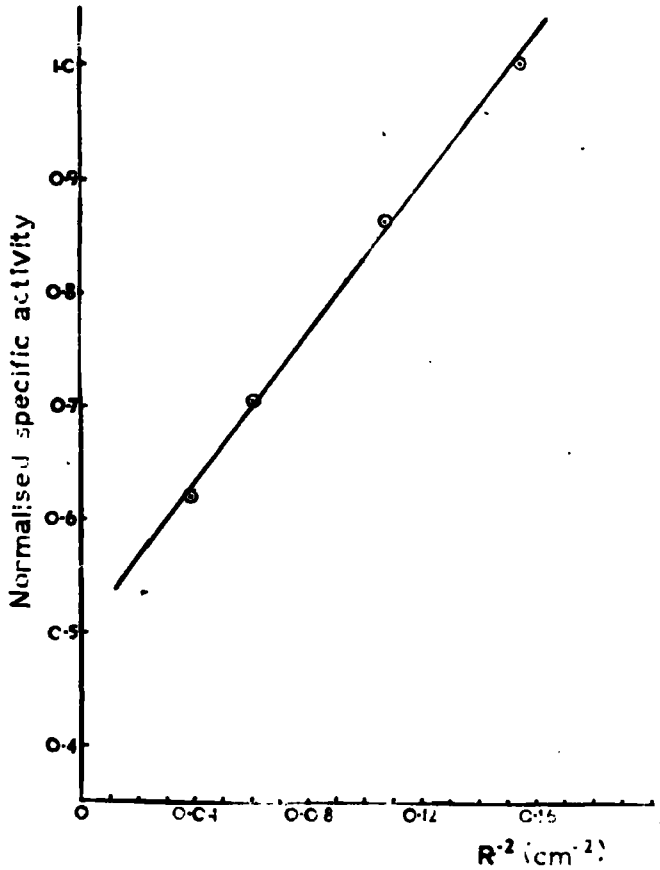

Fig.41 Variation of activity with target distance.

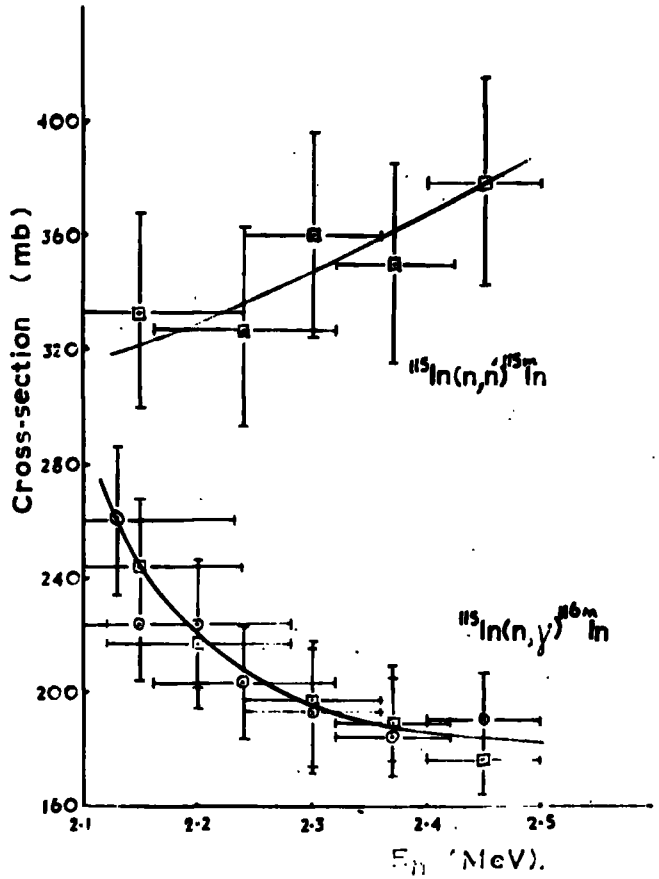

Fig.42 Excitation functions for In reations.

b). Measurement of the cross-sections of the reactions induced in ^{115}In between 2.1 and 2.5 MeV.

The excitation function for the following two reactions have been measured between 2.1 and 2.5 MeV.

$^{115}In(n,\gamma)^{116m}In$ ($t_{\frac{1}{2}} = 54.0 \pm 0.5m$) (Q = +6.610 MeV)

$^{115}In(n,n^1)^{115m}In$ ($t_{\frac{1}{2}} = 4.5 \pm 0.1$ hr) (Q = -0.335 MeV)

Experimental procedures.

Indium foil 99.95% pure and 0.005" thick was obtained from Johnson Matthey and Co. Ltd. Five or six strips 0.4 cm wide were positioned side by side encircling the target, and subtending angles between 95 and 140° to the incident deuteron beam. The indium foils were irradiated, sandwiched between two 660 mg cm^{-2} thick cadmium foils, for periods of up to 90 minutes. The direct neutron flux was measured by the associated particle method, by counting protons on the Ortec solid state counter as described in Chapter 2 and Chapter 3.

After an irradiation each foil was tightly rolled, and dropped inside a semi-micro test tube which was placed inside a brass tube set at the centre of the face of a 3" x 3" NaI(T1) scintillation crystal. For the ^{115m}In activity the window of the spectrometer was set on the 0.335 MeV photopeak while for the ^{116m}In activity both the 1.085 and 1.27 MeV photopeaks

were counted. Counter efficiences were calculated from the data of Crouthamel[42] and absorption curves of Davisson and Evans[62].

Since the decay scheme of ^{115m}In is fairly simple, the counter efficiency was calculated directly and found to be 7.71% (allowing for the internal conversion constant of 0.98). The decay scheme for ^{116m}In, however, is extremely complex and the following equation was derived in an attempt to calculate the counter efficiency for this isomer; the notation is the same as that described in Part 1 of this Chapter.

$$N = No\Big[P_{1.27}(0.02(1 - T_{1.77}) + 0.10(1 - T_{1.487}) + 0.15(1 - T_{0.82})(1 - T_{0.460}))$$

$$+ (P_{1.085} + P_{1.27} - P_{1.035}\, P_{1.27})(0.42 + 0.06(1 - T_{1.37}) + 0.08(1 - T_{0.460}))\Big].$$

The calculated efficiency was 7.5%.

Results and comparison with other work.

The results of the two irradiations made on indium are presented in Tables 39 to 41 and Fig. 42. The values for the $^{115}In(n,\gamma)^{116m}In$ reaction are almost a constant factor of two higher than the data published in the compilation of Hughes[110]. On the other hand the values for the inelastic scattering cross-section are in close agreement with the only other determination that of Martin et al[111]. A possible explanation of the disparity in the (n,γ) cross-section lies in the estimation of

the counter efficiency from a complex decay scheme, although it seems rather unlikely that such errors could give rise to a discrepancy of this order.

Estimation of error.

Errors of 10% could arise from the measurement of sample target distances and the calculation of the absolute neutron flux. The estimation of the counter efficiency of ^{115m}In should be less than 10% in error but that for ^{116m}In could perhaps be about 50%. This gives a total error for $^{115}In(n,n^{1})^{115m}In$ cross-sections of $\pm$ 14% and for the $^{115}In(n,\gamma)^{116m}In$ cross-section $\pm$ 50%.

Sample No.	No. of target nuclei x 10^3/N	Ao obs. c/m. x 10^{-3}	Ao corrt. d/m. x 10^{-4}	Mean angle of sample (degrees)	Square of mean separation of sample and target (cm^2)	Rn thick (400 KeV)	Mean neutron energy (MeV)	Calculated cross-section (mb)
Table 39. Irn No. K3 Result for $^{115}In(n,\gamma)^{116m}In$ cross-section.								
1	2.495	3.98	5.31	97° 5'	5.141	1.626	2.45 ± 0.05	190
2	2.352	3.57	4.76	104° 55'	5.423	1.568	2.37 ± 0.05	184
3	2.318	3.58	4.77	112° 0'	5.891	1.491	2.30 ± 0.07	193
4	2.344	3.59	4.79	118° 50'	6.601	1.411	2.24 ± 0.08	203
5	2.435	3.80	5.07	124° 45'	7.497	1.345	2.20 ± 0.08	224
6	2.427	3.41	4.55	129° 55'	8.697	1.290	2.15 ± 0.09	224
7	2.444	3.62	4.83	134° 20'	9.903	1.247	2.13 ± 0.10	260

Counter efficiency = 0.075, Rp thick $(\gamma_{dn}/\gamma_{dp})400KeV = 0.9735$,

Ω p = 1.661×10^{-6} sterad . $\lambda^{116m}In = 0.01283\ min^{-1}$

Proton count correction for decay = 214,600

Sample No.	No. of target nuclei $\times \frac{10^3}{N}$	Ao obs. c/m. $\times 10^{-3}$	Ao corrt. d/m. $\times 10^{-4}$	Mean angle of sample	Square of mean separation of sample and target (cm^2)	Rn thick (400 KeV)	Mean neutron energy (MeV)	Calculated cross-section (mb)
Table 40. Irrn. No. K4 Results for $^{115}In(n,\gamma)^{116m}In$ reaction cross-section.								
1	2.291	4.50	6.00	97° 5'	5.141	1.626	2.45 ± 0.05	176
2	2.427	5.01	6.68	104° 55'	5.423	1.568	2.37 ± 0.05	189
3	2.346	4.88	6.51	112° 25'	5.927	1.487	2.30 ± 0.07	197
4	2.492	4.99	6.65	124° 45'	7.497	1.345	2.20 ± 0.08	217
5	2.494	4.43	5.91	130° 30'	9.947	1.284	2.15 ± 0.09	244

Counter eff. = 0.075, Rp thick (γ_{dn}/γ_{dp}) 400 Kev = 0.9735,

Ω_p = 1.661 x 10^{-6} sterad. $\lambda^{116m}In$ = 0.01283 min^{-1}

Proton count correction for decay = 274,100.

Table 41. Irrn. No. K5 Results for $^{115}In(n,n^1)^{115m}In$ reaction cross-section.

1	"	30.5	39.6	"	"	"	"	379
2	"	29.4	38.1	"	"	"	"	350
3	"	28.2	36.6	"	"	"	"	360
4	"	23.7	30.7	"	"	"	"	326
5	"	19.1	24.8	"	"	"	"	333

Counter eff. = 0.077, Proton count corrt. for decay = 420,900

$\lambda^{115m}In$ = 0.002567 min^{-1}

Part 7.

Measurement of the $^{31}P(n,p)^{31}Si$ reaction cross-section between 2.1 and 2.5 MeV.

The cross-sections of the (n,p) reaction on ^{31}P has been determined by a number of workers (the values have been compiled by Liskien and Paulsen[17]), and others, such as Gonzalez et al[112], have used it as a reference cross-section in this energy region. It was considered to be of interest to measure this fairly well known cross-section, mainly to check the calculations made for the absolute neutron flux determinations.

The details of the reaction are:-

$^{31}P(n,p)^{31}Si$ ($t_{\frac{1}{2}}$ = 2.60 ± 0.05 h) (Q = -0.694 MeV)

Experimental procedures.

AnalaR grade sodium dihydrogen orthophosphate ($NaH_2PO_4.2H_2O$) was packed into Portex 320 polythene tubing (internal and external diameters 0.25 and 0.35 cm respectively). Four 18 cm lengths, each containing about one gram of sample, were wound round the target wall so as to accept neutrons from 90° to 130°. The samples were surrounded with 660 mg cm^{-2} layers of cadmium foil to reduce the effects of background neutrons.

The samples were irradiated in this position for 90 minute periods the absolute neutron flux being determined by the

associated particle method, by counting protons as has been described in Chapters 2 and 3.. After an irradiation, a few drops of silicon carrier solution were added to each sample which was then dissolved and made up to 12 ml with water. 10 ml aliquots of these solutions were counted in the pre-calibrated liquid G.M. counter and the decay followed for several half-lives. No activity other than that of ^{31}Si was observed.

Results and comparison with other work.

The results for the two irradiations made are presented in Tables 42 and 43 and Fig. 43. The agreement between the two runs is good and indicates a smooth increase in the cross-section with increase in neutron energy. The values obtained are a little higher than those of Luscher et al[113], and Ricamo[114] of 40 ± 10 mb at 2.5 MeV. The later work of Grundl[115] et al, however, suggests a lower value, nearer 20 mb at 2.5 MeV while the excitation function determined down to 2.7 MeV by Cuzzocrea et al.[116] (normalising on an absolute point of Grundl) indicates a higher value of around 50 mb. The values obtained here are not greatly different from those published, and therefore the neutron flux calculations were considered to be reasonable.

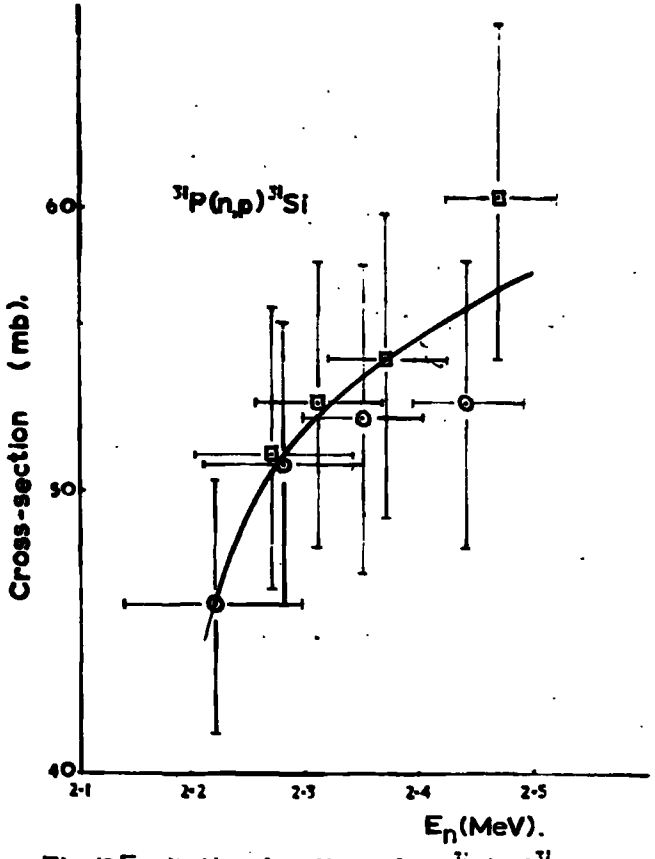

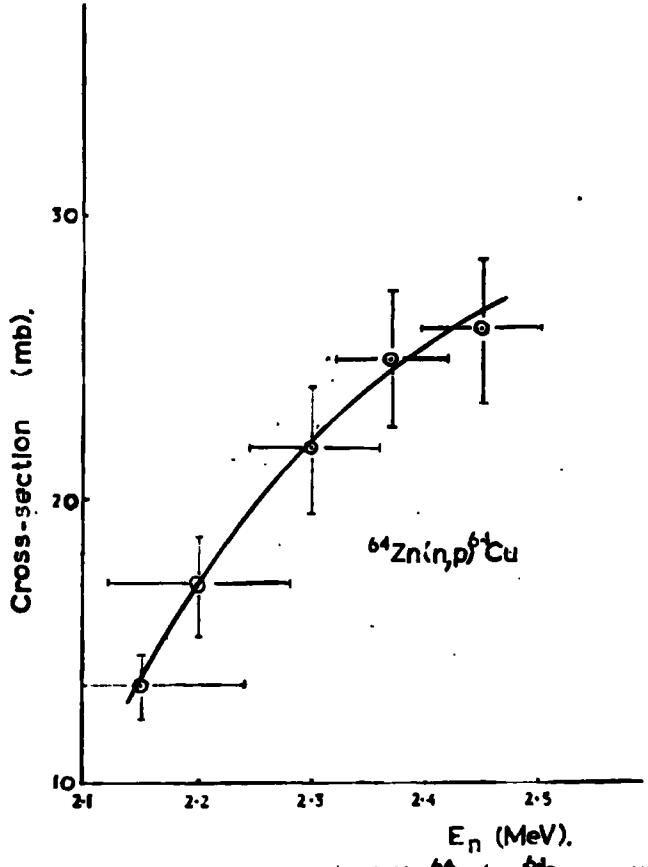

Fig.43 Excitation function of the $^{31}P(n,p)^{31}Si$ reaction. Fig.44 Excitation function of the $^{64}Zn(n,p)^{64}Cu$ reaction.

Estimation of error.

The errors arising from counter standardisation and statistics should not be more than 2% while the solid angle subtended by the solid state counter was determined to $\frac{1}{2}$%. The main errors again come in the determination of the sample-target separation and in calculations of neutron flux, which together should not be more than $\pm$ 10%. The error here was therefore taken as $\pm$ 10%.

Sample No.	No. of target nuclei $\times \frac{10^3}{N}$	Mean neutron energy (MeV)	Calculated cross-section (mb)
Table 42. Irrn. No react			
1	5.223	2.44 ± 0.05	53.1
2	5.689	2.35 ± 0.05	52.6
3	5.714	2.28 ± 0.07	51.0
4	5.673	2.22 ± 0.08	46.0

Counter eff. = 0.0

$R_p(\gamma_{dn}/\gamma_{dp})$400 KeV

$\lambda^{31}Si$ = 0.004376

Table 43. Irrn. No react			
1	5.931	2.47 ± 0.05	60.3
2	5.139	2.37 ± 0.05	54.7
3	5.475	2.31 ± 0.06	53.1
4	5.478	2.27 ± 0.07	51.3

Counter eff. = 0.0

$R_p(\gamma_{dn}/\gamma_{dp})$400 KeV

$\lambda^{31}Si$ = 0.004376

Part 8.

Measurement of the $^{64}Zn(n,p)^{64}Cu$ reaction cross-section between 2.1 and 2.5 MeV.

The details of the reaction studied here are:-

$^{64}Zn(n,p)^{64}Cu$ $(t_{\frac{1}{2}} = 12.8 \pm 0.1h)$ $(Q = +0.209$ MeV).

Only two previous excitation functions of this reaction in the energy range 2.0 to 3.6 MeV are reported in the literature. Both of these are effectively by the same group - Rapaport and Van Loef[117] and Van Loef[118]. The first was made relative to the $^{31}P(n,p)^{31}Si$ reaction at 3.56 MeV from the data of Grundl[115] while the second was made relative to the first. The errors quoted were $\pm$ 20%.

Experimental procedures.

High purity (99.9999%) zinc metal foil (obtained from Koch-Light Ltd.) was irradiated (in the form of strips 0.4 cm wide) and counted in a similar manner to that already described for indium. The γ-ray scintillation spectrometer was set on the 0.51 MeV photopeak to count the annihilation radiation, comparison being made with a standard ^{22}Na source. (The activity of the ^{64}Cu produced was found to be too low to count by the usual annihilation coincidence methods). The single channel annihilation equation for ^{22}Na has been described in

Part 1 of this Chapter while that for ^{64}Cu would be identical with those for ^{13}N and ^{18}F. The counter efficiency obtained was 4.6%.

The neutron flux was again determined by the associated particle method.

Results and comparison with other work.

Only one irradiation was carried out and the results are presented in Table 44 and Fig. 44. The value of the cross-section rises smoothly from 13.5 mb at 2.15 MeV to 26.1 mb at 2.45 MeV. This is in good agreement with that obtained by Rapaport and Van Loef[117] of 10.5 ± 1.5 mb at 1.99 MeV and 30 ± 6 mb at 2.55 MeV. This agreement again lends support for the neutron flux measurement made here.

Estimation of error.

The error in the ^{22}Na standard source was 2% and the counting statistics not more than 1%. Again the main error arises in the neutron flux determination which may be as large as ± 10%. The total error is therefore ± 10%.

Table 44. Irrn. No. K8 Results for $^{64}Zn(n,p)^{64}Cu$ cross-section.

Sample No.	No. of target nuclei $\times \frac{10^3}{N}$	Ao obs. c/m	Ao corrt. d/m $\times 10^{-3}$	Square of mean separation of sample and target (cm^2)	Rn thick	Mean neutron energy (MeV)	Calculated cross-section (mb)
1	6.045	125	2.72	5.141	1.626	2.45 ± 0.06	26.1
2	6.102	119	2.59	5.423	1.568	2.37 ± 0.05	25.0
3	6.060	100	2.17	5.927	1.487	2.30 ± 0.06	21.9
4	6.289	71	1.54	7.497	1.345	2.20 ± 0.08	17.1
5	6.264	44	0.957	9.947	1.284	2.15 ± 0.09	13.5

Counter eff. = 0.046 R_p thick(γ_{dn}/γ_{dp})400KeV

Ω_p = 1,661×10^{-6} sterad. $\lambda^{64}Cu$ = 0.0008998 mi

Proton count corrected for decay = 454,600

Part 9.

Investigation of the possible measurement of (n,particle) reaction cross-sections at 2.5 MeV.

Very few of the cross-sections for nuclear reactions which have favourable Q values appear to have been measured in this energy region. A search was made through the nuclide chart to select those nuclides for which either an (n,p) or (n,α) reaction was energetically possible. Of these the reactions were chosen for which the products had a reasonable half-life, the target nuclide had a natural abundance of more than 5%, and of which the element could be obtained in a convenient form. The choice of nuclides included those with odd and even neutron numbers in case pairing effects made one reaction more probable.

Experimental procedures and results.

The reactions chosen are set out in Table 45. Gram quantities of the elements, or compounds containing the nuclides, were irradiated at 0^{o} to the incident deuteron beam and close up to the target block, so as to obtain the maximum flux available. The samples were irradiated for periods of up to 2 hours in order to obtain an integrated flux of 5×10^{11} n cm^{-2}.

After an irradiation each sample was counted under an end-

window proportional counter and the decay followed down to background. Only in the cases of arsenic and palladium were activities corresponding to products of (n,p) reactions seen. These reactions were:-

$^{75}As(n,p)^{75}Ge$ and $^{105}Pd(n,p)^{105}Rh$

In both of these, the initial count rate amounted to 15 c/m, that is just over the background count rate. It was considered therefore, that if the samples were irradiated in a position of relatively good geometry for good neutron energy resolution (at 90^{o} to the incident beam), where, not only would the flux be reduced by over a factor of ten, but the mean neutron energy would be reduced by about 0.5 MeV to 2.5 MeV, no activity would be observed with the present equipment. Investigations of this field were therefore discontinued.

Table 45. Reactions studied at 3 MeV.

Reaction	$t_{\frac{1}{2}}$	Natural abundance (%)	Q value (MeV)	Compound irradiated
$^{41}K(n,\alpha)^{38}Cl$	37.3m	6.8	- 0.100	K_2CO_3
$^{51}V(n,\alpha)^{48}Sc$	44h	99.75	- 2.04	NH_4CO_3
$^{66}Zn(n,p)^{66}Cu$	5.1m	27.8	- 1.85	Zn
$^{75}As(n,p)^{75}Ge$	82m	100	+ 0.40	As_2O_3
$^{77}Se(n,p)^{77}As$	39h	7.5	+ 0.10	SeO
$^{96}Ru(n,p)^{96m}Tc$	52m	5.6	+ 0.56	$RuCl_3$
$^{99}Ru(n,p)^{99m}Tc$	6.0h	12.7	+ 0.35	"
$^{105}Pd(n,p)^{105}Rh$	36h	22.2	+ 0.22	Pd
$^{109}Ag(n,p)^{109}Pd$	13.6h	48.6	- 0.33	$AgNO_3$
$^{115}In(n,p)^{115}Cd$	54h	95.22	- 0.67	In
$^{120}Sn(n,\alpha)^{117}Cd$	3.0h	32.5	+ 0.77	Sn
$^{123}Sb(n,p)^{123}Sn$	40m	42.75	+ 0.64	Sb_2O_3
$^{197}Au(n,p)^{197}Pt$	19h	100	+ 0.03	Au

Target nucleus	Measured cross-section (mb)	Estimated Statistical error (mb)	Estimated Systematic error (mb)	Calculated values (mb)			
				Levkovskii	Gardner	Mani & Iori	Brown & Muirhead.
Table 46. Results for the (n,p) reactions.							
^{16}O	36.2	0.4	3.0	80	64		20
^{42}Ca	148	7	10	190	184		
^{43}Ca	100	4	8	92	92		
^{44}Ca	40.4	1.5	2.9	46	46		
^{54}Fe	371	40	185	305	496	350	
^{56}Fe	98.3	2.4	5.4	100	124	70	90
^{76}Se	58.8	5.1	4.7	(38.4)	152	45	
^{77}Se	44.7	5.5	3.6	45(26)	76	25	25
$^{78}Se \rightarrow g.s$	20.6	0.7	1.6	(18.3)	38	15	
$^{78}Se \rightarrow e.s$	16.3	6.5	5.2	—			
Table 47. Results for the (n,α) reactions.							
^{78}Se	6.35	0.18	0.50		(3.23)	5	
^{80}Se	2.26	0.15	0.18		(0.41)		
^{82}Se	6.47	0.50	0.81				

Table 48. Results for the (n,2n) reactions.

Target nucleus	Measured cross-section (mb)	Estimated Statistical error (mb)	Estimated Systematic error (mb)
^{14}N	7.42	0.13	0.47
^{19}F	52.1	0.6	3.3
^{48}Ca	868	67	130
^{54}Fe	8.9	0.03	0.6
^{63}Cu	550	6	33
$^{74}Se \rightarrow e.s.$	167	7	14
$^{74}Se \rightarrow g.s.$	458	19	37
^{76}Se	2850	144	360
$^{82}Se \rightarrow e.s.$	860	170	69
$^{82}Se \rightarrow g.s.$	489	95	59

Table 49. Results for the (n,t) reactions.

Target nucleus	Measured cross-section (mb)	Estimated Statistical error (mb)	Estimated Systematic error (mb)	Calculated cross-section Baerg & Bowes (mb)
^{40}Ca	0.006	0.001	0.003	2×10^{-6}
$^{54}Fe \rightarrow e,s.$	2.66	0.42	0.55	
$^{54}Fe \rightarrow g.s.$	<0.31	0.07		1×10^{-6}

Table 50. Results for the reactions at 2.3 MeV.

Reaction	Measured cross-section (mb)	Estimated Systematic error (mb)
$^{115}In(n,\gamma)^{116m}In$	195	97
$^{115}In(n,n^{1})^{115m}In$	360	50
$^{31}P(n,p)^{31}Si$	52.5	5.3
$^{64}Zn(n,p)^{64}Cu$	21.9	2.2

Part 2.

Discussion.

The existing data on nuclear reaction cross-sections is extensive, but reported errors are often large, especially in the older work[illegible], and it was considered useful to apply methods leading to values in which more confidence could be placed. That this has been achieved is shown in the collected results given in Tables 46 to 50; for most measurements statistical errors are only a few per cent and the estimated systematic error is less than 10%. In addition, some cross-sections which do not appear to have been previously reported were measured.

The increased accuracy is considered to arise from the care and attention given to counter calibration and absolute neutron flux determination. Absolute measurement of the neutron flux was used mainly in the determination of the $^{56}Fe(n,p)^{56}Mn$ cross-section, the error of which amounted to less than 5.5%. Other reaction cross-sections could then be measured using this as a reference. The use of both radiochemical separations and β-particle and γ-ray counting techniques enabled the radioactive species to be identified and determined with considerable certainty.

The measurements made here are almost entirely confined

to the middle weight region (except for oxygen, nitrogen and fluorine). Where it has been possible to compare the results with calculated values based on the statistical theory fairly good agreement has been found for (n,p) and (n,α) cross-sections. This supports the now generally accepted view that the compound nucleus process predominates over direct interactions in this region.

Energy spectra, and angular distribution studies of emitted particles, as well as cross-section values, indicate that both processes occur over the entire mass range. Since the energy of emission of charged particles from the decay of the compound nucleus is in general lower than for those emitted from direct interactions, the latter process is favoured on moving to heavier nuclei because of the increased height of the Coulomb barrier. Strohal et al.[119] have pointed out that compound nucleus formation is still the most probable interaction where Coulomb barrier considerations are small; this is further supported by the observation that neutron emission is the commonest mode of de-excitation, which is largely a statistical process in the heavy region.

For (n,p) reactions direct effects are evident in both light ($A \leqslant 40$) and heavy($A > 90$) nuclei. The approximate theoretical calculations of Brown and Muirhead[11] (and the extension of their work to heavier masses by Coleman et al.[120])

follow the trend of the experimental data but tend to be low at heavier masses. Three of their values corresponding to the measurements reported here are included in Table 46. These authors calculated the contributions from both processes separately using a Fermi gas model of the nucleus and a three stage interaction process. That is, that the incident nucleus collides with one of the nucleons of the target nucleus, which then emits particles directly or after first forming an excited nucleus. A more general three stage process has been suggested by Weisskopf[121].

Mani and Iori[122] used optical model considerations and calculated (n,p) and (n,α) excitation functions between 5 and 25 MeV for almost all stable nuclei. Their values are in general in good agreement with experimental data up to A = 80 when they begin to diverge. Their values for the cross-sections reported here are also included in Tables 46 and 47 and are in close agreement.

Brown and Muirhead[11] treated the interaction as a volume effect but suggested possible surface interactions for protons because of the resulting reduced Coulomb barrier. Surface interactions must be of even more importance in the case of (n,α) reactions because of the very low penetrability of this particle through nuclear matter. Colli et al.[123] have suggested that this hypothesis is further supported by the Pauli exclusion principle which would diminish the possibility of more effective

interactions in the occupied internal states.

The results for the measurement of (n,p) reaction cross-sections for three adjacent isotopes of both calcium and selenium (Table 46) show that the Levkovskii[10] trend is only partially obeyed here. In each case the cross-section of the lightest isotope is only 1.5 times that of the next, while the predicted factor of 2 is observed between the heavier pair. For the (n,α) cross-sections on selenium (Table 47), however, the values first decrease and then increase. It has been suggested by Gardner[12] that the constant factor is a Q value effect.

Both Levkovskii[124] and Gardner[12] have derived empirical formulae, the latter on the basis of the statistical model, which predicts (n,p) cross-sections at 14 MeV. Later Gardner[20] added Q value and pairing energy effects. Both equations give reasonable agreement with experimental data but in general Levkovskii's simpler treatment gives the better fit. When Levkovskii's calculations were checked, however, some disagreement, usually small, was found with almost all the values quoted. In the case of selenium they are about a factor of two high. The predicted values are also included in Table 46 together with those calculated in the present work (bracketed). The good agreement is the more surprising since the statistical model process is expected to be highly sensitive to variations

in Q value, pairing energies and neutron and proton shell closure, all of which the equations ignore.

Chatterjee's[125] plot of (n,p) cross-sections against proton and neutron number of the residual nuclei reveals minima corresponding to proton shell closure but no similar effects corresponding to neutron shell closure. Gardner[20] disclaims this as a shell effect and attributes it to the increase in the N/Z ratio with increasing A of stable nuclei on changing from one region to the next.

Colli[126] has suggested that (n,d) reactions differ from (n,p) reactions in proceeding entirely through direct interactions.

For (n,α) reactions both mechanisms are again present, but the direct effects are reduced. The statistical mechanism makes the major contribution to this process in the mass range 20 - 70. Facchini et al[127] have noted that on plotting cross-sections against neutron number, besides the general decrease in value with increasing N, maxima occur at the neutron magic numbers 50 and 82. At these magic numbers the competing (n,n^1) process has a small cross-section corresponding to a minimum in the level density parameter, and therefore α-particle emission is favoured. On comparison with values calculated from the statistical model they find agreement with experimental values for $A < 60$ and at 50, 82 and perhaps 126.

They suggest, therefore, that in the other mass regions where the compound nucleus mechanism is reduced, direct effects occur.

Chatterjee[128] again noticed minima corresponding to proton shell closures on plotting (n,α) cross-sections against proton number, Z. He again failed to notice minima corresponding to neutron shell closures. Wille and Fink[129] also searched for neutron shell effects at N = 82 and concluded that these effects were negligible. Neither of these workers mention the maxima observed by Facchini et al.[127]

By including Coulomb barrier effects Gardner[21] has extended his emperical formula to predict (n,α) cross-sections in the range $6 \leqslant Z \leqslant 30$. His predictions again agree quite well with the experimental values available although discrepancies were found for ^{16}O and ^{26}Mg. His calculations have been extended in the present work to selenium (Z = 34) by assuming that A_Z, a stability line parameter, is 2Z + 8. The values obtained are compared with experiment in Table 47 and are found to be a little low. The lack of a Q value for the (n,α) reaction of ^{82}Se prevented the calculation of this cross-section.

In order to explain high (p,α) cross-section values and energy spectra for heavy nuclei, Wilkinson[130] and Hodgson[131] have suggested a cluster model direct interaction process.

Here quasi-free α-particles or tritons in the nuclear surface are respectively knocked out or picked up by the incident proton. Similar considerations were suggested for (n,α) reactions which require the preformation of α-particles and ^{3}He particles.

A similar process might be applied to (n,t) reactions. Estimates from the statistical model of the cross-sections for this type of reaction by workers such as Baerg and Bowes[72] and Heinrich and Tanner[22] are in general considerably lower than the experimental values. (The values calculated by Baerg and Bowes for reactions at 14.5 MeV are included in Table 49). This together with the direct nature of (n,d) reactions, suggests that direct reaction effects may be present.

The suppression of charged particle emission by the Coulomb barrier on moving to heavier masses causes the (n,2n) and (n,n^1) reactions to become more probable. These two reactions almost completely account for the non-elastic reaction cross-section in the heavy mass region. The results of many workers - (e.g. Paul and Clarke[7], Wille and Fink[132] and Khurana and Hans[133]) were explained by the statistical theory although in some cases the experimental values were rather low.

Recently Bormann[15] has made an extensive survey of (n,2n) reactions and suggested that the low values are explained by

maxima in the competing (n,n^1) reaction. He plotted (n,2n) cross-sections against A separately for even-proton and odd-proton nuclei. In the even-proton nuclei he observed minima corresponding to magic neutron numbers 28 and 50 and maxima at 82 and 126. For odd-proton nuclei minima were observed at N = 20, but maxima at 28, 50, 82 and 126. The minima at low magic numbers corresponded to minima in reaction Q values. The maxima, however, were explained by showing that the nuclear level density parameter and pairing energy go through minima at magic neutron numbers so causing a change in the distribution of nuclear levels which causes a minimum in the cross-section for the (n,n^1) process. Between magic numbers the (n,n^1) reaction cross-sections rise to several hundred millibarns but these are reduced towards magic numbers of the target nucleus where the (n,2n) cross-section almost reaches the full calculated statistical model value.

In the measurements of the present work, the very low value for the $^{54}Fe(n,2n)$ cross-section of 8.9 mb corresponds to a minimum at the neutron shell closure for N = 28.

Agreement between experimental measurements and theoretical values can be seen to be reasonable; this applies to many of the reaction cross-sections at 14 MeV, although the agreement is rarely very close. It is hoped that work on excitation

functions, angular distributions and energy spectra will provide more information. The study of rarer reactions should be facilitated as higher neutron fluxes and separated isotopes become available.

Appendix A

Experimental techniques used for the reference reaction $^{56}Fe(n,p)^{56}Mn$.

(i) Standard method.

The $^{56}Fe(n,p)^{56}Mn$ reaction has been widely used by previous workers in this laboratory as a reaction relative to which other measurements could be made. The technique developed involves irradiating about 0.5g of iron in the form of foil for the sandwich method, or granules for the homogeneous mixture method; the iron may then be rapidly separated from the rest of the sample by mechanical means (electromagnetically for the homogeneous mixture). The pure ($\geqslant$ 99.8%) iron foil came from the Research Department of the United Steel Co. Ltd., and the granules (99.9% pure) from the Bureau of Analysed Samples Ltd. (B.C.S. No. 149/1).

After separation 0.5g of iron was dissolved in 10 ml of a standard acid solution (50% 5N sulphuric acid, 50% 5N nitric acid and 0.5 mg ml^{-1} manganese (II) carrier) and made up to 12 ml with further acid mixture. A 10 ml portion of this was counted in a liquid G.M. tube previously calibrated for ^{56}Mn in this acid mixture. The efficiency of the counter used in the present work was 7.67 $\pm$ 0.15%.

(ii) Amended method used in the irradiation of nitrogen and fluorine.

In the irradiation of nitrogen and fluorine (Chapter 4 part 3), a non-standard method was unfortunately used to dissolve the iron. Here 0.5g was dissolved in 5 ml of 8N hydrochloric acid and 0.25 ml of 20 volume hydrogen peroxide with the addition of 1 mg manganese (II) chloride to act as a carrier. The solution was made up to 25 ml with water and 10 ml were counted in the liquid sample G.M. tube.

To standardise this method three irradiations were carried out in which 1g of iron granules was irradiated close to the D,T target block, thoroughly mixed, divided into two 0.5g samples and dissolved using the two methods described.

The results of the measurements gave a ratio between the methods of 1.055 ± 0.002 representing a counting efficiency of 8.09% for the hydrochloric acid solution.

(iii) Amended method used with the increased neutron flux of the S.A.M.E.S. machine.

The higher specific activity induced in the iron by the larger flux at Canterbury made the standard solution method described above unsuitable. It was considered that to reduce the quantity of iron irradiated with a sample was inconvenient and would lead to errors in the flux measurement; the following

dilution procedure was therefore employed to reduce the activity of the sample so that it could be counted on the day of an irradiation.

An 0.5g quantity of iron was dissolved in 20 ml of the standard acid mixture which was then made up to 100, 250, 500 or 1000 ml with water depending on the amount of activity expected. A 10 ml portion was withdrawn and counted in the usual way.

The efficiency of the counter for the above dilutions relative to that for the standard acid solution was determined by irradiating 2.1g of iron granules, dissolving them in 50 ml of acid mixture and counting samples corresponding to the dilutions stated. The results of the three comparisons made are shown in Table 51.

Table 51. The variation of counter efficiency with dilution.

Dilution	Density ($20^{o}C$) g ml^{-1}	Counter efficiency (%)			Mean efficiency (%)
		1	2	3	
Standard	1.2170	7.67	7.67	7.67	7.67
100 ml	1.0371	8.03	7.96	7.97	7.99 ± 0.02
250 ml	1.0117	8.03	8.00	7.98	8.00 ± 0.02
500 ml	1.0063	8.08	8.03	8.06	8.06 ± 0.02
1000 ml	0.9997	8.03	8.04	8.07	8.05 ± 0.01

(iv) Comparison of sandwich and granule techniques in poor geometry conditions.

In general the sandwich technique was used only in relatively good geometry conditions when foils were to be irradiated some 2 - 5 cm from the target block. In the irradiations of calcium and selenium, however, the sandwich technique was employed since a rapid chemical separation was required; also the foils could be wrapped in polythene to prevent transfer of recoil nuclei. The foils used were 2 cm in diameter with a separation of 0.3 cm. The distance between the target and the front foil was 0.3 cm.

To determine the ratio of the neutron flux at the foils to that passing through the sample the following procedure was carried out. 0.5g of iron granules was intimately mixed with finely powdered sucrose to form a homogeneous mixture. This was then irradiated between two iron foils in identical conditions to those described above. Both foils and granules were dissolved and counted under the same conditions and the ratios of the activities induced in each determined. Three irradiations were carried out with foil separations of 0.2, 0.3 and 0.4 cm. Within the experimental error a constant ratio of 1.049 was found and this factor was therefore applied as a correction to the activity of the iron in irradiations of calcium and selenium.

REFERENCES

1) N. Bohr and F. Kalckar, Kgl. Danske Videnskab Selskab 14 (1937) No. 10.

2) M.G. Mayer, Phys. Rev. 74 (1948) 235: M.G. Mayer and J.H.D. Jensen, The Elementary Theory of Nuclear Shell Structure, Wiley, 1955.

3) G.J. Fischer, Phys. Rev. 108 (1957) 99.

4) V.J. Ashby et al., UCRL-5054 (1958).

5) N. Bohr, Nature 137 (1936) 344.

6) V.F. Weisskopf and D.H. Ewing, Phys. Rev. 57 (1940) 472.

7) E.B. Paul and R.L. Clarke, Can. J. Phys. 31 (1953) 267.

8) H.G. Blosser, Oak Ridge Natl. Lab. Drawing ORNL-LR-DWG: 13811 (1957).

9) H.G. Blosser, C.D. Goodman and T.H. Handley, Phys. Rev. 110 (1958) 531.

10) V.N. Levkovskii, Soviet Physics JETP 33 (1957) 1520.

11) G. Brown and H. Muirhead, Phil. Mag. 2 (1957) 473.

12) D.G. Gardner, Nuclear Physics 29 (1962) 373.

13) A. Chatterjee, Nucleonics 22 (8) (1964) 108.

14) A. Chatterjee, Nucleonics 23 (8) (1965) 112.

15) M. Bormann, Nuclear Physics 65 (1965) 257.

16) H. Neuert and H. Pollehn, EURATOM - Report EUP 122.e (1963).

17) H. Liskien and A. Paulsen, EURATOM - Report EUR 119e (1963).

18) A. Chatterjee, Nuclear Physics 60 (1964) 273.

19) A. Chatterjee, Phys. Rev. 134 (1964) B374.

20) D.G. Gardner and A.D. Poularikos, Nuclear Physics 35 (1962) 303.

21) D.G. Gardner and Yu-Wen Yu, Nuclear Physics 60 (1964) 49.

22) F. Heinrich and F. Tanner, Helv. Phys. Acta 36 (1963) 257.

23) A. Poularikos and D.G. Gardner, Annual Prog. Rept. Nuclear Chem. p.14 (1963).

24) M. Cevolani and S. Petralia, Nuovo Cim. 26 (1962) 1328.

25) J.D. Hemmingway, R.H. James, E.B.M. Martin and G.R. Martin, Proc. Roy. Soc. Ser. A 292 (1429) (1966) 180.

26) A.E. Johnsrud, M.G. Silbert and H.H. Barschall, Phys. Rev. 116 (1959) 927.

27) J.F. Barry, Reactor Sci. Technology 16 (1962) 467.

28) B. Kern and W. Kreger, Phys. Rev. 112 (1958) 926.

29) D.L. Allan and M.J. Poole, Proc. Roy. Soc. (London) 204A (1950) 500.

30) G. Preston, P.F.D. Shaw and S.A. Young, Proc. Roy. Soc. (London) 226A (1954) 206.

31) E.B.M. Martin and G.R. Martin, Handbook for Cockcroft-Walton Accelerator, Londonderry Laboratory

for Radiochemistry, University of Durham.

32) J.R. Morton and D.S. Stark, Trans. Farad. Soc. 56 (1960) 351.

33) G. Dernaley and A.B. Whitehead, Nucl. Instr. and Meth. 12 (1961) 205.

34) R.L. Chase, W.A. Higinbotham and G.L. Miller, IRE Trans. on Nucl. Sci. NS-8 (1961) 147.

35) J.L. Blankenship, IRE Trans. on Nucl. Sci. NS-7 (1960) 190.

36) R. Redstone and M.C. Rowland, Nature 201 (1964) 1115.

37) L.N. Large and H. Hill, Nucl. Inst. and Meth. 34 (1965) 100.

38) K. Fiebiger, Z. Naturforsch. 11a (1956) 607; Z. Angew. Phys. 9 (1957) 213.

39) J. Davies, Thesis, University of Durham, 1960.

40) B.D. Pate and L. Yaffe, Can. J. Chem. 33 (1955) 929.

41) B.W. East, Thesis, University of Durham, (to be submitted 1966).

42) C.E. Crouthamel, Ed., Applied Gamma-Ray Spectrometry, Pergamon Press, New York, 1960.

43) R.L. Heath, Scintillation Spectrometry, Gamma-Ray Spectrum Catalogue, 2nd. Ed., 2 vols. Phillips Petroleum Co., 1964.

44) D. Redon, G.S. Mani, J. Delaunay - Olkowsky and C. Williamson, Nucl. Inst. and Meth. 26 (1964) 18.

45) E.B.M. Martin and J.D. Hemmingway, private communication.

46) B.P. Bayhurst and R.J. Prestwood, Nucleonics 17 (3) (1959) 82.

47) P.J. Campion, Int. J. App. Rad. Isotopes 4 (1959) 232.

48) A.H. Wapstra, Alpha-Beta and Gamma-Ray Spectroscopy, Ed., K. Siegbahn, North Holland, Amsterdam, vol. 1, p539, 1965.

49) J.L. Putman, Chapter 26; Beta and Gamma-Ray Spectroscopy, Ed., K. Siegbahn, North Holland Amsterdam, 1955.

50) D.T. Stevenson and M. Deutsch, Phys. Rev. 83 (1951) 1202.

51) W.F. Biller (thesis), University of California Radiation Laboratory Report UCRL-2067 (1952).

52) E.C. Freiling and L.R. Bunney, Nucleonics 14 (9) (1956) 112.

53) J.D. Buchanan, Radiochemica Acta 4 (1965) 28.

54) J. Benveniste and J. Zenger, UCRL-4266 (1954).

55) E.M. Gunnersen and G. James, Nucl. Inst. and Meth. 8 (1960) 173.

56) S.J. Bame and J.E. Perry, Phys. Rev. 107 (1957) 1616.

57) L. Ruby and R.B. Crawford, Nucl. Inst. and Meth. 24 (1963) 413; UCRL-10752 Suppl. (1963).

58) C.F. Wandel, T. Hesselberg Jensen and O. Kofoed-Hansen, Nucl. Inst. and Meth. 4 (1959) 249.

59) J.L. Tuck, Nuclear Fusion 1 (1961) 201.

60) H.V. Argo, R.F. Taschek, H.M. Agnew, A. Hemmendinger and W.T. Leland, Phys. Rev. 87 (1952) 612.

61) F. Everling, L.A. Koenig, J.H.E. Mattauch and A.H. Wapstra, Nuclear Data Tables (1960), vols 1 and 2.

62) C.M. Davison and R.D. Evans, Revs. Mod. Phys 24 (1952) 79.

63) J. Terrel and D.M. Holm, Phys. Rev. 109 (1958) 2031.

64) M. Bormann, S. Cierjacks, R. Langkau and H. Neuert, Z. Physik. 166 (1962) 477.

65) D. Santry and J. Butler, Can. J. Phys. 42 (1964) 1030.

66) D.M. Chittenden, D.G. Gardner and R.W. Fink, Phys. Rev. 122 (1962) 860.

67) J.E. Brolley, J.L. Fowler and L.K. Schlacks, Phys. Rev. 88 (1952) 618.

68) B. Grimeland, E.Kjellsby and J. Vines, Phys Rev. 137 (1965) B 878.

69) R.N. Glover and E. Weigold, Nuclear Physics 29 (1962) 309.

70) J.M. Ferguson and W.E. Thompson, Phys. Rev. 118 (1960) 228.

71) Nuclear Data Sheets, National Academy of Sciences - National Research Council, Washington, D.C.

72) A.P. Baerg and G.C. Bowes, Can. J. Chem. 39 (1961) 684.

73)

74) M.M. Depray, G. Legros and M.R. Salin, J. Phys. Rad. 21 (1960) 377.

75) D.L. Allan, Proc. Phys. Soc. 70 (1957) 195.

76) H. Neuert and H. Pollehn, Z. Naturf. 16a (1961) 230.

77) C. Carles, Compte Rendus, 257 (1963) 659.

78) L.A. Rayburn, Phys. Rev. 122 (1961) 168.

79) D.L. Allan, Nuclear Physics 24 (1961) 274.

80) P. March and W. Morton, Phil. Mag. 3 (1958) 143.

81) R. Storey, W. Jack, and A. Ward, Proc. Phys. Soc. 75 (1960) 526.

82) W. Cross, R.L. Clarke, K. Morin, G. Slinn, N.M. Ahmed and K. Beg, Bull. Am. Phys. Soc. 7 (1962) 335.

83) E.B.M. Martin and G.R. Martin, private communication.

84) J.D. Dudley and C.M. Class, Phys. Rev. 94 (1954) 80.

85) I. Heertze, L. Delvenne, W. Naget and A.H. W. Aten Jr., Physica 30 (1964) 1762.

86) D.O!Brill, N.A . Vlasov, S.P. Kalinin and L.S. Sokolov, Doklady (Soviet Physics) 6 (1961) 24.

87)

88) J. Picard and C.F. Williamson, Nuclear Physics 63 (1965) 673.

89) C.F. Williamson, J. Phys. Rad. 22 (1961) 651.

90) M. Bormann, E. Fretwurst, P. Schenka, G. Wrege, H. Buttner, A. Lindner and H. Meldner, Nuclear Physics 63 (1965) 438.

91) V.J. Ashby, H.C. Catron, L.L. Newkirk and C.J. Taylor, Phys. Rev. 111 (1958) 616.

92) K.W. Seeman and W.E. Moore, Bull. Am. Phys. Soc. 6 (1961) 237.

93) J.De Juren, R. Stooksberry and M. Wallis, Phys. Rev. 127 (1962) 1229.

94) J. Kantele and D.G. Gardner, Nuclear Physics 35 (1962) 353.

95) A.B. Lillie, Phys. Rev. 87 (1952) 716.

96) H.C. Martin, Phys. Rev. 93 (1954) 498.

97) R.M. Engelbrecht and F.A. McCoy, Anal. Chem. 28 (1956) 1772.

98) E. Weigold and R.N. Glover, Nuclear Physics 32 (1962) 106.

99) C.S. Khurana and I.M. Govil, Nuclear Physics 69 (1965) 153.

100) P. Hille, Oesterr. Akad. Wiss., Math-Naturw. Kl., Ang. (1961) 200; Chem. Abstracts 57 (1962) 349.

101) B.L. Cohen, Phys. Rev. 81 (1951) 184.

102) V. Levkovskii, JETP (Soviet Physics) 45 (1963) 305.

103) M. Hillman, Nuclear Physics 37 (1962) 78.

104) NAS - NS 3043 p4.

105) A.I. Vogel, Quantitative Inorganic Analysis 2nd. Ed. Longmans. 1955.

106) Iu. A. Nemilov, A.N. Pisorevskiiand L.D. Soshin, JETP (Soviet Physics) 35 (1959) 555.

107) Von K. Fritze and W. Kiefer, Radiochimica Acta 4 (1965)

166.

108) S.K. Mangal and C.S. Khurana, Nuclear Physics 69 (1965) 158.

109) A. Cohen and P.H. White, Nuclear Physics 1 (1956) 73.

110) D.J. Hughes and R.B. Schwartz, BNL-325 (1955).

111) H.C. Martin, B.C. Diven and R.F. Taschek, Phys. Rev. 93 (1954) 199.

112) L. Gonzalez, J. Rapaport and J.J. van Loef, Phys. Rev. 120 (1960) 1319.

113) E. Luscher et al., Helv. Phys. Acta 23 (1950) 561.

114) R. Ricamo, Nuovo Cim. 8 (1951) 383.

115) J.A. Grundl, R.L. Henkel and B.L. Perkins, Phys. Rev. 109 (1958) 425.

116) P. Cuzzocrea, G. Pappalardo and R. Ricamo, Nuovo Cim. 17 (1960) 634.

117) J. Rapaport and J.J. van Loef, Phys. Rev. 114 (1959) 565.

118) J.J. van Loef, Nuclear Physics 24 (1961) 340.

119) P. Strohal, N. Cindro and B. Eman, Nuclear Physics 30 (1962) 49.

120) R.F. Coleman, B.F. Hawker, L.P.O'Conner and J.L. Perkin, Proc. Phys. Soc. 74 (1959) 215.

121) V.F. Weisskopf, Rev. of Mod. Phys. 29 (1957) 174.

122) G.S. Mani and I. Iori, Nuov. Cim. 32 (1964) 1092.

123) L. Colli, U. Facchini, I. Iori, G. Marcazzan and A. Sona, Peaceful Uses of Atomic Energy Vol. 14, P/1375 (1958).

124) V.N. Levkovskii, Soviet Physics JETP 18 (1964) 1.

125) A. Chatterjee, Nuclear Physics 47 (1963) 512.

126) L. Colli, Progress in Fast Neutron Physics, Ed. Phillips and J.B. Marion, Chicago (1963).

127) U. Facchini and E. Saetta-Menichella, Nuclear Physics 51 (1964) 460.

128) A. Chatterjee, Nuclear Physics 49 (1963) 686.

129) R.G. Wille and R.W. Fink, Phys. Rev. 118 (1960) 242.

130) D.H. Wilkinson, Phil. Mag. 4 (1959) 215.

131) P.E. Hodgson, Nuclear Physics 8 (1958) 1.

132) R.G. Wille and R.W. Fink, Phys. Rev. 112 (1958) 1950.

133) C.S. Khurana and H.S. Hans, Nuclear Physics 28 (1961) 560.

ACKNOWLEDGEMENTS

I wish to record my thanks to the following:

Professor G.R. Martin for his supervision and interest throughout the course of this work.

Mrs. E.B.M. Martin for helpful advice and discussion.

Mr. R.J. Oliver for valuable practical assistance and for running the neutron generators.

To the University of Durham for the award of a Research Studentship during the tenure of which this work was undertaken.